In-Situ Ethylene Polymerization with Organoclay-Supported Metallocenes for the Preparation of Polyethylene-Clay Nanocomposites

by

Abolfazl Maneshi

A thesis
presented to the University of Waterloo
in fulfillment of the
thesis requirement for the degree of
Doctor of Philosophy
in
Chemical Engineering

Waterloo, Ontario, Canada, 2010

AUTHOR'S DECLARATION

I hereby declare that I am the sole author of this thesis. This is a true copy of the thesis, including any required final revisions, as accepted by my examiners.

I understand that my thesis may be made electronically available to the public.

Abstract

In-situ polymerization is one of the most efficient methods for production of polymer clay nanocomposites. In-situ polymerization of olefins using coordination catalysts is a type of heterogeneous polymerization. In order to achieve acceptable clay nanolayer dispersion in the polyolefin matrix, the clay layer exfoliation and particle break up during the polymerization are essential requirements. A literature review on polyolefin/clay nanocomposite is given in *Chapter 2*.

In *Chapter 3*, we present a new mathematical model, which is as an extension of the multigrain model (MGM), to describe the intercalative polymerization and expansion of clay interlayer spaces during polymerization using clay-supported metallocenes. The results from the model show that, under the studied conditions, mass transfer is not a strong factor controlling clay exfoliation and particle break up. If the polymerization active sites are supported uniformly on all clay surfaces, effective exfoliation will be achieved after a relative short polymerization time.

In practice, obtaining good dispersion of clay nanolayers with uniform properties requires that the active sites be exclusively located on the clay nanolayer surfaces, and not extracted by the solvent to form a homogeneous solution. Factors favouring active site extraction would result in nanocomposites with poor properties. In addition, high polymerization activities, stable polymerization runs, and ease of supporting are other criteria for a successful in-situ polymerization. For this purpose we established a catalyst supporting method by which most of these requirements were met. In this method, the water content on the clay surface, which is considered as poison for the metallocene catalyst, was used to produce MAO upon reaction with trimethylaluminum (TMA). Using this method, polymerization was highly active in absence of MAO cocatalyst, knowing that MAO cocatalyst promotes active site extraction from the clay surface and results in poor powder morphology. Chapter 4 describes the development of this supporting methodology.

Chapter 4 also investigates the effect of the organic modification type existing on the clay surface on the success of catalyst supporting and in-situ polymerization. We found that using the proposed supporting procedure, only tertiary ammonium type modification enhanced the in-situ polymerization, whereas the quaternary ammonium worsened the catalyst supporting efficiency and led to catalyst with poor or no polymerization activity. It is suggested that, in addition to enhancing clay surface-organic solvent compatibility (which facilitates catalyst supporting), the tertiary ammonium cation reacts with the in-situ produced MAO and increases the stability of the cocatalyst bonded to the clay surface.

The effect of different polymerization conditions on the polymerization behavior and nanocomposite structural properties, such as catalyst loading during supporting, polymerization temperature and triisobutylaluminum (TIBA) concentration, were studied in *Chapter 5*. It was found that TIBA acts merely as scavenger. High polymerization activities were obtained with low Al/Zr ratios (Al from TIBA) and increased Al concentration decreased the polymerization activity and also the quality of powder morphology. Catalyst loading in the supporting step showed to have an important role in determining the final

properties. The clay particles with higher catalyst loading resulted in better exfoliation and powder morphologies

The effect of solvent type during catalyst supporting and polymerization was studied in *Chapter 6*. It was shown that catalyst supporting in n-hexane resulted in polymerizations with higher activities and polymers with higher molecular weight were produced. Polymerization with catalyst supported in hexane showed different ethylene uptake profiles, suggesting different mechanism of exfoliation. It is suggested that using this catalyst, the clay is mostly exfoliated before polymerization started.

Similar to the original clay, the catalyst supporting efficiency on the organically modified clay was close to 100 percent. However, comparing the polymerization activities of these catalysts to those that were supported directly in the reactor just before the polymerization (in-reactor, or in-situ, supported catalysts) shows that a considerable fraction of the active sites are deactivated during the prolonged contact between catalyst and clay support surface. In *Chapter 5,* it was shown that the in-reactor supported catalyst had considerably higher polymerization activities, up to 40 percent of that of the homogeneous catalyst. Nanocomposites made with in-reactor supported catalysts had powder morphology and nanaolayer dispersion comparable to those made with clay-supported catalysts.

Acknowledgements

Now that this thesis is being submitted, I see my name on its cover, but the fact is that I see many faces and names hidden in every line of my thesis, a small number of which I would like to mention, as the full listing would be a separate volume to this thesis.

First of all, I would like to praise my God for giving me incredible companies along my life journey, a part of which was my PhD study.

I would deeply appreciate my dear wife Fatima, for being patient and giving me courage to conquer difficulties in different aspects of my student life.

I would like to appreciate my dear son, Mostafa (Erfan), who has been a real supporter to me from his birthday on. Believe it or not, I have learnt many things from his straightforward and loving attitude that helped me improve my lifestyle.

My supportive family from back home provided me with a great deal of support, without which I could not be here talking about achievements. I would like to thank them and I wish I could inherit only a smart part of their kindness, love and patience.

I am grateful Professor Joao Soares and Professor Leonardo Simon for being more than supervisors to me. I have learnt many things from them that will be my assets for the rest of my life. I would like to give special thanks to Professor Joao Soares for his great deal of support during hardships in my PhD thesis.

I would like to express my appreciation to my Committee members, Prof. Tomhas Duever, Prof. Gunter Scholtz, and Prof. Pu Chen, for their concern and guidance in planning and performing my PhD thesis, and also to my external examiner, Prof. S. Wanke for giving me valuable comments to enhance my PhD thesis.

The helpful staff in our department did a great job. I would like to thank Pat Anderson, Lorna Kelly, Liz Bevan, Dennis Herman, Ralph Dickhout, Ravindra Singh, Rosemary Anderson, and many others.

I would like the give special thanks to my dear labmates: Saeid Mehdiabadi, Yiyoung Choi, Anthony Shin, Ravindra Reddy, Ahmad Al-shaiban, Mohamad Al-saleh who gave me a great deal of support.

I would like to thank my friends in the Chemical Engineering Department for their kindness and company: Ali Mohsenipour, Keyvan Nowroozi, Nima Rezaei, Sohrab Zendehboudi, Rafat Parsaei, Omid Mohammadzadeh, Reza Gheslaghi, Ashraf Amin, Majid Soltani, Bahram Zargar, Diroush Abedi and many more.

I would like to express my appreciation to many people in other research groups outside the department for their great deal of cooperation and support. Fred Pearson in McMaster, with his excellent expertise in TEM, helped me a lot to prepare valuable TEM images. Nina, Jalil, Maria, Michael, Katja, Brian and many more people in the Chemistry Department helped me very much to perform my characterizations.

Last, but not least, I would like to express my gratitude to the Iranian Ministry of Science, Research and Technology for providing me the financial support for the major part of my PhD studies, and to NSERC, for providing funds for general consumables in the labs.

At the end, I would like to thank many other people who have directly or indirectly contributed to my PhD thesis and who have not been mentioned above. Thank you all.

Dedication

To my beloved ones.

Table of Contents

List of Figures

List of Tables

Chapter 1

Introduction

Polymer-clay nanocomposites are a new generation of composite materials in which the addition of a small weight fraction of clay can significantly improve the mechanical and barrier properties of the base polymer, provided that the intrinsic properties of clays, such as high surface area of the individual layers (as high as 750 m^2/g) and high aspect ratios are achieved when they are distributed in the polymer matrix.

Among polymer clay nanocomposites, polyolefin-clay nanocomposites find applications in the automotive and packaging industries. These nanocomposites combine excellent barrier and mechanical properties with lower weights than those of conventional composites. In addition, they are less expensive than engineering polymers with similar properties.

Currently, the only commercial production method for polyolefin-clay nanocomposites is melt mixing. In this method, clay layers are dispersed within the polymer matrix under high shear rates allowing polymer chains to diffuse into the interlamellar spaces between the clay layers. Usually, due to the low compatibility between polar clay surfaces and non-polar polymer chains, the clay must be subjected to organic modification through ion exchange reactions with bulky ammonium cations prior to melt mixing to improve the stability of the final nanocomposite. Functionalized polymers, such as polyethylene or polypropylene grafted with anhydride may also be used to ensure good compatibility between the organic and inorganic phases.

In-situ polymerization is an interesting alternative technique for the preparation of polyolefin-clay nanocomposites because, when properly done, it leads to better clay exfoliation and dispersion in the polymer matrix than melt mixing. In this technique, a coordination catalyst (such as Ziegler-Natta, metallocene, or late transition metal complex) is supported onto the clay layers and the polyolefin is made in situ, between the clay layers, leading to their exfoliation and dispersion into the formed polymer matrix.

From modeling point of view, mass transfer (monomer) during polymerization with heterogeneous Ziegler-Natta catalysts and silica-supported metallocene are commonly described with the multigrain model. The multigrain model, however, is not adequate to describe polymerizations with clay-supported catalysts because it does not account for the presence of the clay galleries. Since in-situ polymerizations required the supporting of a catalyst onto clay particles, it is important to investigate whether intraparticle monomer mass transfer limitations take place during polymerization and, if they are relevant, how they affect particle morphology evolution and polymer microstructure.

In this thesis, a single gallery model, as an extension to the multigrain model is developed to investigate the importance of mass transfer through the nanometer scale geometries on the expansion uniformity of the clay which is used as a support material for polymerization catalyst. This model is described in Chapter 3.

From experimental point of view, in order to benefit for advantages of in-situ polymerization techniques, several requirements must be met for it to be used in the industry: the

polymerization activity must be relatively high, clay exfoliation must be efficient, and the morphology of the polyolefin (reactor powder) must be acceptable for operation in commercial reactors.

Several difficulties must be surpassed to prepare good polyolefin-clay nanocomposites by in situ polymerization. Water molecules, which act as a catalyst poison, are an intrinsic part of clay structures and must be removed or neutralized before polymerization can take place. Poor clay surface – organic solvent compatibility that results in non homogenous polymerization conditions and inadequate clay dispersion must be accounted for. Catalyst and cocatalyst extraction from the clay surfaces must be eliminated, or at least reduced to an acceptable level. These aspects are still poorly understood, despite the good number of literature published in this field in the last decade. The main objective of this thesis is to clarify some of these issues and to suggest a methodology for the effective production of polyolefin-clay nanocomposites using metallocene catalysts supported onto organically modified clays. The experimental sections are covered in Chapters 4, 5 and 6 of this thesis

Chapter 2

Literature Review and Background

2.1 Introduction

This chapter provides a literature review on olefin polymerization and polyolefin properties with emphasis on in-situ polyolefin/clay nanocomposite production, which is the main topic of this thesis.

2.2 Polyethylene

Polyethylene is a polymer with the simplest chemical formula for the repeating unit (CH_2-CH_2). It is commonly sold as a copolymer with α-olefins (mainly 1-butene, 1-hexene, or 1-octene). Thanks to the remarkable ability of coordination polymerization catalysts to tailor polymer molecular structures, and despite its simple structural formula, polyethylene has a versatile range of properties among modern commodity resins. Based on differences in chain structure, crystallinity, and density, polyethylene is classified into different categories, including high density polyethylene (HDPE, ≥ 0.941 g·cm^{-3}), low density polyethylene (LDPE, 0.915–0.935 g·cm^{-3}), linear low density polyethylene (LLDPE, 0.915–0.94 g·cm^{-3}), ultralow density polyethylene (ULDPE, <0.915 g·cm^{-3}), and ultrahigh molecular weight polyethylene (UHMWPE, with molecular weight averages of several million grams per mol). Schematics for the three main types of polyethylene are shown in Figure 2.1. HDPE, LLDPE and UHMWPE are made with coordination polymerization catalysts, while LDPE is made with free-radical polymerization at high temperature and pressure. The main difference between LDPE and the other polyethylene types is that LDPE has both long and short chain branches (LCB and SCB), while most resins made by coordination polymerization have mainly SCBs.

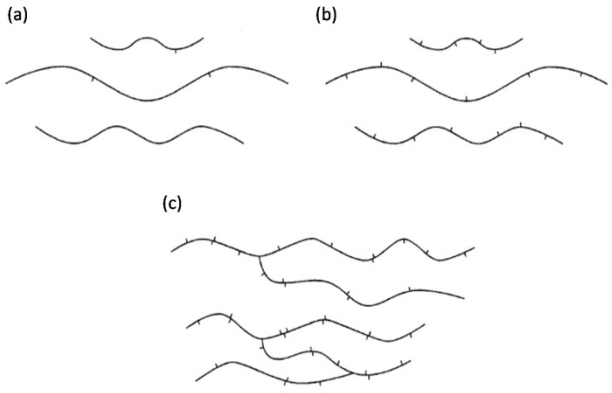

Figure 2.1. Different polyethylene structures: (a) HDPE, (b) LLDPE, and (c) LDPE.

2.2.1 Coordination Catalyst for Ethylene Polymerization

The discovery of coordination catalysts for olefin polymerization was a breakthrough in the production of polyethylene and polypropylene because the polymerization conditions with these systems are much milder than with free radical polymerization, and the control of the polymer microstructure is considerably enhanced. Today, coordination polymerization is the dominant method for the industrial production of polyolefins. Ziegler-Natta and Phillips catalysts have been used since the early fifties, and are still responsible for most of the industrial production of polyolefins. Metallocene catalysts started being used in the late eighties, and their impact on the industrial production of polyolefins is increasing rapidly because they make polyolefins with more uniform microstructures [1] that result in physical properties which, are different from those obtained with Ziegler-Natta or Philips catalysts. Metallocene catalysts are also highly active, and can be supported on a variety of inorganic and organic carriers, making the change from the older Ziegler-Natta or Phillips technologies to metallocene-catalyzed polymerization relatively simple, in a process that has been dubbed *drop-in technology*.

2.2.2 Metallocene Catalysts for Olefin Polymerization

Metallocenes are transition metal complexes in which a central metal atom from group IV is sandwiched between two cyclopentadienyl (or cyclopentadienyl-derivative) rings; an alkenyl group may connect the two cyclopentadienyl rings (the bridge). The hydrogen atoms on the ligands and the bridge can be substituted by other groups to change the reactivity and stereoselectivity of the catalyst. A typical metallocene is shown in Figure 2.2. The metal (M) is normally Ti, Zr or Hf; X is normally Cl or a methyl group; and the R-substituents are often H or methyl groups, but can also be other ring structures.

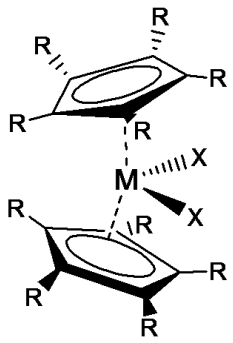

Figure 2.2. General chemical structure of metallocenes.

2.2.2.1 Polymerization Mechanism

Olefin polymerization with a metallocene catalyst follows the general coordination polymerization mechanism, which includes repeated coordination steps of monomer

molecules to the catalyst active site, and successive insertions into the metal-alkyl bond between the catalyst centre and the growing polymer chain.

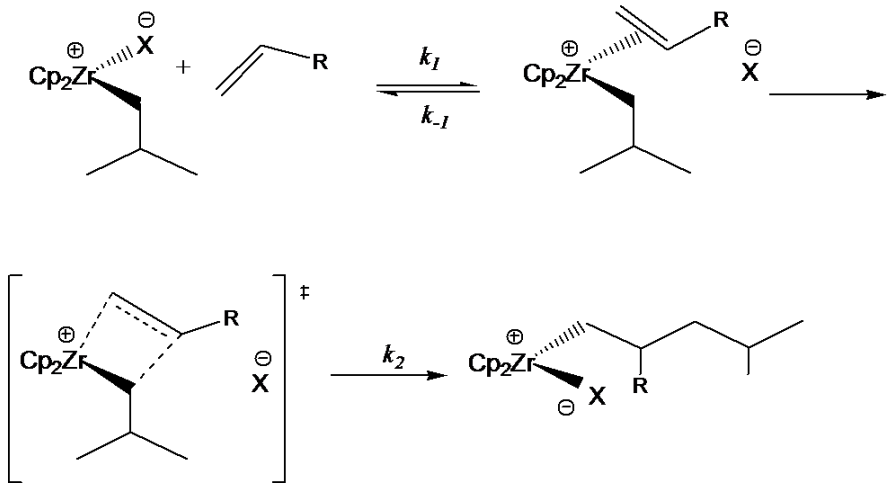

Figure 2.3. Monomer coordination and insertion with a metallocene catalyst [2]

Figure 2.3 shows that the active site for ethylene polymerization is a positively charged metal center. The group IV metallocene catalysts are generated from a neutral metallocene precursor complex that is activated by a cocatalyst. The cocatalyst abstracts a ligand from the metallocene, generating an ion pair composed of a low-valence cation and a charge-balancing non-coordinating counter-ion. Different types of cocatalysts can be used to activate a metallocene catalyst, but methylalumoxane (MAO) is one of the best cocatalysts available. MAO is an oligomer produced by the controlled hydrolysis of trimethylaluminum (TMA) [3, 4].

2.2.3 MAO

There is still some controversy regarding the proper molecular structure of MAO. It has been suggested that MAO has a linear, cyclic, or even a three-dimensional cage structure [3, 5, 6]. The general formula accepted for MAO is given in Figure 2.4.

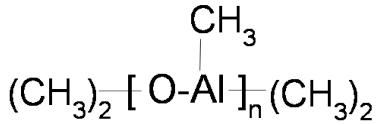

Figure 2.4. General MAO formula.

Different roles have been proposed for MAO in coordination polymerization using metallocenes. As a cocatalyst, MAO generates and stabilizes the cationic species active for olefin polymerization. The reaction between MAO and a zirconocene is shown in Figure 2.5. Before producing active centers, for metallocene di-halides, MAO functions as methylation agent.

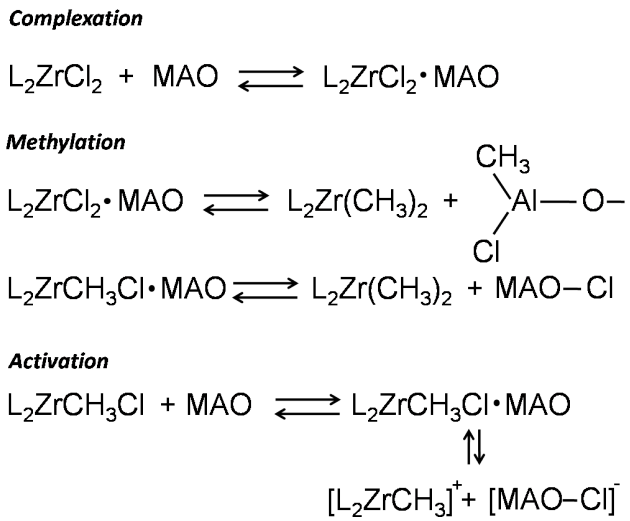

Figure 2.5. Reaction between MAO and a zirconocene [7].

MAO is a Lewis acid and has a high reactivity towards water and other oxygen-containing molecules that can poison the catalyst. Therefore, MAO is used as impurities scavenger before introducing the catalyst into the reactor.

Usually, to achieve high activities, high ratios of MAO to metallocene (Al/M ratio), typically from 1,000 to 10,000, are required in olefin polymerizations with unsupported metallocenes.

Increasing the Al/M ratio results in higher polymerization activity up to a maximum value, after which a further increase in the Al/M ratio will have little effect on the polymerization rate or may even cause a decrease in activity. Initially, the polymerization rate increases because the MAO molecules surrounding the active centers help stabilize them. However, after a given Al/M ratio, higher MAO concentrations may deactivate the active sites, as proposed in Figure 2.6.

Deactivation

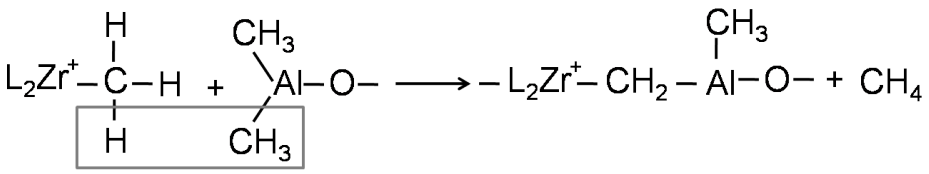

Figure 2.6. MAO deactivation mechanism.

2.2.3.1 MAO production methods

Alkylaluminoxanes, including MAO, are generally produced by the controlled hydrolysis of their corresponding alkylaluminum compounds [8-10]. Among the various aluminoxanes available commercially, MAO is the most difficult to prepare because of the extreme reactivity of TMA. Usually TMA:H_2O ratios higher than unity are found to produce more efficient MAOs [8-10]. MAO synthesis procedures are classified into direct and indirect methods.

In the direct method, the alkylaluminum is reacted with water under mild conditions. They are classified according to the way water is made available for reaction with the alkylaluminum:

- *Reaction with water in solvents:* Water is dissolved in an organic solvent such as benzene
- *Inert gas as water carrier:* A nitrogen stream acts as a carrier for water vapor
- *Condensation method*: Water vapor is condensed into a cooled solution of alkylaluminum
- *Molecular sieve method:* Water adsorbed onto a molecular sieve serves as the water source
- *Ice method:* Ice is contacted with an alkylaluminum solution at temperatures below the freezing point of water

Direct methods are hazardous and runaway reactions may occur due to the high reactivity of TMA and water.

In the indirect method, also called *crystal water method*, water is present in the form of salt hydrates. Since the crystal water is released more slowly, a controlled reaction is guaranteed. The hydrated salts generally used in the synthesis of aluminoxanes are $CuSO_4{\cdot}5H_2O$, $FeSO_4{\cdot}7H_2O$, $Al_2(SO_4)_3{\cdot}18H_2O$, $Al_2(SO_4)_3{\cdot}15H_2O$, $Ti(SO_4)_2{\cdot}8H_2O$, $LiBr{\cdot}2H_2O$, and $LiI{\cdot}2H_2O$. The mole ratio of TMA to water in the hydrated salt may vary from 4:3 to 1:3.5. The temperatures used for MAO synthesis through the indirect method are in the range of -78°C – 80°C, and reported yields vary from 35–45%.

The quality of MAO produced depends on the CH_3/Al ratio and the degree of TMA oligomerization. It is reported that highest productivities are obtained with MAO of higher degrees of oligomerization [11].

Generally, after partial TMA hydrolysis, a fraction of TMA remains strongly bonded [12] into the MAO product and is considered to affect the MAO characteristics. It has been suggested that TMA present in MAO is responsible for the mono methylation of zirconocene dichloride, which corresponds to the first step of the activation process [13, 14].

Trito et al. [15] compared reactions of MAO and TMA with $Cp_2TiMeCl$ and concluded that MAO was a better alkylating agent and that it had a greater capacity for producing and stabilizing active centers. Giannetti et al. [11] studied the effect of TMA on the polymerization activity and molecular weight of polyethylene produced by $(Ind)_2Zr(CH_3)_2$ –MAO and $Cp_2Zr(CH_2C_6H_5)_2$–MAO systems, and found that the catalytic activity decreased with increasing [TMA]/[MAO] ratios. They also showed that the effect of TMA on molecular weight of polyethylene depended on the type of metallocene catalyst. Increased TMA concentration resulted in drastic drop of molecular weight with $Cp_2Zr\ (CH_2C_6H_5)_2$, but it did not show any significant effect when $(Ind)_2\ Zr\ (CH_3)_2$ was used.

A TMA poisoning effect has also been noted by Pédeutour et al. [16]. They investigated the activation of *rac*Et$(Ind)_2ZrCl_2$ by "TMA-depleted" MAO for 1-hexene polymerization and concluded that it activated the zirconocene at lower than usual Al/Zr ratios (Al/Zr ≈ 50–200) in homogeneous conditions.

MAO is not easily soluble in aliphatic organic solvents. To overcome this problem, the bulkier tri-isobutyl aluminum (TIBA) is hydrolyzed together with tri-methyl aluminum (TMA) to synthesize a modified MAO with more methyl groups. The product is called modified methyl-aluminoxane (MMAO) and has increased solubility in aliphatic solvents.

2.2.4 Catalyst Supporting

Metallocene catalysts are soluble in organic solvents and can be used directly in solution or precipitation polymerization. In solution polymerization, the temperature is kept high enough so that both catalyst and polymer chains are soluble in the reaction medium; in precipitation polymerization, the catalyst is soluble in the reaction medium, but the polymer precipitates as it is formed. As a drawback [17], metallocene catalysts in dissolved forms are unsuitable for the production of polyethylene or isotactic polypropylene in gas phase or slurry processes.

Most commercial Ziegler-Natta olefin polymerization reactors require a heterogeneous catalyst; therefore, metallocenes have to be supported onto a carrier to be used with these processes. A supported metallocene/MAO catalyst was first suggested by Sinn et al. [18] and Kaminsky et al. [19]. Many types of supported metallocene catalysts since then have been reported; they have been surveyed recently by Ribeiro et al. [20].

2.2.4.1 Criteria for an Acceptable Supported Catalyst

A supported catalyst needs to achieve the following improvements to be used in existing olefin polymerization reactors:

1. The supported catalyst should have activity comparable to that of the homogeneous catalyst [17].
2. MAO requirements (Al/M ratio) should be as low as possible for economic viability.
3. The supported catalyst should produce polymer with high molecular weight when needed, at the temperatures commonly encountered in industrial polymerization reactors.
4. Supported catalysts must produce polymer particles with high bulk density and controlled powder morphology.
5. The enhanced MWD control provided by metallocene catalysts should not be lost during catalyst supporting.
6. For the case of polypropylene, the support should not affect adversely the catalyst stereochemical control.

2.2.4.2 Catalyst Supporting Methods

Various metallocene supporting methods are reviewed in the literature [17, 21-23]. They are classified in three main types:

A. Absorption or in-situ production of MAO on the support followed by metallocenes impregnation and washing the catalyst. The supported catalyst is used in combination with additional MAO or other alkylaluminum in polymerization

B. One step supporting of pre-activated metallocene/MAO. The supported catalyst will be used in combination with an alkyl aluminum compound for polymerization.

C. Direct supporting of the catalyst onto the support and activation with a cocatalyst in the polymerization reactor (support/catalyst + cocatalyst)

These catalyst supporting methods are illustrated in Figure 2.7.

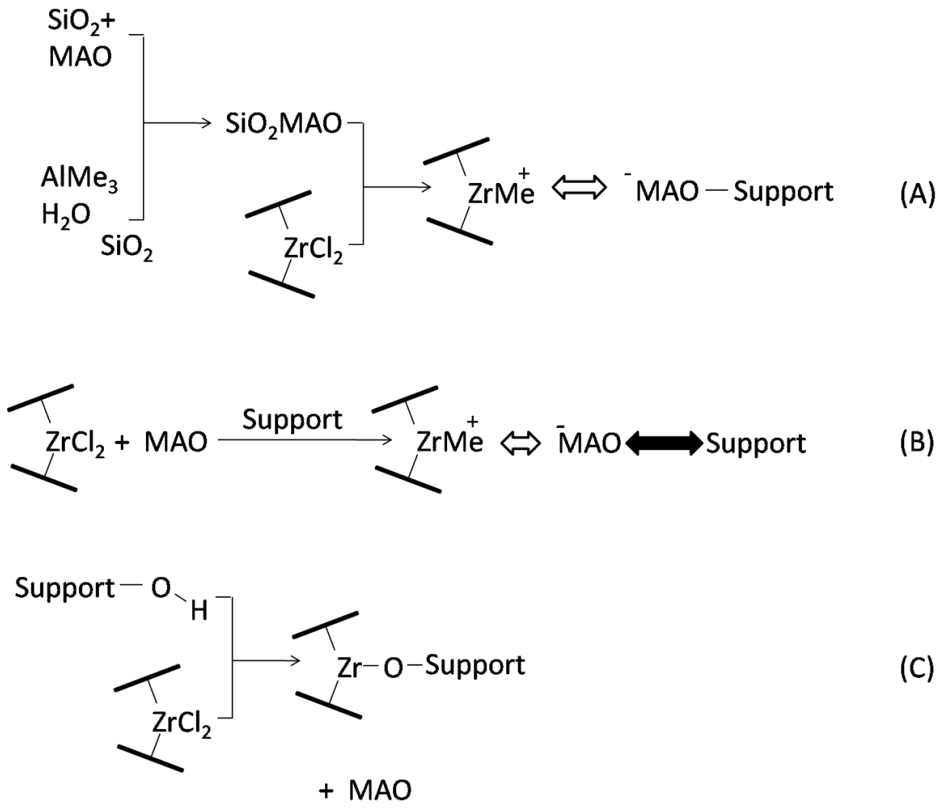

Figure 2.7. Different metallocene supporting methods [24].

2.2.5 Polymer Particle Growth

Catalyst particle break up and growth during olefin polymerization has been studied in detail by several research groups [25-28].

Laboratory scale olefin slurry polymerizations typically start with injection of catalyst particles (support containing the catalyst) with average diameters in the range of 15-60 μm, into the reactor. The monomers can be gaseous or liquid, and a hydrocarbon diluent may also be present, forming the continuous phase of the reactor. The monomer is either dissolved in the diluent or, in the case of propylene, present alone in the liquid phase. Hydrogen is commonly used as a chain transfer agent. When a supported catalyst is used, monomer must diffuse through the boundary layer around the catalyst particle and through its pores to reach the active sites, where polymerization occurs at a turnover rate that may be as high as 10^4-10^5 monomer insertions per second for metallocene catalyzed solution polymerization. Upon polymerization, the formed polymer is deposited onto the catalyst surface, forming a layer around the active sites. For polymerization to continue, monomer must be absorbed onto the surface of this polymer layer and diffuse through it until reaching the active sites.

After filling up the catalyst support pores, the hydrodynamic pressure caused by the growing polymer breaks the support into many fragments that are known as micrograins, microparticles, or primary particles. If the catalyst is properly designed, the polymer layers will act as a binder, keeping the microparticles together into a larger macroparticle. As a consequence, the morphology of the catalyst particle is replicated in the morphology of the polymer particle (replication phenomenon).As a result, for a successful particle break up the particle size distribution (PSD) of the polymer should resemble the PSD of the catalyst particles.

Since the monomer must diffuse through the macroparticle pores and the polymer layer surrounding the microparticles, mass transfer resistances may affect the observed polymerization rate. In addition, heat transfer limitations may also result because olefin polymerizations are exothermic (approximately 100 kJ/mol). If heat is not removed efficiently from the growing polymer particle, hot spots may form, leading to increased catalyst deactivation, polymer softening or melting, and reactor fouling.

2.2.5.1 Single Particle Modeling

It is convenient to classify olefin polymerization models in three different levels: macro-, meso-, and microscale, as explained below:

1) *Macroscale* (>1m) includes detailed description of the reactor hydrodynamics for modeling mixing, reactor stability, and particle size distributions.
2) *Mesoscale* ($>10^{-3}$–10^{-2}m) includes interparticle, intraparticle, and particle-wall interaction mass and heat transfer models. This, in turn, requires models for particle morphology evolution and monomer adsorption. This scale also links the continuous approach used at the macroscale and the discrete approach needed at the microscale.
3) *Microscale* includes modeling of polymerization kinetics, the nature of active site types, diffusion of monomer in the polymer, and crystallization of polymer molecules.

2.2.5.2 Physical Models

Physical models for olefin polymerization try to explain phenomenon such as broad MWDs through inter- and intraparticle heat and mass transfer resistances [29]. If the catalytic sites are identical and are uniformly distributed throughout the particles, then the radial variations in monomers concentration and temperature lead to different rates of chain growth and termination across the polymer particles. If mass and heat transfer limitation are significant, polymer chains with different average properties are produced at different radial positions, even if all of the sites were chemically identical.

Three main types of physical models have been proposed in the literature: the solid core model, the polymer flow model, and the multigrain model (Figure 2.8). The solid core model ignores particle break-up. In this model, polymer is considered to grow around a solid catalyst core. The solid core model contradicts experimental observations and has only historical

value, but it is mentioned here because it is a component of the multigrain model. The polymer flow model (PFM) [25, 30-32] assumes that growing polymer chains and catalyst fragments form a continuum. This model uses the classical pseudo homogeneous approximation, commonly used when modeling heterogeneous catalytic reactors. In the PFM, heat and mass transfer take place throughout a pseudo homogeneous polymer matrix. Although the PFM is a significant improvement over the solid core model, it does not explicitly consider the catalyst particle fragmentation and the heterogeneous nature of the resulting polymer particle.

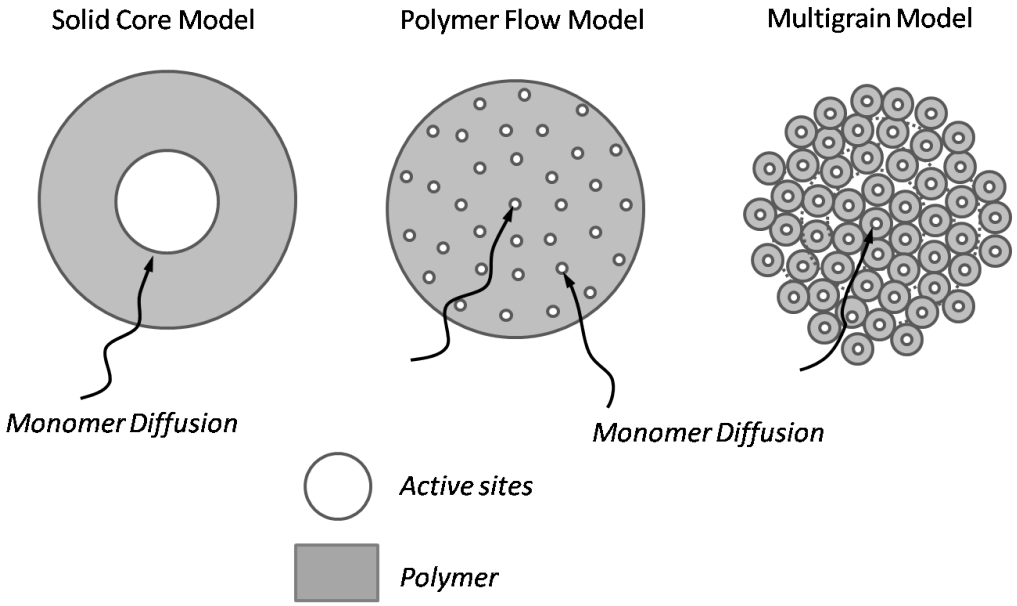

Figure 2.8. Three classes of physical models [25].

The multigrain model [25, 32-37] gives a more detailed description of phenomena taking place during polymerization with supported catalysts. Instead of using the pseudo homogeneous approximation as the PFM, the MGM considers the heterogeneous nature of the polymer particles. Mass and heat transfer resistances are considered to take place in two levels, at the macroparticle and the microparticles that compose it. As shown in Figure 2.9, the polymeric particle (macroparticle or secondary particle) is formed by an agglomerate of microparticles or primary particles. Each microparticle is a fragment of the original catalyst particle, with all active sites located on its external surface, surrounded by dead and living polymer. During polymerization, monomer diffuses through the pores of the macroparticle, adsorbs onto the polymer layer surrounding the microparticle, and diffuses through it to the active sites on the microparticle surface. The newly formed polymer chains push the previously formed layer, thus increasing the radius of the microparticles and, consequently, the size of the macroparticle.

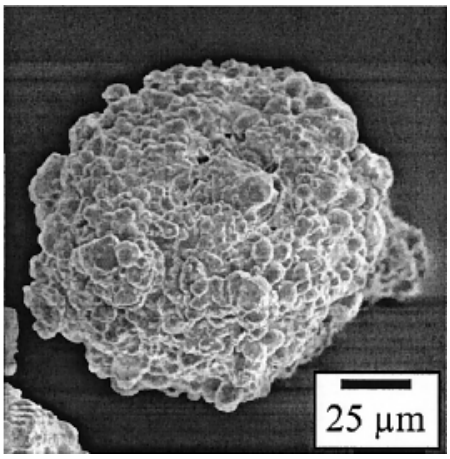

Figure 2.9. A typical macroparticle, composed of several microparticles [27].

The MGM is the most widely used particle growth model for olefin polymerization with Ziegler–Natta catalysts. It has been used to describe heat and mass transfer resistances for homo- and copolymerization of ethylene, propylene, and higher α-olefins, in slurry and gas-phase reactors.

Ideally, the mechanical strength of the catalyst particle is sufficiently high to prevent its disintegration into smaller fragments (as this may lead to fines), but low enough to allow controlled progressive expansion during polymerization. As the polymerization proceeds, the initial catalyst support fragments and is dispersed within the growing polymer matrix (Figure 2.10).

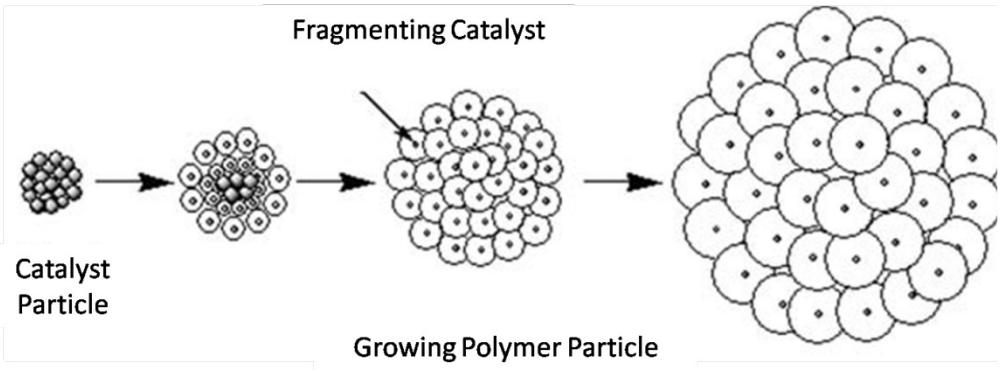

Figure 2.10. Schematic representation of a model for the growth of a single polymer particle [38].

Extensive fragmentation and uniform particle growth are key indications that the replication process is proceeding as desired. These features dependent on a high support surface area, a homogeneous distribution of active centers throughout the particle, and free access of the monomer to the innermost zones of the particle.

For silica-supported catalysts, it has been observed that polymer growth starts at the particle surface and propagates inwards, leading to the formation of a polyolefin shell around the catalyst particle. This makes difficult the free access of the monomer to active sites within the particle. Fink [28] has highlighted that this mechanism of particle growth is associated with a kinetic profile in which an initial induction period is followed by an acceleration period after which, in the absence of chemical deactivation, a stationary rate is obtained. Figure 2.11 represents such a profile. Depending on the extent of catalyst loading, from low to high, the actual time for each stage may be considerably shortened.

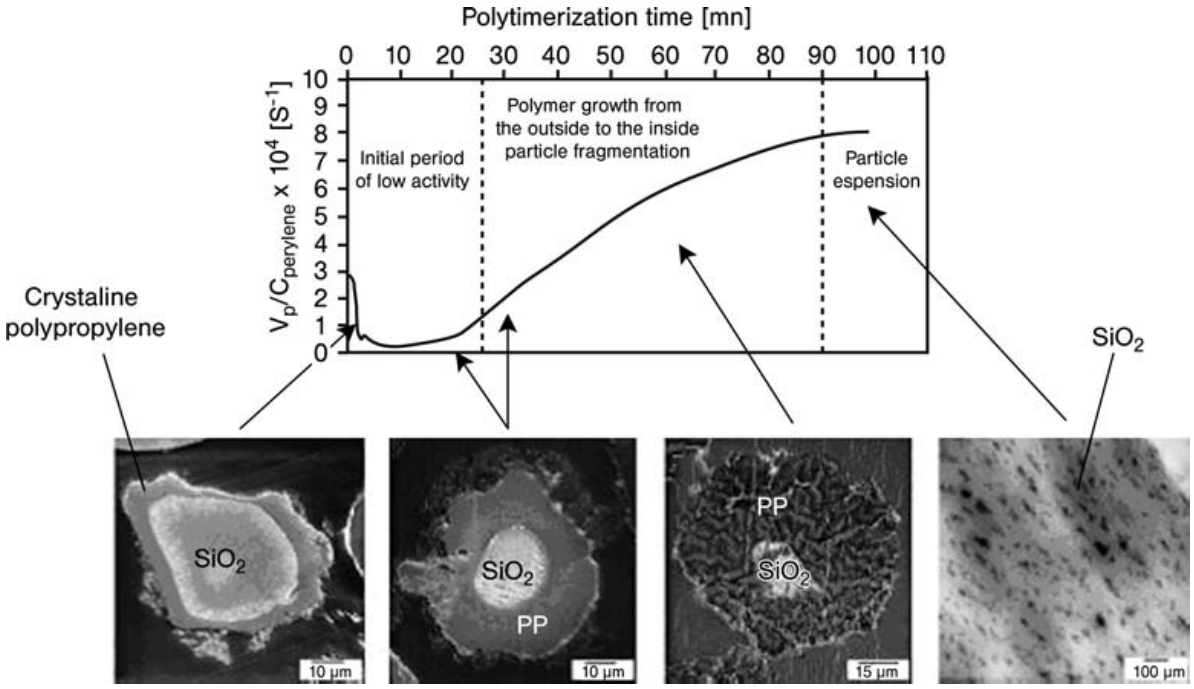

Figure 2.11. Schematic polymer growth and particle expansion from experimental analysis [28].

It has been reported that the polymerization temperature has a considerable effect on particle break up [39, 40] and, therefore, on the final particle morphology.

2.3 Layered Silicates – Clay Materials

In mineralogy, the term "clay" is used for a variety of polycrystalline materials that are described in detail in clay science, mineralogy properties and characterization textbooks [41-44]. Herein, we will focus on aspects related to catalyst supporting and particle growth, i.e. clay chemistry, crystalline structure and geometry.

Clay materials can be present in fibrous, tubular, lath shaped, and planar geometries. In this section, our focus will be on the planar clay varieties called smectites that include

montmorillonites, the type of clay used to support catalysts in this thesis. These clay minerals consist of two basic units, an octahedral sheet and a tetrahedral sheet.

The octahedral sheet is comprised of closely packed oxygen atoms and hydroxyl groups, in which aluminum, iron, and magnesium atoms are arranged in octahedral coordination (Figure 2.12).

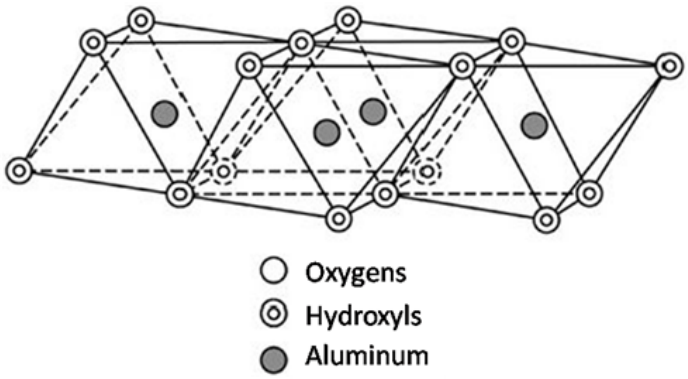

Figure 2.12. Sketch of a clay octahedral sheet [44].

The second structural unit is the silica tetrahedral layer, having a silicon central atom and four oxygen atoms, or possibly hydroxyl groups, arranged in the form of a tetrahedron. These tetrahedra form a hexagonal network that is repeated infinitely in two horizontal directions to form a silica tetrahedral sheet (Figure 2.13).

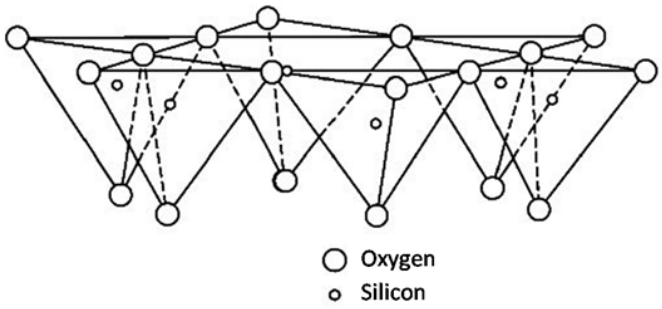

Figure 2.13. Silica tetrahedral sheet [44].

The silica tetrahedral sheet and the octahedral sheet are joined by sharing the apical oxygen atoms or hydroxyl groups, to form a 1:1 clay mineral layer (kaolinite) or a 2:1 clay mineral layer (montmorillonite). The structure and composition of the major industrial clays, kaolins and smectites are very different, even though they are comprised of octahedral and tetrahedral

sheets as their basic building blocks. The arrangement and composition of the octahedral and tetrahedral sheets account for most of the differences in their physical and chemical properties.

2.3.1 Smectite Clays

In smectite minerals, the basic layer is composed of an alumina octahedral layer sandwiched between two silica tetrahedral layers by sharing the apical oxygen atoms of the silica tetrahedral sheets and designated as a 2:1 layer mineral (Figure 2.14). Water molecules and cations occupy the space between the 2:1 layers. Their theoretical formula is $(OH)_4Si_8Al_4O_{20}.nH_2O$ (interlayer) and their theoretical composition without the interlayer material is SiO_2 (66.7%), Al_2O_3 (28.3%), and H_2O (5%). However, smectites have considerable substitutions in their octahedral sheet, and some in their tetrahedral sheet, that create a charge imbalance on the layer structure which is balanced with alkali or earth alkali metal cations. The most common smectite mineral is calcium montmorillonite, in which the layer charge deficiency is balanced by the interlayer calcium cations and water. The basal spacing of calcium montmorillonite is 14.2Å. Sodium montmorillonite occurs when the charge deficiency is balanced with sodium ions and water and its basal spacing is 12.2Å.

The smectite particles are very small. Because of their small crystalline domains they are considered as structurally disordered; therefore, the X-ray diffraction data of smectites are sometimes difficult to analyze [45]. A typical scanning electron micrograph of sodium montmorillonite is shown in Figure 2.15. Sodium montmorillonite, which is the focus of this thesis, is comprised of very small thin flakes with “cornflake texture”, having a high surface area of about 150–200 m^2/g.

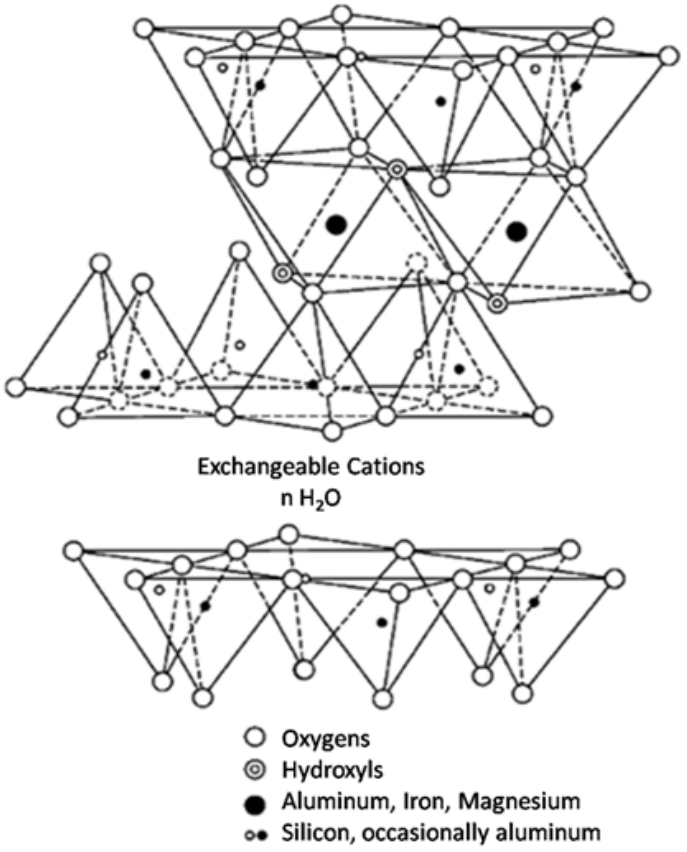

Figure 2.14. Sketch of the structure of smectites [44].

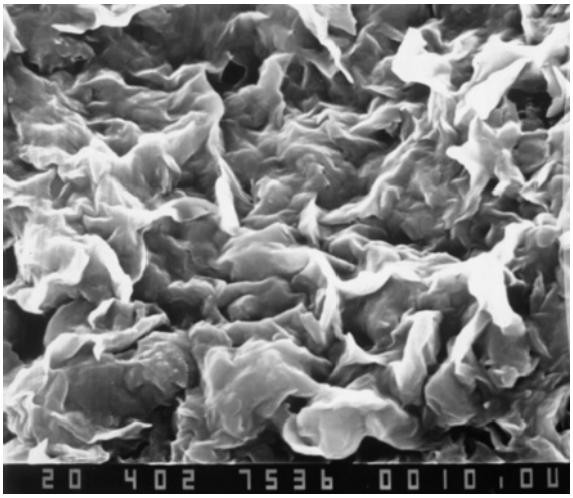

Figure 2.15. Scanning electron micrograph of a sodium montmorillonite [44].

For smectites, substitution of Al^{3+} by Fe^{3+}, Fe^{2+} and Mg^{2+} in the octahedral sheet is common. There can also be some substitution of silicon atoms by aluminum atoms in the tetrahedral sheets, which again creates a charge imbalance. The isomorphous substitution of bivalent cation for a trivalent on the octahedral layer, results in a positive charge deficiency in the octahedron layer and enhances the Lewis base behavior of the hexagonal cavity on the silicate layer,sufficient to form complexes with dipolar molecules and cations with their hydration sphere [42].

2.3.2 Clay Particle Morphological Hierarchy

The clay particle morphology may be divided in several structural levels, as illustrated in Figure 2.16. The elementary structure is the clay *layer*. As discussed previously for montmorillonite, these layers are composed of tetrahedral and octahedral sheets. A *particle* is an assembly of layers. Tactoid stacking of clay layers is a specific type of particle assembly. An assembly of particles will be referred to as an *aggregate*. Aggregates may combine to form the assembly of aggregates shows as superstructure D in Figure 2.16.

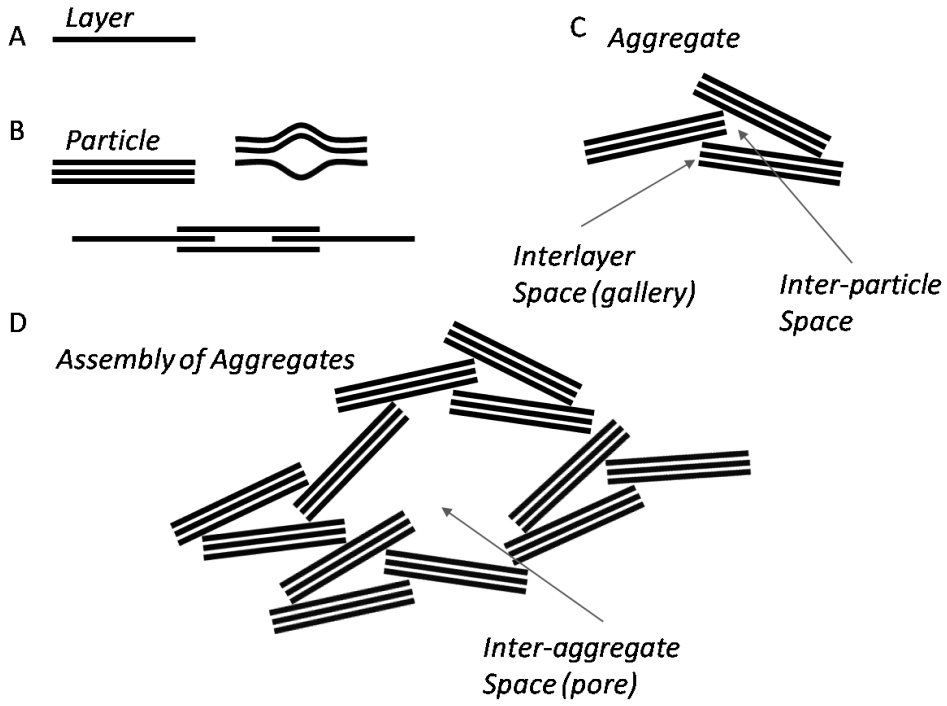

Figure 2.16. Structural hierarchy of clays: (A) clay layer; (B) a particle made up of stacked layers; layer transition and deformation can give rise to a lenticular pore; (C) an aggregate, showing an interlayer space and an inter-particle space; and (D) an assembly of aggregates, enclosing an inter-aggregate space (pore) reproduced from [41].

In practice, clay minerals are highly anisometric, often having irregular particle shape and broad particle size distribution. The distribution of cation exchange capacity is not uniform and, therefore, a distribution of interlayer spacing can be detected in the montmorillonite clays. The individual layers are flexible and can be curved as depicted in Figure 2.16 [46]. Clay mineral particles, in particular those of montmorillonites, are never crystals in the strict sense [46]. In fact, a montmorillonite 'crystal' is more equivalent to an assemblage of silicate layers than to a true crystal (Figure 2.17).

Figure 2.17. Schematic view of montmorillonite particles with curvature [46].

Montmorillonite particles seen in the electron microscope never have the regular shape of real crystals but look like paper torn into irregular pieces. The core of the particles is surrounded by disordered and bent silicate layers with frayed edges. Layers, or thin particles composed of a few layers protrude from the packets and enclose wedge-shape pores. The particles reveal many points of weak contacts between the stacks of the layers. At these 'breaking points' the particles may easily disintegrate during interlayer reactions, or as a result of mechanical forces that influence rheological behavior. The electrostatic attractions between the layers and the interlayer cations increase the stacking order in more highly charged 2:1 clay minerals; the domains with equally spaced layers become thicker and the influence of the defects on the shape and position of the basal spacing (001) reflections, the characteristic of interlayer spacing in X-ray diffraction, decreases.

2.3.3 Clay Chemistry

The distinctive structure of clay materials is a great potential towards different types of chemical reactions. The interlayer cations can be exchanged with various types of cations. The highest possible cation exchange on the clay surface is called cation exchange capacity (CEC). In addition to the interlayer cations, montmorillonite clays also have silanol and aluminol groups on the edge surface that can be used in cation exchange reactions, depending on the

acidic properties of the reaction medium. The substitution within the lattice is responsible for about 80% of the total cation exchange capacity; the hydroxyl groups on the edge surface account for the remaining 20% [44]. The reactivity of the latter fraction depends on the pH of the dispersion medium. Sodium montmorillonite has a high cation exchange capacity, generally ranging from 80 to 130 meq/100 g. The high electrical charge on the lattice enables sodium montmorillonite to exchange the interlayer water and associated cations with more polar organic molecules, such as ethylene glycol, quaternary amines, and polyalcohols.

Clay minerals can interact with different types of organic compounds in particular ways. The penetration of organic molecules into the clay interlayer space is called intercalation. Intercalated guest molecules can be displaced by other suitable molecules. Water molecules in the interlayer space of smectites can be displaced by many polar organic molecules. Neutral organic ligands can form complexes with the interlayer cations. The interlayer cations can be exchanged by various types of organic cations. Alkylammonium ions, mainly quaternary alkylammonium ions, are widely used in modifying smectites for industrial applications. The silanol and aluminol groups on the edge surfaces of montmorillonite clays can be used for grafting reactions.

The adsorption of neutral molecules on smectites is driven by various chemical interactions: hydrogen bonds, ion–dipole interaction, co-ordination bonds, acid–base reactions, charge-transfer, and van der Waals forces. Polar molecules such as alcohols and amines form intercalation complexes with montmorillonite clays. Even acids are intercalated. The intercalation can be performed from the vapor, liquid, and even solid state.

In intercalation from solution, solvent molecules are generally co-adsorbed in the interlayer space. Guest molecules may be intercalated in dried clay minerals or may displace the water molecules of hydrated montmorillonite. The displacement of interlayer water molecules depends on the hard-and-soft-acid-and-bases (HSAB) character of the interlayer cations and the interacting groups of the guest molecules. HSAB, also known as the Pearson acid–base concept, is widely used in chemistry for explaining stability of compounds, reaction mechanisms and pathways. In the HSAB concept, chemical species are classified by their Lewis acidic and basic properties by the terms 'hard' or 'soft'. 'Hard' applies to small species which have high charge states, and are weakly polarizable. 'Soft' applies to large species which have low charge states and are strongly polarizable [47]. Water molecules around hard cations like Na^+, Mg^{2+}, and Ca^{2+} are displaced only by HO– or O= containing compounds but not by amines. In contrast, amines as soft bases displace water molecules from soft interlayer cations like Cu^{2+} and Zn^{2+} [48]. Aliphatic and aromatic amines can be directly coordinated to the interlayer cations (Figure 2.18a) or bound by water bridges (Figure 2.18b) [48]. The type of bonding is mainly determined by the hardness or softness of the cations due to the HSAB concept. While soft cations such as Zn^{2+}, Cd^{2+}, Cu^{2+}, and Ag^+ bind amines directly, water bridges are formed between amines and hard cations (alkali and earth alkali ions, Al^{3+})[1].

[1] These cations do not form stable amino complexes in water.

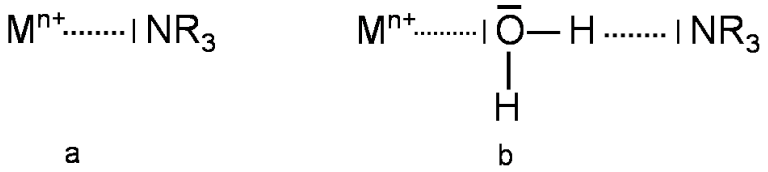

Figure 2.18. Coordination of amines to the interlayer cations: a) directly, b) by water bridges.

In addition to the coordination bonds, ionic bonds are often observed, especially in aqueous dispersions when the base is protonated due to acidic solution pH [49, 50] or to the increased acidity of interlayer water molecules (Figure 2.19).

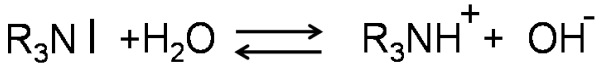

Figure 2.19. Ionic bond when a base is protonated in acidic pH solution.

The ratio of protonated base to unprotonated base in the interlayer space of the clay is different from the ratio in homogeneous solution (outside the interlayer space of the clay), mainly because of the increased acidity of water in the interlayer space. In addition, protonation is enhanced by the ability of the negatively charged clay mineral surface to lower the chemical potential of the protonated form of the base relative to the neutral form, and therefore drive the equilibrium towards protonation in Figure 2.19.

Two types of acid sites, Brønsted and Lewis acid sites, are available on the clay surface. Brønsted acidity mainly arises from interlamellar water, since silanol groups at the edges are only weak-acidic centers. Lewis acidic sites on clay mineral surfaces are usually coordinately unsaturated Al^{3+} ions that can accept electron pairs from donor molecules. In the presence of water, the Lewis acidic species are hydrated and their Lewis acidity is masked. As the electron pair of nitrogen groups cannot displace water molecules from Al^{3+} ions, Lewis acidity of these Al^{3+} ions only develop after thermal decomposition of the water molecule, i.e. when the heated clay mineral is reacted with a base in the absence of water. Exchange of the sodium and calcium ions by several di-ammonium cations showed a certain selectivity strongly influenced by the solvent [51].

2.4 Polymer- Clay Nanocomposites

Potentially large clay surface areas can be exposed to the polymer matrix when only a small weight percent of clay is used in the composite. When there is complete separation of the individual clay nanolayers (each with thickness of 0.7 nm), the composite qualifies as a nanocomposite. Polymer-clay nanocomposites are an emerging group of materials that received a great deal of attention not only because of their potential industrial applications, but

also from a fundamental point of view. Useful reviews on this topic have been published by Alexandre and Dubois [52], and Sinha, Ray and Okamoto [53].

Different morphologies for polymer-clay composites are sketched in Figure 2.20. Microcomposites are clay-polymer compounds wherein the clay is predominantly present as large size aggregates, with dimensions larger than 1 mm. To be called a nanocomposite, it is necessary that the polymer-clay system have the following characteristics: (i) intercalated clay layers, formed when the polymer chains are inserted into the interlayer space; and (ii) exfoliated (or delaminated) clay layers, formed when the silicate layers are no longer close enough to interact with each other. Polymer-clay nanocomposites can have morphologies ranging from exfoliation to intercalation. Purely exfoliated clay–polymer compounds are by definition those in which the clay layers are individually dispersed in the polymer.

Only a few examples of complete exfoliation can be found in the literature, but many published transmission electron microscopy (TEM) micrographs show small regions in a compound where complete exfoliation occurred. According to most TEM nanocomposite micrographs, a range of layer separation states are available. Perfectly exfoliated compounds constitute one end of the spectrum; the other end is represented by clay mineral–polymer compounds in which the polymer is intercalated as a monolayer into the clay mineral. The reality of nanocomposites is that even in cases where exfoliation appears to have taken place, little if any individual platelets can be found in the compound, and most often exfoliation only leads to one layer or few layers.

Distinguishing between the two types of structures on the basis of their mechanical properties is often not possible, as some interesting properties were found also for intercalated structures, and mechanical properties do not always improve with increasing interlayer expansion [54, 55]. Further, exfoliated nanocomposites can revert to the intercalated morphology under certain conditions. In the melt, mass transport of the polymer entering the interlayer space is rapid, and the polymer chains exhibit mobility similar to or faster than the polymer self-diffusion [56]. If the thermodynamic conditions are favorable for intercalation, the polymer can crawl in and out of the interlayer space until equilibrium is reached. Changes in physical conditions (such as external pressure, temperature and shear rate) disturb this equilibrium, and the polymer may eventually leave the interlayer space.

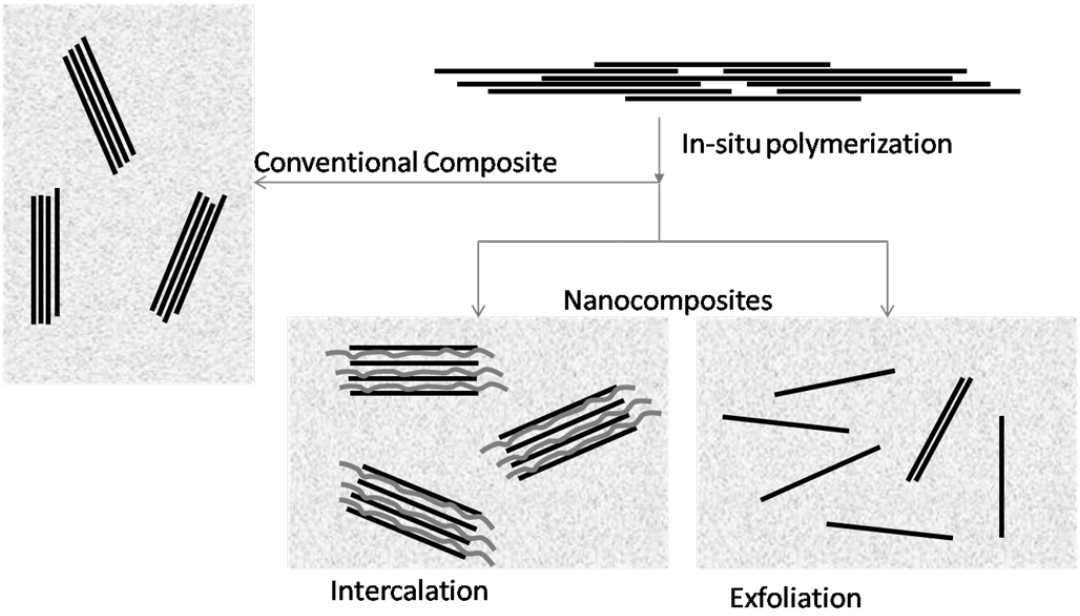

Figure 2.20. Different structures proposed for clay-polymer materials arranged as nano- and microstructure solids.

2.4.1 Preparation of Polyolefin-Clay Nanocomposites

There are two major methods for preparing polyolefin-clay nanocomposites: a) in-situ polymerization and b) direct mixing through melt compounding. Both may be used in the raw (untreated) state, or after a specific clay modification.

Polar polymers can be directly intercalated into smectites from solutions of the polymers in polar solvents (e.g. water, alcohols, etc.), and in some cases from the melt [48]. The mechanism of this interaction is based in each case on the formation of hydrogen bonds between the functional groups of the polymers with the mineral surface. This interaction occurs directly with the siloxane surface of the clay mineral layer or with the water molecules coordinated to the interlayer cations, through water bridges. However, for non-polar polyolefins for which no functional group is available to interact with the siloxane surface of the clay, additional methods are demanded to increase the compatibility between the two phases. The clay surface may be modified with organic compatibilizers to render it more organophilic and decrease the interfacial energy between clay surface and polymer chains, facilitating the diffusion of polyolefin molecules. Polymeric compatibilizers, such as maleic anhydride-modified polyolefins, may also be used to achieve better composite morphology. Currently, the melt mixing method is vastly used for the preparation of polyolefin-clay nanocomposites.

In-situ polymerization is another important method for the production of polymer-clay nanocomposites. This process consists on the intercalation of monomers between the clay layers, followed by their polymerization. In contrast to hydrophilic monomers, which are

easier to polymerize in the interlayer space, low polarity monomers such as styrene can be efficiently polymerized in the interlayer space only if the clay was previously modified.

2.4.1.1 Clay Modification Methods for In-Situ Polymerization

Clays are often modified using several types of treatment. In this section, we will review the most common clay modification approaches used to make them more suitable as supports for in-situ polymerization processes.

Organic modification is a common technique that is applied to clay surface to enhance the efficiency of in-situ polymerization organic monomers. In this technique, bulky anions such as ammonium or phosphonium ions with long alkyl chains (C_{10}-C_{18}) substitute the small interlayer alkali ions to increase the clay basal spacing and render the hydrophilic clay layers more organophilic. Organically modified clays are called organo-clays [57, 58].

For the production of polyolefin-clay nanocomposites, the polymerization catalyst needs to be fixed on the clay surface, which then acts as a support for the coordination catalyst. In the in-situ polymerization method, the compatibility between the clay surface and reagents has a great impact on the efficiency of in-situ polymerization method. In order to enhance the surface compatibility between hydrophilic clays and organic solvent that carries the reactants, the clay is modified by cation exchange with alkylammonium ions. The most common alkylammonium species for preparation of organoclays are quaternary ammonium compounds containing alkyl, phenyl, benzyl and pyridyl groups (Table 2.1).

Several interlayer structures were proposed for alkylammonium-exchanged montmorilonites. The alkyl chains generally lay flat on the clay surface as mono- or bilayers. Other arrangements, such as pseudo-trimolecular and paraffin-type arrangements, have also been proposed [48].

Table 2.1. Quaternary ammonium cations frequently used to prepare organoclays.

Quaternary cation	Abbreviation	Formula
Tetramethylammonium	TMA	$(CH_3)_4N^+$
Trimethyl phenylammonium	TMPA	$C_6H_5N^+(CH_3)_3$
Benzyl trimethylammonium	BTMA	$C_6H_5CH_2N^+(CH_3)_3$
Hexadecyl pyridinium	HDPY	$C_5H_5N^+(C_{16}H_{33})$
Benzyl dimethyl teradecylammonium	BDTDA	$C_6H_5CH_2N^+(C_{14}H_{29})(CH_3)_2$
Hexadecyl trimethylammonium	HDTMA	$C_{16}H_{33}N^+(CH_3)_3$
Dioctadecyl dimethylammonium	DODMA	$(C_{18}H_{37})_2N^+(CH_3)_2$

To achieve an acceptable in-situ polymerization process to produce polyolefin-clay nanocomposites, the immobilized active site on the clay surface should be preserved from deactivation. Pristine clays such as Na^+ montmorillonite are hydrophilic materials and contain substantial amounts of water on their layer surfaces (up to 10 wt. %), accompanying alkali metal cations. Water is a poison [59, 60] for the majority of olefin polymerization catalysts; therefore, direct contact between pristine clay and polymerization catalysts produces supported catalysts with very low polymerization yields or completely inactive catalysts [61].

In the clays minerals, depending on their structure, different forms of water are available [34, 42, 49, 51-54] that can be determined using thermal gravimetric analysis (TGA): a) physically adsorbed water (also called zeolitic or free water, generally released below 100°C), b) bound water (released below 300°C) and c) structural water (released around 600°C). As a result of water displacement during organic modification, the water content in organo-clays is considerably lower than in pristine clays (typically less than 0.2 wt. %).

For organoclays being used as support in in-situ polymerization methods, the organic modifier must not significantly affect the activity of the polymerization catalyst. As an example, oxygen-containing modifiers would result in catalyst deactivation. Organic modification of clay has been reported to enhance the in-situ polymerization efficiency [62, 63]. For example, Liu et al. [62] compared the polymerization of ethylene with Cp_2ZrCl_2 supported on sodium montmorillonite and montmorillonite modified with methyl glycinate hydrochloride. They found that the organically modified clay had a considerably higher catalyst loading (214 μmol/g vs 9.8 μmol Zr/g support) and higher polymerization activity under the same conditions.

Thermal treatment is another modification method for clay surface before catalyst supporting. During thermal treatment, and consequent removal of water at different temperature ranges, the clay porosity and acidity change. In fact, acidity, porosity, and cation exchange capacity (CEC) of clays are closely related to their water content [48]. Clay mineral surfaces have both Brønsted and Lewis acid sites. In smectites, strong Brønsted acidity derives from dissociation of water that is directly coordinated to interlayer cations. The acid strength increases with the polarizing power of the cations, i.e. with decreasing size and increasing charge. The smaller is the amount of hydration water present on the clay surface, the greater would be the polarization of the remaining water molecules and hence their ability to donate protons. Dehydrated interlayer cations also act as Lewis acids. A certain degree of Lewis acidity is beneficial in activation of metallocene catalyst for polymerization [14, 59, 61]. Both Brønsted and Lewis acidity vary greatly with the nature of the interlayer cation. Irrespective of the type of interlayer cation, maximum Brønsted activity is attained at about 150°C and tends to zero on further heating. Maximum Lewis acidity is achieved after thermal activation at 250–300°C and does not change noticeably up to 500°C [48].

Treatment with alkyl aluminum compounds such as AlR_3, with R representing an alkyl group such as methyl (Me), ethyl (Et) or tertiary isobutyl (i-Bu), can remove the residual water on the clay surface and protect the upcoming coordination catalyst from deactivation, because alkyl aluminum compounds are highly reactive to moisture due to the strength of the Al-O bond (-350 $kJ.mol^{-1}$) versus the Al-C bond (-255 $kJmol^{-1}$) [64].

Complete removal of water from clay surface enquires thermal treatment at elevated temperatures, about 400- 600°C by which the clay structure is partially collapsed and its CEC is decreased. Therefore, even after thermal treatment, alkyl aluminum compounds may be used to passivate the residual water. For the case of organo-clays, the water content decreases considerably after organic modification [65], but it is still large enough in the form of hydrating water, to cause significant catalyst deactivation. High temperature treatment may degrade the organic modification of organo-clays and therefore alkyl aluminum treatment is accompanied with moderate thermal treatment for further reduction of adsorption water. In addition, the alkyl aluminum treatment reacts with the hydroxyl group population on the surface of the clay layers [59, 66, 67]. In addition to water removal from clay surface, treating the clay with alkyl aluminum compounds also changes the nature of hydroxyl groups on the edges of the layers, which are believed to decrease the compatibility between clay and non-polar organic solvents [68, 69].

2.4.1.2 In-Situ Polymerization Techniques

Different in-situ polymerization techniques have been reported for the production of polyolefin-clay nanocomposites [52, 59, 61-63, 67, 70-85]. They can be classified into four main categories:

1. *Polymerization in the Presence of Organoclays*

In this method, the organoclay, the catalyst precursor, and the activator (alkyl-aluminum compounds such as trialkyl aluminum (AlR_3) or alkyl aluminoxanes) are added into the reactor and the polymerization is started by introduction of the olefin monomer. This is the simplest in-situ polymerization method, and only very few reports [62, 74, 80] have been published investigating this method for production of polyolefin-clay nanocomposites. In comparison to the other in-situ polymerization methods, this method has the lowest polymerization activities.

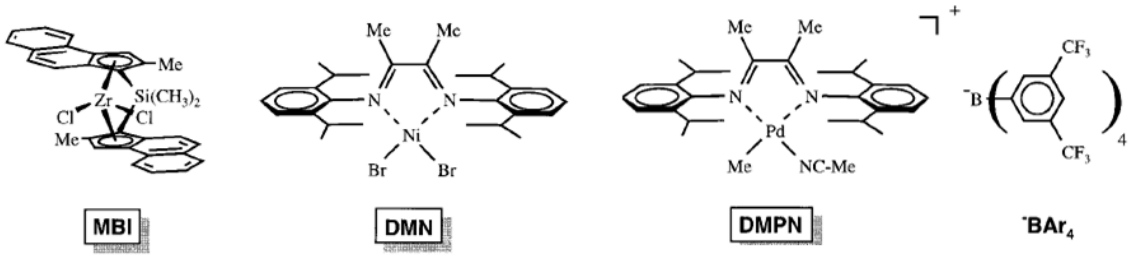

Figure 2.21. Catalyst components MBI, DMN and DMPN/borate [74].

This method was first reported by Heinemann et al. [74] in 1999 for the polymerization of ethylene with different catalysts (MAO-activated zirconocene dichloride, rac-dimethlysilylene bis(2-methyl-benz[*e*] indenyl) zirconium dichloride (MBI) and N,N-bis(2,6-

diisopropylphenyl)-1,4-diaza-2,3-dimethyl-1,3-butadienenickeldibromide (DMN) in toluene and palladium catalyst (DMPN/borate) in methylene dichloride (Figure 2.21) in presence of clays with different types of organic modifications.

The authors reported that the clay exfoliation was better than that achieved by melt mixing. Figure 2.22 compares homogeneous and supported polymerization ethylene uptake curves when MBI was used as a catalyst.

As water present on the clay surface can deactivate the polymerization catalyst [80], the low polymerization activities in this method is supposed to be caused by the remaining water traces on the organoclay surface.

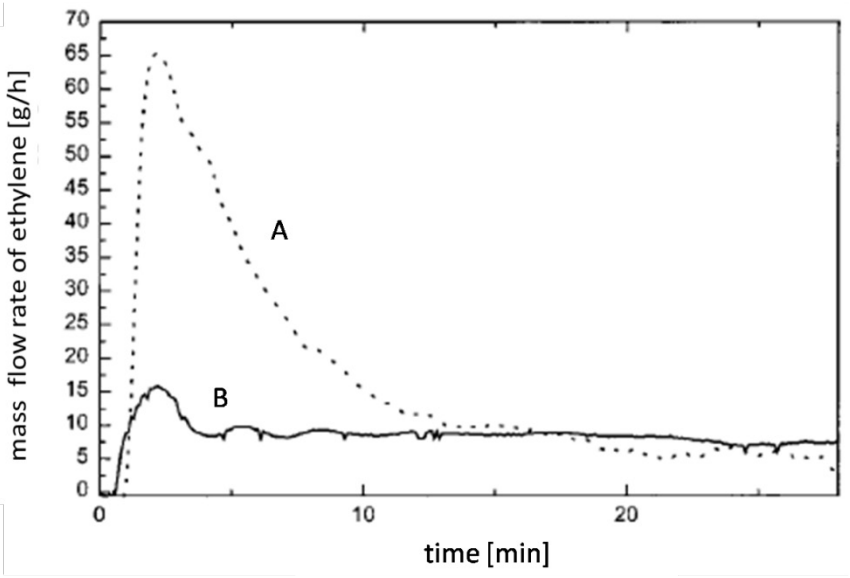

Figure 2.22. Comparison of ethylene uptake for homogeneous polymerization (A) and polymerization in presence of clay (modified with dimethyl stearyl benzyl ammonium chloride-DMDS) (B) with MBI (*T*=48°C *P* = 6 bar; solvent: toluene; total volume in the polymerization vessel: 800 mL; Zr concentration = 1 µmol/L, Al/Zr ratio =4000) [74].

In some reports [70], the organoclay is modified with alkyl aluminum compounds to remove traces of water before being added to the polymerization reactor with the catalyst precursor. Additional alkyl aluminum compounds may or may not be added to the reactor. We represent this category as (Al/clay + cat).

Kuo et al. [80] performed a comparative study between two different in-situ polymerization methods. In Method 1, they contacted an ansa-metallocene catalyst ($Et(Ind)_2ZrCl_2$), MAO, and an organoclay in the reactor and started the polymerization by introducing ethylene. In Method 2, they first treated the organoclay with MAO, impregnated the MAO-treated clay with a catalyst solution, and then used the product to polymerize ethylene. They concluded that in-situ polymerization with Method 2 led to higher catalyst activities and were less

sensitive to clay loading. In addition, a finer and more homogeneous dispersion of polymer/clay particles was obtained when the MAO-treated clay was used. They also reported that extending the treatment time (MAO-treatment: from 1.5 to 2.5 h; catalyst impregnation: from 0.5 to 2 h) had no appreciable effect on the polymerization activity. A TEM micrograph of a polyethylene/clay nanocomposite made with Method 1, shown in Figure 2.23, does not seem to show clay exfoliation.

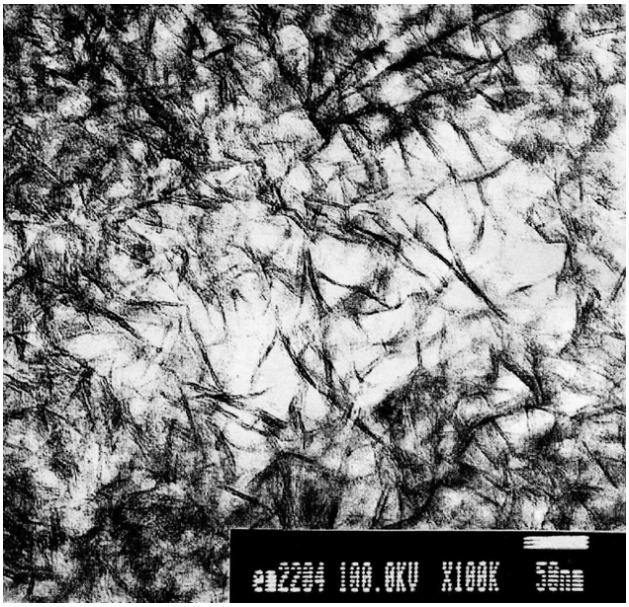

Figure 2.23. TEM micrograph of a thin section of a polyethylene/clay nanocomposite formed using Method 1; 2.4 wt% of clay [80].

In polymerization in presence of MAO-modified clay, especially if additional MAO is added to the reactor, a considerable part of active sites may be formed in solution. Therefore, polymerization may take place in two phases: on the clay-supported sites and with the catalyst molecules in solution. Usually, polymerization with homogeneous catalysts results in higher catalyst deactivation (albeit higher initial polymerization rates) and reactor fouling.

2. *Polymerization with Clay-Supported Catalysts*

In this method, the catalyst is supported onto the clay surface before polymerization. In the first step, the surface of the organoclay is treated with an alkyl aluminum compound, and then impregnated with a catalyst solution. Generally, washing steps are included after each treatment step. Additional alkyl aluminum compound may or may not be used during the course of polymerization. This category represented as (Al/cat/clay) and has been reported by several research groups [62, 63, 70, 72].

Ray et al. [70] treated Cloisite 20A, montmorillonite modified by dimethyl–ditallow ammonium cations containing approximately 65% C_{18}, 30% C_{16}, and 5% C_{14} chains, with a MAO solution, after vacuo-drying at 100°C. The resulting MAO-treated clay was subsequently used for ethylene polymerization in the presence of a late transition catalyst (2,6-bis[1-(2,6-diisopropylphenylimino)ethyl] pyridine iron(II) dichloride) and free MAO in a glass reactor. They compared the result with homogeneous polymerization with the same catalyst in the presence of Cloisite 20A and observed that the supported catalyst was more efficiently exfoliated than when only a mixture of catalyst and clay was used; this comparison lead them to conclude that at least some of the active centers resided within the clay galleries. Inductively coupled plasma (ICP) measurements showed that all MAO and catalyst remained in the solid catalyst after drying.

Lee et al. [63] supported Cp_2ZrCl_2 on Na^+ montmorillonite (MMT) and on an organically-modified montmorillonite, Cloisite 25A (organic modification is shown in Figure 2.24). During the supporting procedure, the clays were treated with modified MAO (MMAO), impregnated with a solution of metallocene in toluene, and washed with toluene after each supporting step. By measuring the Al and Zr loading after each step for Na^+ MMT and Cloisite 25A, the authors concluded that considerably higher Al and Zr loadings were obtained for Cloisite 25A, as shown in Table 2.2.

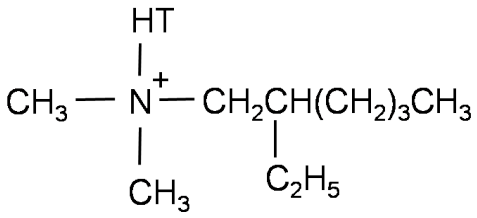

Figure 2.24. Chemical structure of the quaternary ammonium cation used in Cloisite 25A. HT: Hydrogenated tallow (~65% C18; ~30% C16; ~5% C14).

Lee at al. also showed that the modifier content in Cloisite 25A decreased after MMAO treatment from 34 wt% to 4 %, and then to 2.5% after catalyst impregnation. Despite the extraction of about 90 wt% of the ammonium cation during catalyst supporting, X-ray diffraction (XRD) results did not reveal any clay structural collapse due to their removal. In fact, XRD analysis showed that the clay was exfoliated, indicating that the active sites were likely fixed on the surface of Cloisite 25A. XRD investigations, as shown in Figure 2.25, did not reveal any structural collapse due to the removal of organic modifier molecules, and also showed strong evidence of exfoliation, indicating that catalyst molecules were fixed on the surface of Cloisite 25A. As shown in Figure 2.25, the d-spacing peak in Cloisite 25A (25A) greatly deteriorated after MMAO treatment (25A-M) and finally disappeared after complete supporting (25A-MZ).

Table 2.2. Comparison of Al and Zr loading for Na^+ and Cloisite 25A [63].

Sample	Clay (g/L)	Added MMAO (mol/L g)	Supported/ Added MMAO (%)	Added Cp_2ZrCl_2 ($\times 10^4$ mol/L g)	Supported/ Added Cp_2ZrCl_2 (%)
Na^+/MMAO	1.67	0.29	0.65	-	-
25A/MMAO	1.67	0.29	0.80	-	-
Na^+/MMAO/Cp_2ZrCl_2	1.58	-	-	2.1	0.3
25A/MMAO/Cp_2ZrCl_2	1.58	-	-	2.1	14.3

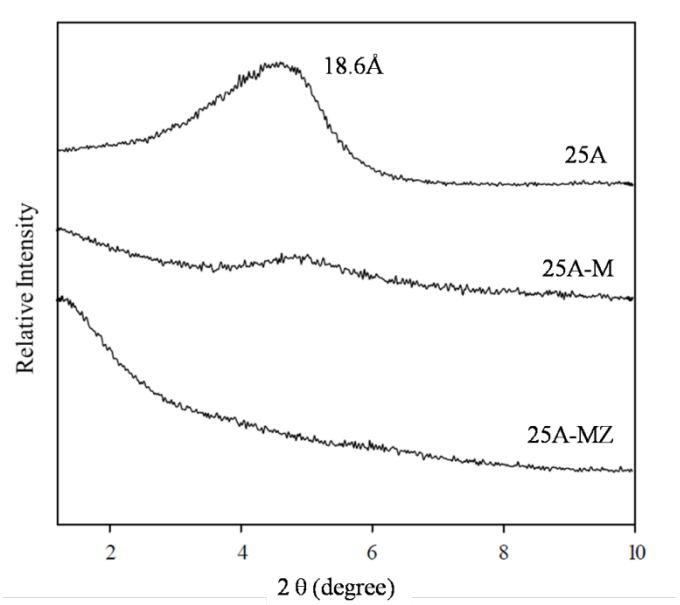

Figure 2.25. X-ray diffraction patterns of Cloisite 25A before supporting (25A), after treatment with MMAO (25A-M), and after catalyst supporting (25A-MZ) [63].

The authors considered this organic modification removal as a result of reactions between oxygen atoms of MMAO and ammonium ions. They also compared three in-situ polymerization methods that were performed under atmospheric pressure of ethylene:

1) Polymerization in presence of MMAO-modified clay (MMAO/clay + catalyst),
2) Polymerization with catalyst supported on MMAO-modified clay (or MMAO/clay/catalyst), with additional MMAO, and
3) Polymerization with catalyst supported on MMAO-modified clay (or MMAO/clay/catalyst), without additional MMAO.

As expected, when Cp_2ZrCl_2/Cloisite 25A was used, high polymerization activities were observed, irrespectively of the polymerization method. The monomer consumption rate with Cp_2ZrCl_2/Cloisite 25A was also higher when MMAO was added during the polymerization. In contrast, the polymerization rate with Cp_2ZrCl_2/Na^+ MMT was very low without the addition of MMAO (Figure 2.26).

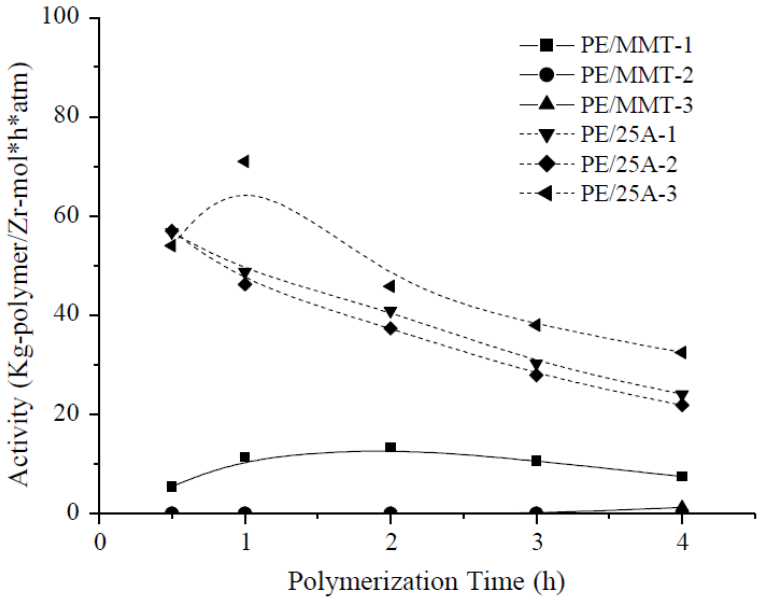

Figure 2.26. Polymerization results using catalyst supported on Na^+ montmorillonite (MMT-MZ: [Al]=5.3×10^{-3} mol/L; [Zr]= 0.2×10^{-5} mol/L) or Cloisite 25A (25A-MZ: [Al]=7.2×10^{-3} mol/L); ethylene pressure: atmospheric; the number at the end of each series represents for the method applied for polymerization

Figure 2.27 shows a TEM image for a polyethylene/clay nanocomposite made with MMAO-treated clay and a homogeneous catalyst with Cloisite 25A, showing the dispersion of the thin clay nanolayers in the polyethylene matrix.

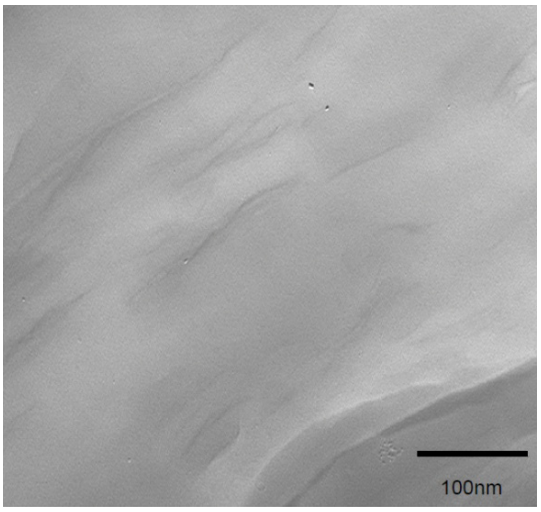

Figure 2.27. TEM image of PE-Cloisite 25A nanocomposite; preparation method: ethylene polymerization (under atmospheric pressure) using MMAO-modified Cloisite 25A and homogeneous metallocene. Polymerization time =2h; 5 wt. % clay.

Dubois et al. [66] used a procedure similar to Lee et al. [63] for Na^+ montmorillonite, hectorite and kaolinite but with a shorter water removal duration (16 h versus 5 days) at higher temperature (105°C versus 40°C). They also tried to deplete the TMA content in the MAO solution by evaporating TMA present in the MAO solution under reduced pressure for two hours, assuming that this would enhance supporting efficiency. The catalysts they investigated were (tert-butylamido) dimethyl (tetramethyl-η^5-cyclopentadienyl) silane titanium dimethyl (CGC) and bis(n-butylcyclopentadienyl) zirconium dichloride. The reaction with MAO and with catalyst was performed for just 1 hour and no washing was done after the impregnation. They performed ethylene polymerization under 70°C and 9-20 bar ethylene pressure. They reported a large amount of MAO needed for high polymerization activities. They also compared polymerization activities of catalyst, when clay was treated with MAO in two different solvents and reported that clay treatment in heptane was more efficient because of surface passivation due to deeper reaction with MAO in toluene and also higher extraction of MAO during washing steps. Although they explained silanol groups on the surface of montmorillonite are responsible for reaction with and fixation of MAO, the observed that kaoilinite, with abundant population of OH groups on its surface, showed to fix lower amount of MAO on its surface after MAO treatment.

3. Alkyl Aluminum-Treated Clays as Catalyst Activator

A number of reports have been published on the olefin polymerization in presence of alkyl aluminum-treated clays as catalyst activator [86-89]. In this work it was tried to replace costly aluminoxane compounds with clay materials.

It is known that the active centre in coordination polymerization is a partly positive- charged. It is also believed that every parameter that can enhance the polarity of polymerization active

center, it can enhance polymerization activity. The reagents that are able to enhance the polarity of active center usually have Lewis Acid characteristics. It was also discussed that by dehydration of clay material, the remaining water molecules on the clay surface will have increased Brønsted acidity. Therefore, dehydration by means of thermal treatment and reaction with TMA removes the harmful water content and creates higher Lewis acidity, useful as a cocatalyst for activation of metallocene catalyst. Usually, during the polymerization MAO or another alkyl aluminum compound is added to the polymerization system, however the clay surface will be the sole location where polymerization is performed. A schematic role of clay surface in activation of polymerization catalyst is shown in Figure 2.28. More details will be discussed in 2.4.1.4.

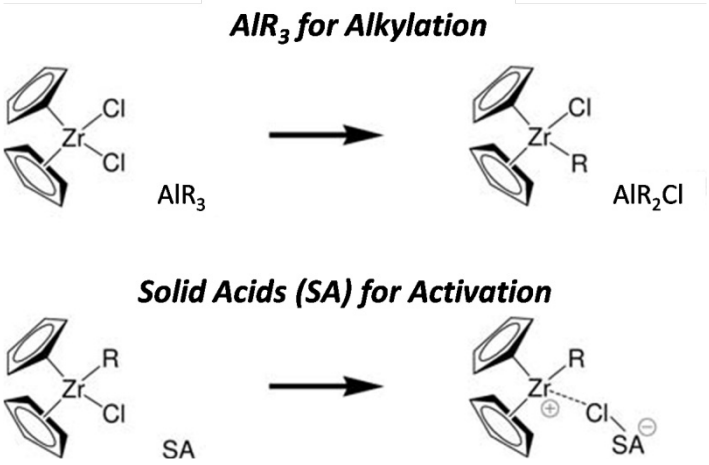

Figure 2.28. Proposed roles of clay surface (SA) as cocatalyst; Alkyl aluminum acts as alkylating agent [14].

4. In-Situ Production of Alkylaluminoxanes

In this method, the water molecules present on the surface of pristine clay are reacted with alkyl aluminum compounds to produce MAO oligomers on the clay surface [61, 81, 90, 91]. The clay modified with in-situ made alkylaluminoxanes can be used directly as a "polymerization cocatalyst", or impregnated with a catalyst solution prior to polymerization. The high temperature thermal treatment to remove surface-bonded water molecules is not required in this case, albeit it has been used by some researchers [61, 90].

Weiss et al. [90] tested kaolinite and montmorillonite as support materials, TIBA and TMA as cocatalysts, and different metallocenes, Cp_2ZrCl_2, Cp_2ZrHCl, Cp_2TiCl_2. They found out that montmorillonite produces supported catalysts with considerably higher polymerization activities than kaolinite. TIBA-treated montmorillonite, in particular, yielded a higher polymerization activity for propylene compared to TMA-treated montmorillonite.

Novoshkonova et al. [81] used two procedures for alkyl aluminum treatment: in the first procedure, they added alkyl aluminums dropwise to the clay until volatile evolution stopped (for instance, when adding TMA, CH_4 will be formed due to the reaction with surface water or

surface hydroxyl groups). In this procedure, the ratio H_2O:alkyl aluminum was shown to be higher than unity. On the second procedure, a ratio of H_2O:alkyl aluminum equal to one was used, and the alkyl aluminum was added in a single step to the clay suspension. The second procedure resulted in higher polymerization activities and extra MAO was not required during polymerization. It was suggested that, in the first procedure, higher degrees of hydrolysis were obtained and fewer alkyl groups were saved for later alkylation of the metallocene; in the second procedure, higher Al:H_2O resulted in partial hydrolysis of the alkyl aluminum compound. In their procedure, they did not mention if they washed the clay after catalyst impregnation. Studies on commercial MAO and MAO formed by this method on the clay surface showed identical behavior during temperature programmed desorption–mass spectroscopy (TPD-MS). The resulting decomposition compounds are consistent with three dimensional structures [5] of the alkyl aluminum compound (alkyl aluminoxane).

In another study, Jeong et al. [61] supported zirconocene dichloride with the same method used by Novoshkonova et al. [81] and investigated the effects of water content and clay surface acidity on ethylene polymerization activity. TMA was added dropwise to the clay suspension and additional TMA was added during polymerization, otherwise catalyst activity was very low and decayed very rapidly as a function of time. Two different acidities were obtained from clays of two different suppliers. Acidity seemed to play a significant role on polymerization activity: for acidic clay samples, irrespective of the water content, polymerization activity was always observed, while no activity was found when the catalyst was supported on basic clay samples.

2.4.1.3 Other Techniques

Despite the fact that organic modifications on the clay surfaces, enhance the dispersion of nanolayers in polymer matrix in in-situ polymerization, it has been found that presence of clay organic modification show some disadvantages on the final physical and mechanical properties [59]; for example they tend to degrade rapidly under the high temperatures existing during polymer extrusion, leading to clay agglomeration and decrease in mechanical properties[92-95]. Scott et al. [59] proposed a techniques to overcome this problem and avoid using clay organic modifiers on the clay structure. By comparing different clay treatments for catalyst supporting and in-situ olefin polymerization, they showed that montmorillonite treatment with mineral acid decreased its original stacking order, as identified by loss of intensity in basal reflection (d(001)) and increased its Lewis acidity. Upon addition of a Ni catalyst ([N-(2,6-diisopropylphenyl)-2-(2,6-diisopropylphenylimino) propanamidato-κ^2-N,N]Ni(η^3-CH_2Ph)), polymerization activity was observed even in the absence of TMA as a passivation agent. They explained their nickel complexes interacting via a Lewis basic site on the ligand backbone with a Lewis acid site on the clay surface was particularly effective at causing polymerization solely on the clay surface and effective dispersion of clay in the polymer matrix, while it did not need any co-catalysts or scavengers for their activation (Figure 2.29).

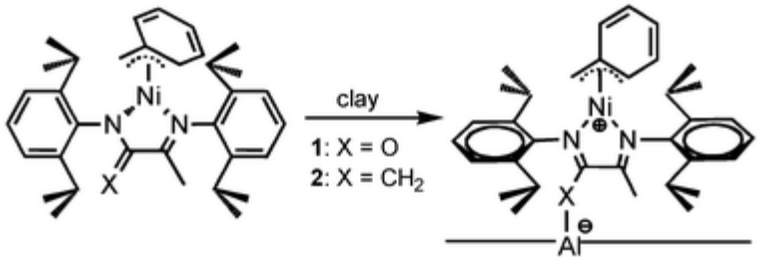

Figure 2.29. Proposed mechanism of for nickel catalysts activation on the surface of clay [59].

On the other hand, when a Cp_2ZrMe_2 solution was added to the acid-treated clay, a very low ethylene uptake was observed and the majority of the gel-like polyethylene was produced by soluble catalyst molecules that were not supported on the clay surface. The authors speculated that the low activity of the clay-supported metallocene was due to severe decomposition of the catalyst in contact with strong Brønsted acidic surface of the clay. Scott et al. also showed that the clay dispersion in the polyolefin matrix is stable during annealing at 170°C for 30 minutes and related this behavior to the high molecular weight and high viscosity at the test temperature (170°C); the retarded structural collapse due to the high molecular weight of the polymer matrix is also mentioned elsewhere [66].

Considering hydroxyl groups as sole opportunities for catalyst supporting on the clay surface, Tang et al. [96] and Wei et al. [79] proposed an indirect supporting method in which a common support such as silica or magnesium dichloride is deposited onto the clay surface from a solution or by the sol-gel method to increase the hydroxyl population on the clay surface, and the catalyst is then fixed on the top of this layer. Tang et al. [96] developed a method in which silica or titanium oxide nanoparticles were fixed on the surface of organically modified clays. This modified clay was subsequently treated with MAO and loaded with a metallocene catalyst. The procedure reported by Wei [79] and Tang [79, 96] was similar: they supported silica nanoparticles on the clay layers using tetraethoxy silane (TEOS), and supported metallocene catalyst after MAO treatment (Figure 2.30).

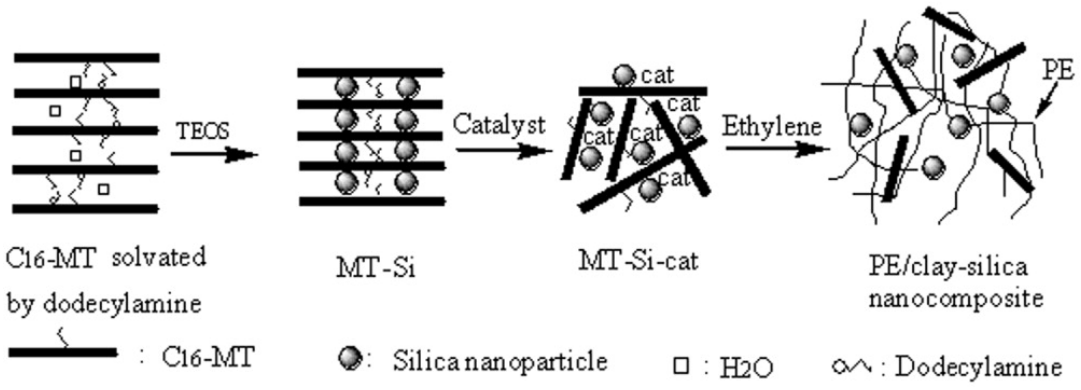

Figure 2.30. Proposed mechanism for formation of MT-Si and the PE/clay-silica nanocomposites [79].

They reported the production of polymer powder with granular morphology and of higher bulk density 0.2 g/cm^3, compared to 0.07 g/cm^3 for homogeneous polyethylene. Although a higher amount of catalyst metal was supported on the silica-treated clay, no improvement in activity was observed. In all heterogeneous cases (with or without silica intermediate) the polymerization activities were lower than those for homogeneous polymerization.

2.4.1.4 Clays as Solid Acid Activators

In many reports on the in-situ polymerization of olefins, the authors depicted clay as a support for polymerization catalyst by providing its Brønsted acid site on the edges of clay layer [75, 76, 85, 90, 97]. Even some reports show trials for increasing the population of hydroxyl groups by acid treatment process [98]

Clays are mainly of acidic nature, or can be activated by acid treatment [5, 14, 58]. Looking back into the classification made in the previous sections for in-situ polymerization methods, one realizes that all methods are related to the fact that clays are intrinsically solid acids able to activate olefin polymerization catalysts. A comprehensive description of solid acids is available by McDaniel et al. [14], where they proposed a new platform for activation of metallocene catalysts that could take the place of expensive MAO or fluoro-organoborate compounds.

During the mid - 1990s it was discovered by the research group at Mitsubishi that certain clays could be calcined and used to activate metallocenes [14, 91]. This activity was attributed to the natural acidity of clays, which were used as cracking catalysts in the past.

One of the main roles of MAO in polymerizations using metallocenes is to function as a Lewis acid, helping to ionize – or at least to polarize – the metallocene compound into cationic like species of the type $[L_2MtCH_3]^+ \cdot [MAO \cdot X]^-$; therefore, in principle, any other Lewis acid may be able to substitute MAO. However, the ability of MAO to alkylate metallocenes and stabilize the resulting cation makes is distinct from other common Lewis acids.

The clay interlayer cations can be involved in ion exchange reactions, changing the clay surface chemistry. Referring to the work of Japanese research groups [99], McDaniel et al. [14] concluded that in using clay as a catalyst support, the polymerization activity can be highly influenced by ion exchange of the natural interlayer cations with other metal cations. Therefore, they proposed that the activation mechanism in clay supported catalyst was significantly different from what is observed in catalyst supported on amorphous silica, by emphasizing a role for the layered structure. They proposed that the high polymerization activity could not be explained by the low population acidic sites on the edges of clay layers but it may come through the ability of clay to conduct ion exchange between the metallocene and the interlayer cations.

In clay materials, positive cations, spaced between the clays sheets, are unusually isolated because they balance negative charges within the interior of the sheets. Thus, the cation is separated from its balancing anion by an “insulating layer” of silica. It is conceivable that

metallocenes are activated by this separation, perhaps by ion exchange, as illustrated in Figure 2.31, where sodium chloride is formed.

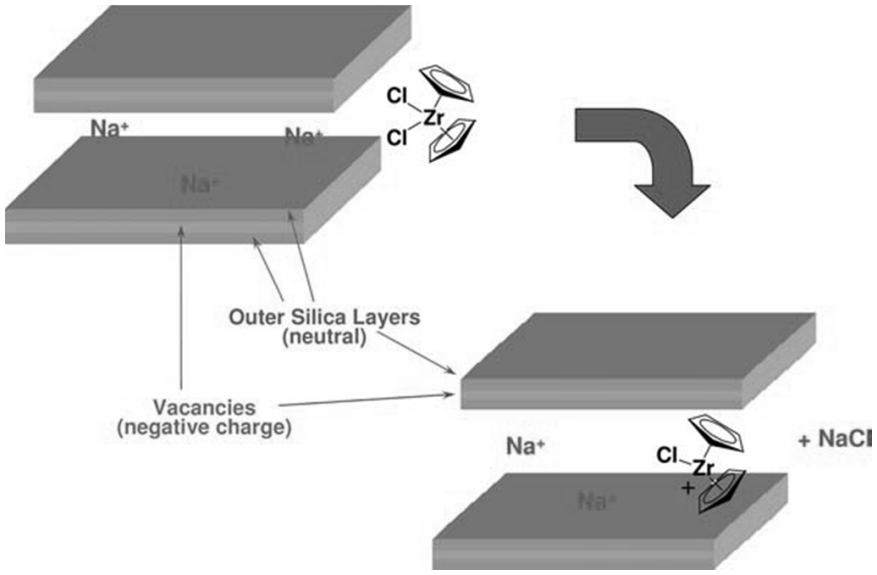

Figure 2.31. Possible mechanism of metallocene activation on clays proposed by McDaniel [14].

As shown in Figure 2.31, in the ion exchange reaction might allow the clay anion and the metallocene cation, as soft ions, and sodium and chloride ions to associate with each other as hard ions. By this mechanism, the high concentration of layer cations, and/or the irreversible nature of the ligand exchange, could help better explain the robust activity in comparison to simple acidic, amorphous, mixed oxides. The ion exchange of metallocenium cation is also discussed by Mariott et al. [100, 101].

2.5 Structure Characterization of Polymer-Clay Nanocomposites

Detailed discussion on the characterization of polymer-clay nanocomposites can be found in several literature reviews [1, 52, 53, 66, 73, 102-104]. The key to understand physical and mechanical properties of polymer nanocomposites and the success of nanocomposite production is to find an insight into nanocomposites morphology and structures. The properties of polymer clay nanocomposites are defined by two major factors, namely i) dispersion and distribution of clay nanolayers within the polymer matrix, and ii) interactions between the polymer chains and nanolayers.

For structural property characterization of nanocomposites, scattering techniques such as X-ray diffraction (XRD) and microscopic techniques such as electron microscopy are mostly employed [104].

XRD is one the most predominant characterization techniques for nanocomposite morphology, offering a convenient and rapid method for initial structural characterization. Changes in the clay structure can be identified using XRD, or specifically wide angle X-ray diffraction [41, 43, 44].

X-rays are a form of electromagnetic radiation, produced when a target metal is bombarded by a stream of fast-moving electrons. X-rays can be diffracted by the atom-bearing planes of crystals. If a beam of X-ray falls on a series of atom-bearing planes at an angle θ, each a distance *d* apart, it follows that for a sharp diffracted beam to be produced.

$$n\lambda = 2d \cdot \sin(\theta) \tag{1.1}$$

where λ is the X-ray wavelength and *n* is an integer.

This phenomenon is observed because a sharp beam is only produced when diffracted rays reinforce each other, that is, when their path length differs by an exact multiple of the wavelength. The above expression is known as Bragg's Law, the integer *n* being the order of the diffraction. The relationship between X-ray diffraction parameters are shown in Figure 2.32. From this figure it can be seen that presence of higher order levels between individual atomic layers will cause higher diffraction intensities.

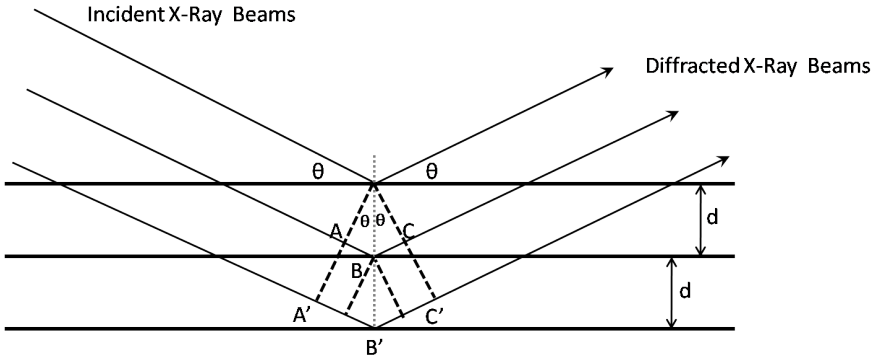

Figure 2.32. Bragg's law equation: 2 θ is the angle between incident and diffracted X-ray beams, *d* is the distance between the atomic planes.

For X-ray characterization, clays are used in the form of a fine powder consisting of a large number of very small crystals, placed into the sample holder which is rotated during exposure to the X-ray beam. A narrow beam of X-rays of known wavelength, produced by bombardment of a copper or other suitable target, is directed onto the specimen, and the diffraction beams are recorded by detectors at different angular positions. Because of the random orientation of the crystals in the sample and the rotation of the sample holder, longer exposure times increase the signal-to-noise ratio. In X-ray diffraction, each set of planes having separation distances *d* may produce a number of peaks on the diffraction pattern for values of *n* from 1 to 3 or higher, but as a rule, the reflections become weaker as the order

increases. Several different sets of d-spacing may be present in any given crystal. The d-spacing for the (0, 0, 1) planes is called the basal spacing, which is characteristics of the relevant mineral and may serve to identify it. For intercalated nanocomposites, in which expansion happened to a finite level, the diffraction peak, depending on the new separation distance in the gallery, will move to new basal position on the graph. Complete exfoliation results in the disappearance of the basal spacing peaks. XRD patterns of different stacking states for three different types of nanocomposites are presented in Figure 2.33.

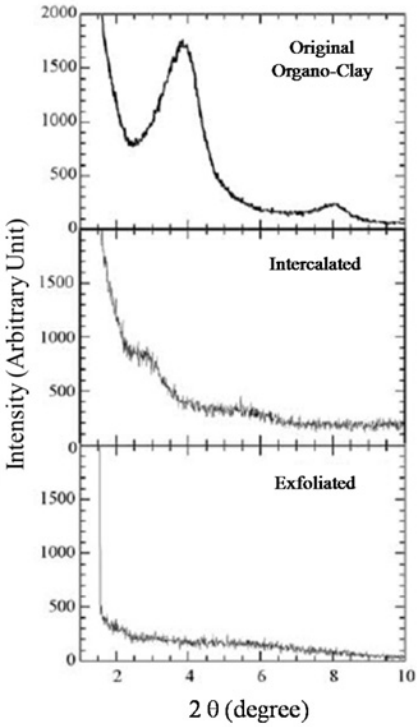

Figure 2.33. Different clay stacking states: (top) original organically modified clay, (middle): intercalated, and (bottom) exfoliated [53].

Despite its convenience, XRD have some limitations. XRD cannot trace the spatial distribution of the silicate layers or any structural non-homogeneity in nanocomposites. Another weak-point of X-ray diffraction analyses appears when the clay content is low: X-ray diffraction is not able to distinguish between different morphologies (exfoliated and intercalated) because of the low diffraction intensity due to the low clay concentration in the composite. These XRD limitations can be overcome by the use of complementary analytical methods such as electron microscopy.

Electron microscopy is a techniques in which images are obtained using electrons and is frequently used when the magnification required is much larger than can be achieved by light microscopes, i.e. particles are smaller that the wavelength of the visible light (< 400 nm). The

emitted electrons with high energy and much lower wavelength (~0.025–0.1Å) compared to that of visible light, allows imaging of the objects in the nanometer scale. Main electron microscopy techniques are available for imaging of nanocomposite structures are scanning electron microscopy (SEM) and transmission electron microscopy (TEM).

Scanning electron microscopy is primarily used in scanning the surface of the samples. The electron gun produces a focused electron beam that scans over the specimen with an electrically conductive surface. For most of the polymers that are electrical isolator, the surface is coated with a thin layer of a conducting material such as gold or carbon. Different signals with varying intensities that are produced by the interaction between the electron beams and atoms are detected by a detector and translated to images.

Usually the samples of nanocomposites are prepared for SEM by means of cold temperature fracture or ultramicrotoming. From polymerization point of view, SEM is useful for characterization of the nascent morphology of the polymer, evaluation of particle break up and in in-situ polymerization technique, similar to what is being done in heterogeneous polymerization.

TEM is another method that is used often in nanocomposites characterization. The popularity of TEM in nanocomposite characterization is due the fact that TEM can detect different clay morphologies and be used to support XRD analysis results. TEM can image the clay internal structure, spatial distribution of the various phases.

Besides its advantages TEM faces some limitations in practice: the preparation of the sample enquires an extremely careful preparation of the sample so that a real representative sample is being examined [105]. Therefore unlike XRD results that represent the average structure for the sample, TEM just shows very small area of the nanocomposite sample, down to few hundred nm^2. Therefore to have reliable information, application of both techniques in structural studies is essential [53, 104].

Chapter 3

A Single-Gallery Model for the In-Situ Production of Polyethylene-Clay Nanocomposites

3.1 Introduction

Coordination polymerization catalysts must be supported on clay for the production of polyolefin-clay nanocomposites by in-situ polymerization. Similarly to other heterogeneous polymerization systems, the break- up of the clay particles and tactoids is an important step in achieving a fine dispersion of clay nanolayers within the polymer phase.

Particle break during olefin polymerization with heterogeneous catalysts is commonly described with the multigrain model (MGM) [25, 32-37]. In the MGM, macroparticles are composed of primary particle agglomerates; the polymerization active sites are assumed to be on the surface of these primary particles. Before using the MGM to describe particle break up with clay-supported catalysts, we need to determine if the layered structure and confined geometries in the clay support influence the polymerization and particle break up. In this chapter, we developed a model for ethylene polymerization in a single clay gallery. This contribution can be seen as an extension to the approach proposed in the MGM.

3.1.1 Clay Structure

The clays commonly used in nanocomposites belong to a structural family known as 2:1 phyllosilicates. Their crystal layers are composed of a central alumina or magnesia octahedral plane fused to two silicate tetrahedron sheets, in a way that the oxygen atoms are part of the silicate tetrahedrons. The total thickness of the crystalline layer is about 1 nm and the lateral dimensions vary from around 300 nm to several micrometers, depending on the type of layered silicate [56]. Isomorphic substitution within the layers, for instance replacement of Al^{3+} by Mg^{2+} or of Mg^{2+} by Li^{+}, causes an imbalance of electrostatic forces that generates residual negative charges on the layer surfaces. The spaces between layers are called *galleries* or *interlayers*. The surface charges within the galleries are counterbalanced by cations such as Na^{+}, which are located inside the galleries (Figure 3.1.). A typical clay particle is composed of many of these layers stacked together in an assembly, called a *tactoid.*

In nature, layered silicates are found as rocks or powders, with micron-sized flaky particles, as shown in Figure 3.2. The typical dimension of clay particles found in powders varies from 10 μm to 0.1 mm. Each of these particles is formed by the agglomeration of smaller, flaky particles with dimensions varying from 1 to 10 μm. These particles will be called macroparticles in our mathematical model. Each macroparticle is itself composed of several tactoids, which are several nanometers thick and up to a micron in lateral dimensions. An electron micrograph of a typical clay agglomerate is shown in Figure 3.3.

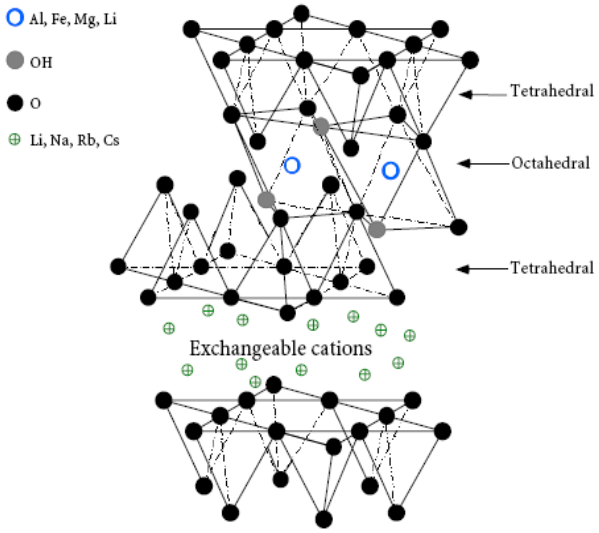

Figure 3.1. Generic structure of layered silicates.

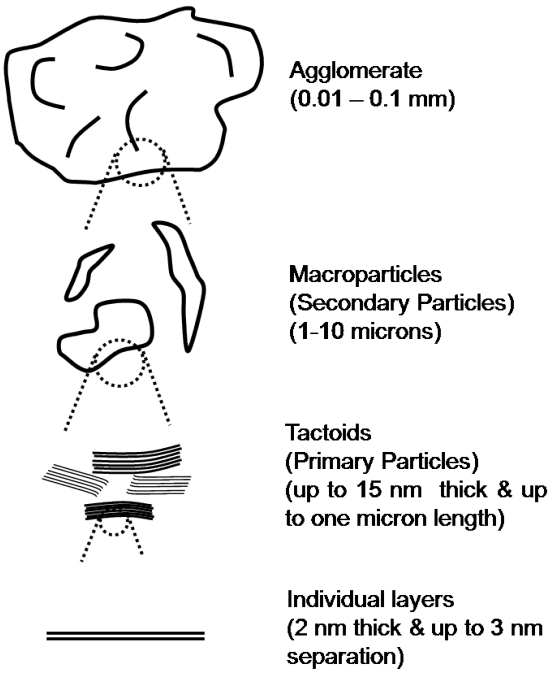

Figure 3.2. Structure of clay particles.

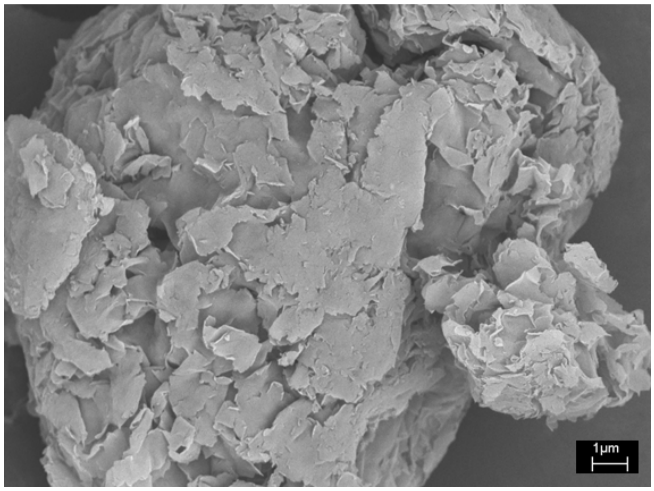

Figure 3.3. SEM image of a clay (montmorillonite) particle.

Usually, clays used in the production of nanocomposites are subjected to an ion-exchange treatment in which small cations are substituted with larger and weaker cations, such as quaternary alkyl ammonium ions, to make them more hydrophobic. The advantages of this treatment is twofold: it increases the compatibility between the clay surface and the polymer phase, and also widens the interlayer spacing between the clay platelets, favoring the diffusion of polymer chains during the intercalation and exfoliation steps.

In the production of polymer-clay nanocomposites, the main objective is to separate and disperse the nanolayers as much as possible in the polymer phase. In the in-situ polymerization technique, the catalyst sites are supported onto the clay surface and polymer is produced directly between the clay galleries; as a consequence, the growing polymer chains separate and disperse the layers within the polyolefin matrix. The active sites are assumed to be fixed on the external and internal surfaces of the clay. Particle break up is needed to expose all available active centers to the polymerization environment and it is, consequently, an essential step during the in-situ production of polyethylene-clay nanocomposites.

The MGM is one of the most commonly used models to describe particle fragmentation and growth in heterogeneous polymerization with coordination catalysts [25]. In this model, each catalyst particle (macroparticle) is considered to be composed of a large number of smaller particles (microparticles). Active sites are supposed to be present on the surface of the microparticles. Monomer molecules diffuse through the pores of the macroparticle and the polymer layer surrounding the microparticles to react on the surface of the microparticle.

When clay is used as a catalyst support, the active sites are not only supported on the surface of the microparticles, but they are also located within the clay galleries. Therefore, before exfoliation takes place destroying the ordered structure of clay nanolayers, monomer has to diffuse through these galleries. Figure 3.4 illustrates a schematic of our proposed model, called *multilayer model* (MLM).

The primary particle (called macroparticle) and secondary particle (called tactoids) are shown on the left side of the Figure 3.4, together with a typical radial profile for monomer concentration ($C \times r$). On the right side, the morphological change of clay layers, from a tightly packed tactoid (before polymerization) to a random distribution of single layers (exfoliation after polymerization), is presented. One assumption is that each primary particle can be composed of more than one tactoid but, for simplicity, just one tactoid is shown for each primary particle in Figure 3.4.

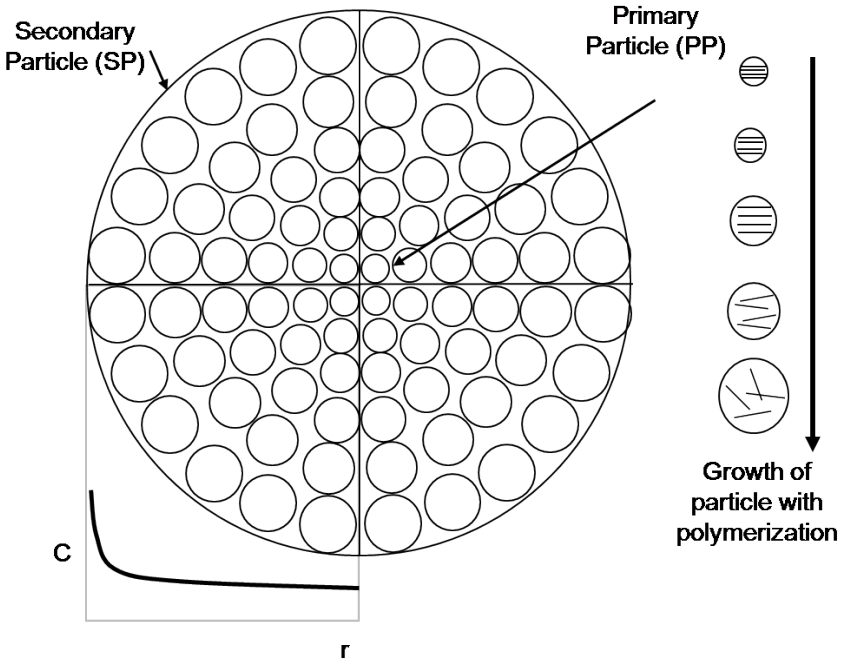

Figure 3.4. A schematic of the multilayer model (MLM).

3.1.2 Interlayer Polymerization: Model Description

The geometry of montmorillonite (MMT) layers is irregular. Our model, however, assumes that the MMT layers can be described as regular discs; this is a reasonable approximation and provides a convenient symmetry for simplifying the model. According to our model, monomer diffuses from the opening to the center of the galleries formed by two parallel discs, and the polymerization occurs on the active sites supported on the internal surfaces of the MMT discs.

Figure 3.5 shows that individual clay layers have radius R and initial spacing h. The catalyst is loaded onto the surface inside the clay galleries with a constant concentration C. The galleries are surrounded by monomer with a concentration M_b, which is equal to the concentration at a given radial position inside the pores of the macroparticles.

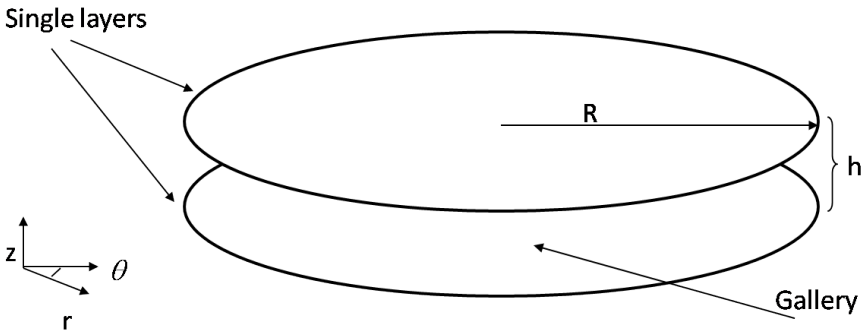

Figure 3.5. Model for a clay gallery.

The partial differential equation for diffusion and reaction in cylindrical coordinates is

$$\frac{\partial M}{\partial t} = \frac{1}{r}\frac{\partial}{\partial r}\left(D\, r\, \frac{\partial M}{\partial r} \right) - R_v \tag{3.1}$$

where M is the monomer concentration inside the gallery, r is the radial position, and D is the effective monomer diffusivity inside the gallery. The term R_v is the polymerization rate per unit volume, given by

$$R_v = k_p \cdot M \cdot C \tag{3.2}$$

where k_p, and C are the propagation rate constant and concentration of active sites in position r and time t, respectively.

Equation (3.1) is subjected to the following boundary and initial conditions

$$M(r = R, t) = M_b \tag{3.3}$$

$$\frac{\partial M}{\partial r}(r = 0, t) = 0 \tag{3.4}$$

$$M(r, t = 0) = 0 \tag{3.5}$$

The following dimensionless variables were defined for the model

$$t' = \frac{t}{R^2 / D} \tag{3.6}$$

and

$$r' = r / R \tag{3.7}$$

$$M' = M / M_b \tag{3.8}$$

Applying these variable transformations, we obtain the following dimensionless equation

$$\frac{\partial M'}{\partial t'} = \frac{1}{r'}\frac{\partial}{\partial r'}\left(r' \frac{\partial M'}{\partial r'} \right) - \frac{R^2}{D} R_v \tag{3.9}$$

Correspondingly, the initial and boundary conditions become

$$M'(r'=1, t') = 1 \tag{3.10}$$

$$\frac{\partial M'}{\partial r'}(r'=0, t') = 0 \tag{3.11}$$

$$M'(r', t'=0) = 0 \tag{3.12}$$

The following additional assumptions were made in the model:

a. The polymerization is isothermal.
b. At the beginning of the polymerization, the catalyst is uniformly distributed on the surfaces inside the gallery.
c. Monomer concentration in the secondary particles (macroparticles) is constant.
d. The catalyst does not deactivate.

In the complete version of the MLM, monomer concentration may vary as a function of radial position in the secondary particle.

The model also assumes that, as polymer is produced on the active sites, it starts filling the interlayer "empty" volume (free volume), finally pushing the clay layers apart when no more free volume is available. A schematic of this mechanism is shown in Figure 3.6. One can envision this process of polymer accumulation inside the galleries as a collection of compressed springs, finally exceeding the forces pulling the layers together and causing them to exfoliate.

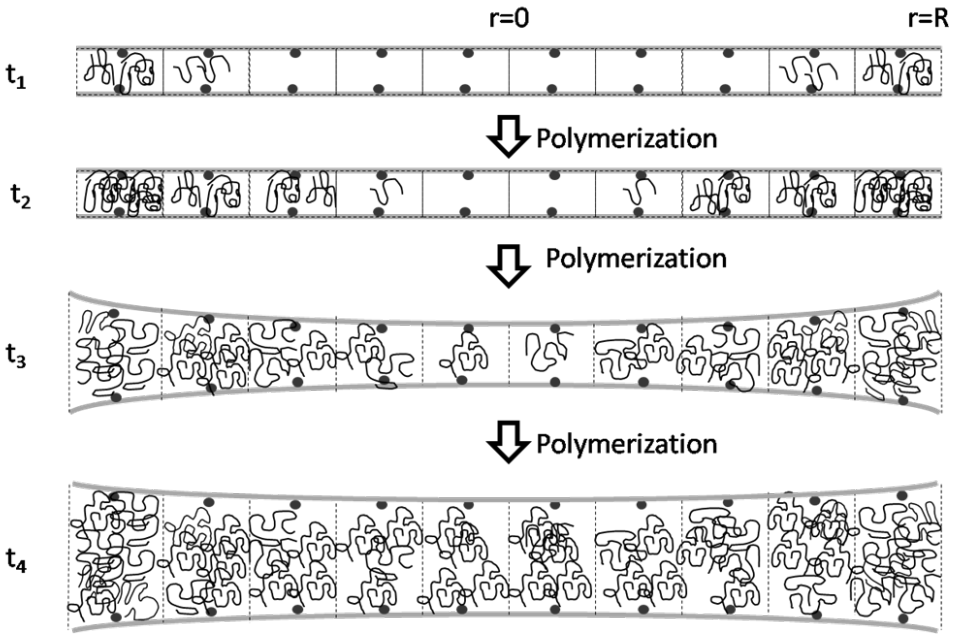

Figure 3.6. Schematic of the expansion mechanism in the gallery due to polymerization. Dots represent active sites and coils are polymer chains.

Equation (3.11) was discretized using explicit finite differences. If we select n as the number of nodal points along the radius r, then the size of each radial element is given by

$$\Delta r' = \frac{1}{n-1} \tag{3.12}$$

The time interval $\Delta t'$ is selected to ensure the solution is stable. For most simulations, $\Delta t'$ is typically in the range of 2.5×10^{-5} to 2.5×10^{-3} seconds.

For internal elements ($1 < i < n$), the finite difference form of Equation (3.9) becomes

$$M(i,t'+1) = M(i,t') + \Delta t' \cdot \left[\begin{array}{l} \frac{1}{r'} \cdot \left(\frac{M(i,t') - M(i-1,t')}{\Delta r'} \right) \\ + \left(\frac{M(i-1,t') - 2M(i,t') + M(i+1,t')}{(\Delta r')^2} \right) - \frac{R^2}{D} K_p \cdot C(i,t') \cdot M(i,t') \end{array} \right] \tag{3.13}$$

For $i = n$ (gallery edge), the monomer concentration is assumed to be M_b

$$M(n,t'+1) = \text{constant} = M_b \tag{3.14}$$

for $i = 1$ (gallery centre)

$$M'(1,t'+1) = M'(1,t') + \left[2 \cdot \frac{(M'(2,t') - M'(1,t'))}{(\Delta r')^2} - \frac{R^2}{D} k_p \cdot C(2,t').M'(2,t') \right] \cdot dt' \tag{3.15}$$

The volume of each element is initially defined as

$$V(1,t'=0) = h(i,t'=0) \cdot A(i) \tag{3.16}$$

where, *A(i)* is the corresponding cross sectional area of the ith element

$$A(i) = 2\pi \cdot r(i) \cdot \Delta r \tag{3.17}$$

For every new $\Delta t'$, new values for M and the amount of polymer produced in every section of the gallery (M_p), are calculated using Equation (3.2), $\Delta t'$ and volume of the element, and are added to the old value

$$M_p(i,t'+1) = M_p(i,t') + R_v \cdot \Delta t' \cdot V(i,t') \cdot \frac{R^2}{D} \tag{3.18}$$

The volume of polymer produced in element i is

$$V_p(i,t'+1) = M_p(i,t') / d_{PE} \tag{2.19}$$

where d_{PE} is the density of nascent polyethylene.

Since we assume that the polymer made in one element stays in that element, the element volume cannot be smaller than the polymer volume. When this happens, the element is expanded to a new volume given by

$$V(i,t'+1) = V_p(i,t'+1) \tag{3.20}$$

and

$$h(i,t'+1) = V(i,t'+1) / A(i) \tag{3.21}$$

and a new catalyst concentration inside the volume is calculated to account for the element volume expansion. The clay volume fraction is calculated with Equation (3.22)

$$V_{clay}(\%) = \frac{V_L}{V_P + V_L} \times 100 \tag{3.22}$$

where, V_L and V_P are volume of a single layer and volume of polymer produced in a single gallery, respectively.

3.1.3 Model Evaluation and Discussion

A sensitivity analysis was performed using the model parameters listed in Table 3.1, with different values for the propagation rate constant (k_p) and the monomer diffusion coefficient (D).

Table 3.1. Model parameters.

Parameter	Value
M_b (mol/cm^3)	1×10^{-4}
C (mol/cm^3)	5×10^{-6}
h (Å)	10
R (nm)	100
d_{PE} (g/cm^3)	0.95

Active site concentration was estimated based on the average catalyst loading ($\overline{C}$), specific surface area of the clay (A_s), and volume of the element. Assuming $\overline{C}$ = 20 μmol/g and A_s = 700 m^2/g, each clay layer will have n_c moles of active centers given by

$$n_c = 2\pi R^2 \cdot \overline{C} / A_s \tag{3.23}$$

The gallery volume is given by

$$V = \left(\pi R^2\right) \cdot h \tag{3.24}$$

We assumed that the initial distance between two layers in the gallery was h_0 = 1.0 nm. The catalyst concentration, C, is then given by

$$C = n_c / V = \left(2\overline{C}\right) / \left(A_s \cdot h\right) \tag{3.25}$$

Assuming that A_s = 700 m^2/g and $\overline{C}$ = 20 μmol/g, we arrive at the following value C = 1.1×10^{-4} mol/cm^3. Arbitrarily assuming that only 5% of the catalyst sites remain active after supporting, C =5×10^{-6} mol/cm^3. The ranges considered for propagation rate constant (k_p) and the monomer diffusion coefficient (D) are shown in Table 3.2. These values are within the range reported in the literature for propylene slurry and gas-phase polymerization[28, 36, 37, 106, 107]. Values for the diffusion coefficient inside the gallery were selected from the MGM literature [26, 28, 34, 36, 37, 107-109].

Table 3.2. Parameter range for sensitivity analysis

Parameter	Value
k_p (cm^3/mol.s)	1×10^{4} - 5×10^{6}
D (cm^2/s)	1×10^{-7} - 1×10^{-4}

Figure 3.7 show how the monomer concentration profile varies as a function of polymerization time. Despite the high propagation rate and low diffusion coefficient values used in this simulation, the monomer concentration gradient becomes practically uniform in less than a minute. As illustrated in Figure 3.8, the clay platelets expand uniformly from the center to the opening of the galleries, with just a slight higher plate separation at the very end of the plates. Figure 3.8 also shows that up to 1 minute, no expansion has happened, because the produced polymer was not enough to completely fill the space between the two parallel discs that define the gallery. Evidently, the time at which the expansion starts depends on the amount of polymer produced (which is a function of the catalyst concentration, monomer concentration, and the propagation rate constant) and the initial gallery spacing. According to the model, after 5 minutes of polymerization, the clay content is 24.1 vol. % and the new spacing distance is about 2.2 times higher than the initial spacing.

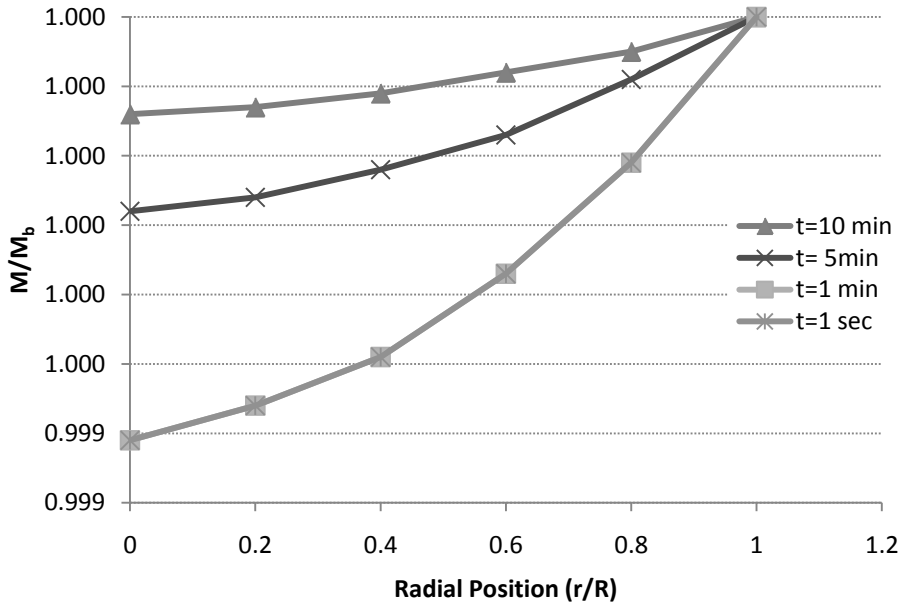

Figure 3.7. Normalized monomer concentration profiles (M/M_b) up to 10 minutes of polymerization. Model parameters: $k_p = 5\times10^5$ cm^3/mol.s, $D = 1\times10^{-7}$ cm^2/s, $h_0 = 1.0$ nm.

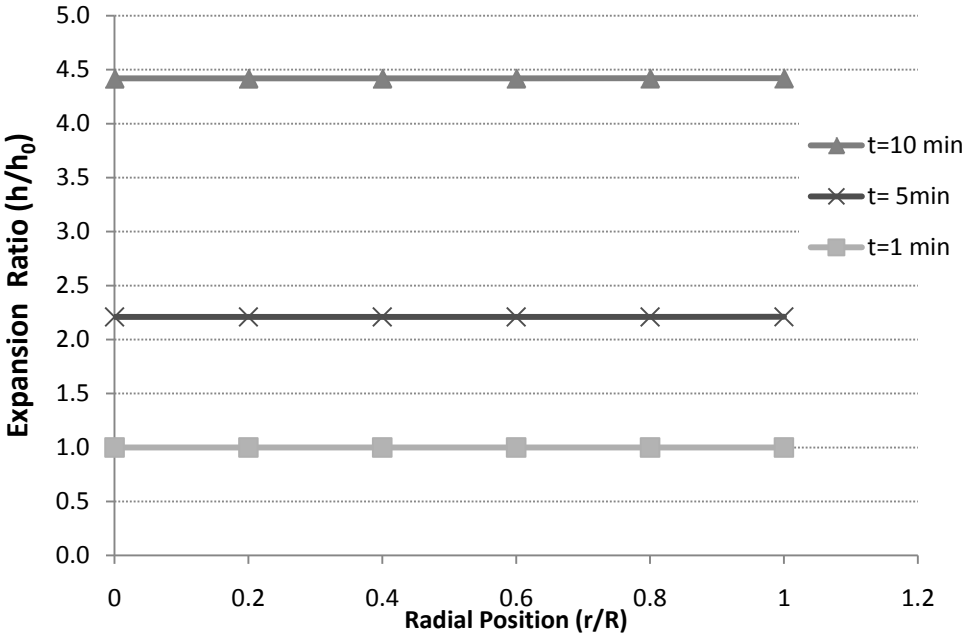

Figure 3.8. Sequences of gallery expansions; Model parameters: $k_p = 5\times10^5$ cm^3/mol.s, $D = 1\times10^{-7}$ cm^2/s, $h_0 = 1.0$ nm; clay contents (vol%) : 61.3 (t=1 min), 24.1 (t=5 min) and 13.7(10 min).

The active site is assumed to be located on the internal surface of the gallery. In classical heterogeneously catalyzed reactions, the competition between pore diffusion and reaction determines the reactant's concentration profile within the catalyst particle. For these systems, a characteristic dimensionless parameter, known as Thiele modulus is useful to quantify the reactant profiles inside the catalyst pores.

Similarly, in the model developed here, the Thiele modulus can be used to investigate the importance of diffusivity and polymerization rate on the expansion behaviour of single clay galleries.

For this system, the Thiele modulus is defined as

$$\phi = R\sqrt{\frac{k_p \cdot C}{D}} \tag{3.26}$$

Considering the variability of D, k_p, and C (Table 3.2) and assuming a variations of catalyst concentration between 5×10^{-6} and 2.5×10^{-5} mol/cm^3 (five times higher than current concentration), the Thiele modulus, ϕ, can be varied between 2.2×10^{-4} and 0.5. For the previous simulation, with results shown in Figure 3.7 and Figure 2.8, the Thiele modulus equals 0.05.

Figure 3.9 shows that highest possible Thiele modulus, ø, in this model only slightly affected the monomer concentration profile inside the gallery and as shown in Figure 3.10, the variations of Thiele modulus have not resulted in a significant difference in basal spacing at different radial positions.

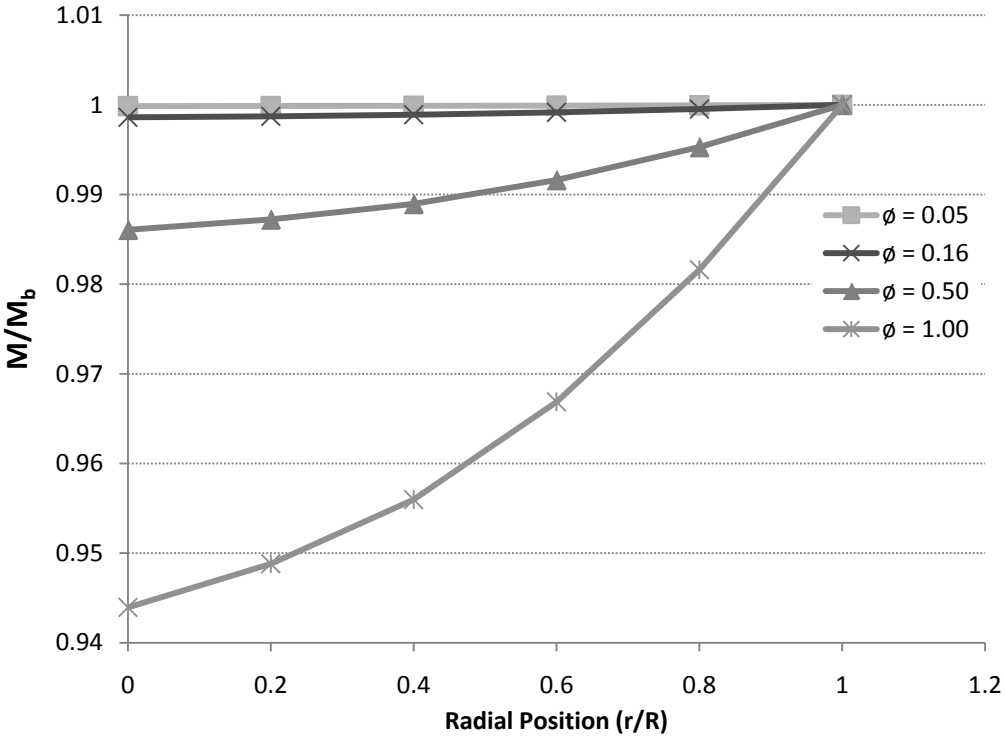

Figure 3.9. Effect of Thiele modulus (ø) on the monomer concentration profile inside the gallery; kp=5×10^5; t=10 min.

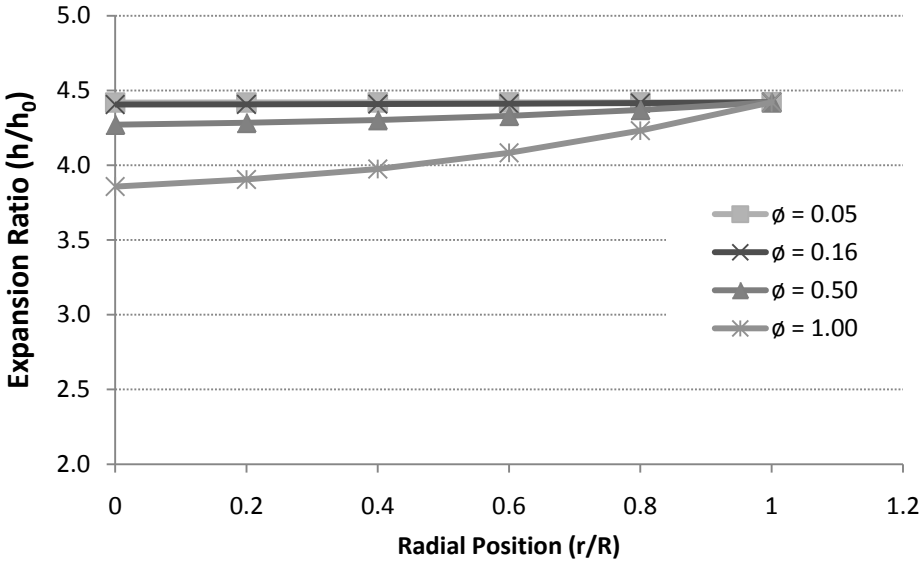

Figure 3.10. Effect of Thiele modulus (ø) on the monomer concentration profile inside the gallery; kp=5×10^5; t=10 min.; clay content = 14.2 (ø=1.0), 13.81 (ø=0.5), 13.68 (ø=0.16) and 13.67(ø=0.05).

From the simulation results, it appears that within the practical ranges for propagation rate constants (k_p), monomer diffusivity (D) and catalyst concentration inside individual galleries (C), there would be no diffusion limitation inside the gallery and the expansion would occur uniformly.

3.2 Macroparticle Model: MLM

The interlayer polymerization model can be implemented into the macroparticle model to generate the multilayer model (MLM). As shown in Figure 3.4, the macroparticle is composed of several concentric spherical shells, each concentric shell containing N_T tactoids (which may varies from shell to shell), and each tactoid contain N_L clay layers. Due to the non-uniform radial expansion of the radial shells in the macroparticle, the radial positions are updated during the simulation. Furthermore, as the particle growth may not be uniform, differential mass balance equations are defined for the macroparticle and solved using explicit finite differences.

The variation of monomer concentration $M_{s,i}$ in a given volume of $V_{s,i}$, located in radial position of $r_{s,i}$ in the macroparticle is obtained by

$$\left[M_{s,i}(t+\Delta t)-M_{s,i}(t)\right]=\left(D_{s,i+1}\cdot A_{s,i+1}\cdot\frac{M_{s,i+1}-M_{s,i}}{r_{s,i+1}-r_{s,i}}-D_{s,i}\cdot A_{s,i}\cdot\frac{M_{s,i}-M_{s,i-1}}{r_{s,i}-r_{s,i-1}}\right)\cdot\Delta t-\frac{MP_{t,i}}{V_{s,i}} \tag{3.27}$$

where $D_{s,i}$, $A_{s,i+1}$ and $A_{s,i}$ are diffusion coefficient, external and internal surfaces in the ith shell in the macroparticle. Assuming a uniform concentration active sites within the spherical shell and that the geometries of the layer in the tactoids within the macroparticle are similar, the total mass of polymer produced in the ith sell would be

$$MP_{t,i}=N_{T,i}\cdot\left[\left(N_{L,i}-1\right)\cdot MP_{g,i},+MP_{s,i}\right]=R_{v,i}V_i \tag{3.28}$$

where, $N_{T,i}, N_{L,i}$, $MP_{g,i}$, $MP_{s,i}$ are the number of tactoids, number of layers in a single tactoid, moles of polymer produced inside clay layers, and moles of polymer produced on the external surfaces of the tactoids, all in the ith shell with volume of V_i respectively. $MP_{g,i}$, $MP_{s,i}$ are calculated according to Equations

$$MP_{g,i}=k_p\cdot C_{g,i}\cdot M_{s,i}\cdot V_{g,i}.\Delta t \tag{3.29}$$

and

$$MP_{s,i} = k_p \cdot n_{c,i} \cdot M_{s,i} \cdot V_{s,i} . \Delta t \tag{3.30}$$

The boundary condition at the surface of the macroparticle, at $r_s = R_s$, is given by

$$D_s \frac{\partial M_s}{\partial r_s} = K_s \left(M_{b,s} - M_s \right) \tag{3.31}$$

where K_s is the mass transfer coefficient in the external film around the macroparticle and $M_{b,s}$ is the monomer concentration in the polymerization medium. Assuming that K_s is large enough, Equation (3.31) is simplified to Equation (3.32)

$$M_s \left(r = R_s \right) = M_{b,s} \tag{3.32}$$

The boundary condition at the center of the macroparticle, at $r_s = 0$ is

$$\frac{\partial M_s}{\partial r_s} = 0 \tag{3.33}$$

The initial condition in the macroparticle is assumed to be:

$$M_s \left(r_s, t = 0 \right) = 0 \tag{3.34}$$

Table 3.3 shows the model parameters used to simulate the polymerization at the macroparticle level. As it was shown earlier, due to small geometry of the gallery, its simulation parameters such as diffusivity has no tangible effect on the course of simulation and therefore they are not evaluated here.

The differential equation from Equation (3.27) is solved with the explicit finite difference method, similar is to what was used in the single gallery model. After each Δt time sequence, the polymer produced from the external surfaces of the tactoids increased the volume of the shell. The polymer produced inside the galleries did not affect the shell volumes until the galleries started to expand.

Before interlayer expansion:

$$V_i = V_i + \frac{N_{T,i}.MP_{s,i}}{d_{PE}} \tag{3.35}$$

After interlayer expansion:

$$V_i = V_i + \frac{N_{T,i}.\left(\left(N_{L,i}-1\right)\cdot MP_{g,i},+MP_{s,i}\right)}{d_{PE}} \tag{3.36}$$

Accordingly, the new values of the radii of the shells were then calculated by the new values of the shell volumes.

The monomer concentration profile in the macroparticle and the corresponding interlayer spacing after 10 minutes are shown in Figure 3.11 . The clay content was calculated to be 6.3 vol %. The layer expansion over the macroparticles radial positions is quite uniform. The monomer concentration profiles and corresponding expansion profiles in the macroparticle are shown for different polymerization times in Figure 3.12 and Figure 3.13, respectively. As can be observed, by knowing the initial macroparticle radius of 10 μm, the particle starts to noticeably grow after 3 min polymerization. By this time, as can be learned from Figure 3.13, the interlayer spaces have been filled completely and from that point on, the polymer production will result in expansion of macroparticle together with polymer fraction made at external surfaces.

Table 3.3. Macroparticle model parameters

$M_{b,s}$ (mol/cm^3)	5×10^{-4}	D_g (cm^2/s)	1×10^{-7}
C_g (mol/cm^3)	5×10^{-6}	D_s (cm^2/s)	5×10^{-5}
h (Å)	10	ε	0.5
R (nm)	1×10^{2}	d_{PE} (g/cm^3)	0.95
R_s (μm)	10	K_p (cm^3/mol.s)	1×10^{5}

C_g: catalyst concentration inside galleries; D_g: diffusivity inside gallery; D_s: diffusivity within macroparticle; ε: porosity; R_s: macroparticle radius;

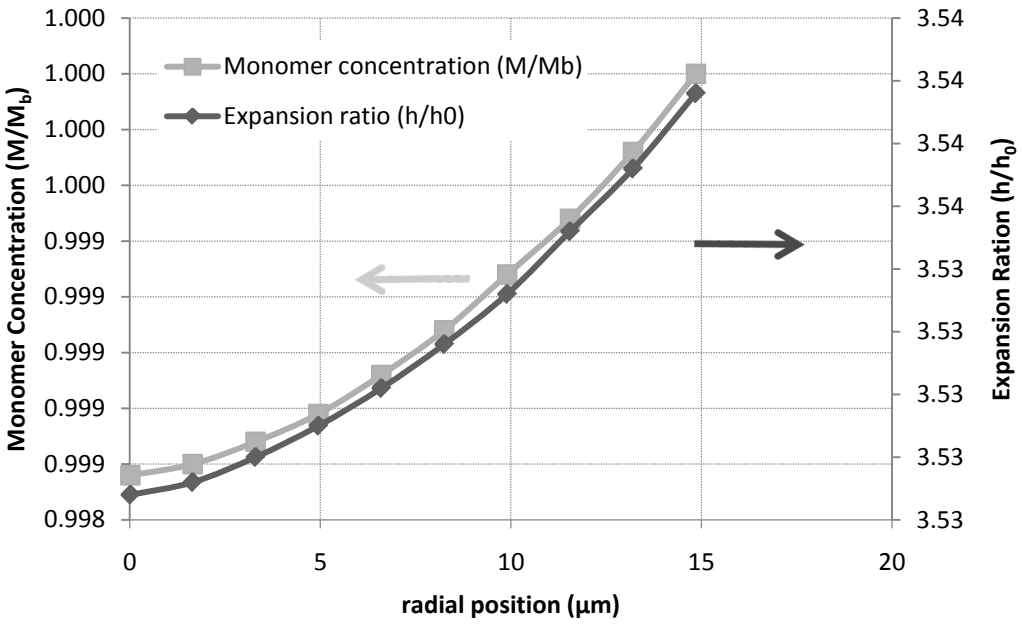

Figure 3.11. Monomer concentration profile and gallery expansion profile inside the macroparticle after 5 minutes polymerization; clay vol. %= 6.2; model parameters summarized in Table 3.3

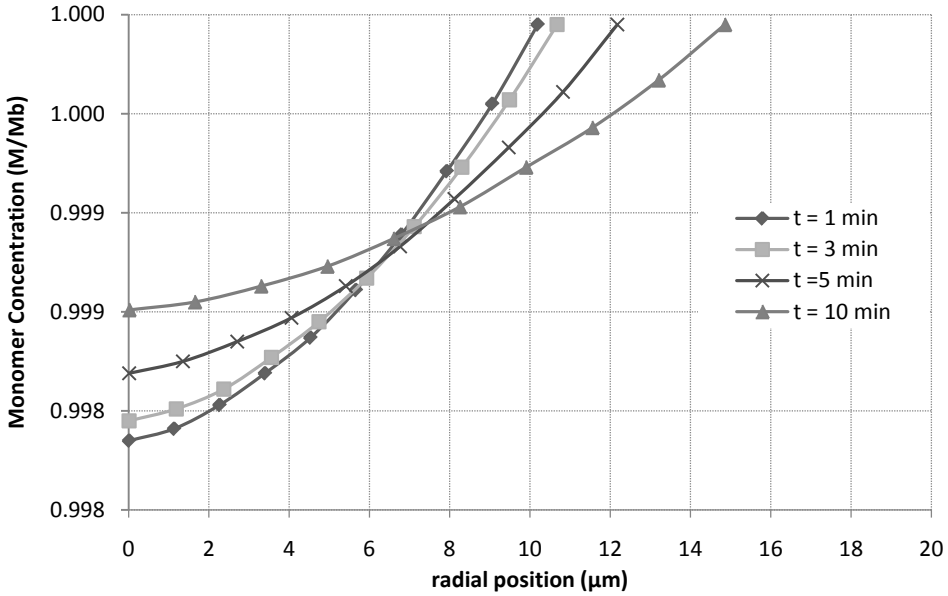

Figure 3.12. Radial profiles of monomer concentration during particle growth after different polymerization times.

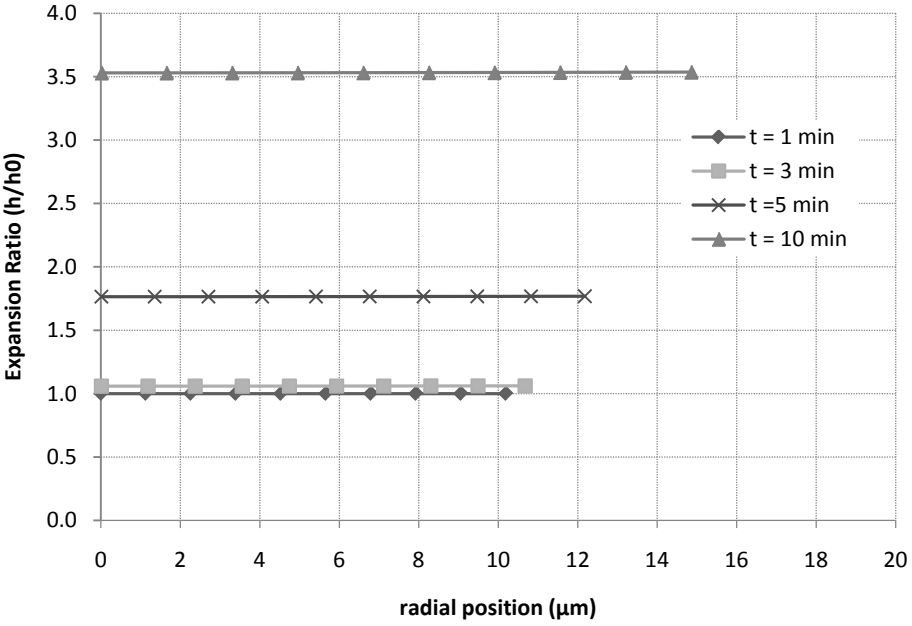

Figure 3.13. Interlayer spacing at different radial positions of macroparticle for different polymerization times; the clay vol.%: 40.0(1 min), 18.2 (3min), 11.7 (5 min) and 6.2 (10 min).

According to the macroparticle model, under practical polymerization conditions and assuming uniform distribution of active sites on the clay layers and within the galleries, a uniform gallery expansion in different positions of the macroparticle is observed.

Regarding the limited supply of the active site precursors during supporting, uniform distribution of active site is provided only if all clay surfaces are accessible in the first moments of supporting. In case of diffusion limitation for the catalyst precursors during catalyst supporting, the external surfaces will have higher concentrations of polymerization active sites. Theoretically, the catalyst can be loaded on the clay surface as high as its cation exchange capacity, ca.1 mmol/g or 1000 μmol/g. Comparing the assumed 20 μmol/g catalyst supply in this work to the theoretical capacity of clay proposes that the assumed clay loading would be majorly resided on the external surfaces in case of diffusion limitation. And the catalyst concentration in the galleries would be considerably lower than what is assumed for homogeneous distribution. Consequently, polymerization rate and expansion will not be achieved in desired clay loading. For example if the catalyst concentration inside the galleries decreases by half, and instead the minority external surfaces (e.g. 10% total surfaces) receive the rest of active sites, the same level of expansion in homogeneous case will be achieved in a twice longer time at which, the clay loading will be also half.

3.3 Conclusions

In order to use multigrain model (MGM), we created a reaction-diffusion model to simulate the monomer diffusion into gallery spacing and intercalative polymerization. By assuming uniform distribution of polymerization active sites on the clay individual layers, the model predicts achieving uniform monomer concentration profile in the beginning of the polymerization reaction, even under extreme conditions, inside the gallery and therefore it is possible to assume a uniform polymerization rate under normal conditions in the macroparticle model. The macroparticle modeling results showed that the under normal conditions and some simplifying assumptions, a uniform expansion of galleries is achieved. To modify this model into a more practical model, experimental observations and data are required.

3.4 Nomenclature

$A(i)$ Surface area of the ith element in the gallery

A_s Specific clay surface area in the macroparticle

C Catalyst concentration inside the gallery

$\overline{C}$ Average catalyst loading on the clay surface

C_g Active site concentration in the gallery

D Effective monomer diffusivity inside the gallery

D_g Diffusion coefficient in the gallery

$D_{s,i}$ Diffusion coefficient in the ith shell in the macroparticle

D_s Diffusion coefficient in the macroparticle

K_s Mass transfer coefficient in the external film around the macroparticle

M Monomer concentration inside the gallery

M' Normalized monomer concentration in the gallery

$M_{b,s}$ Monomer concentration in the polymerization medium

$MP_{g,i}$ Moles of polymer produced inside clay layers, in the ith shell in the macroparticle

$MP_{s,i}$ Moles of polymer produced on the external surfaces of the tactoids, in the ith shell in the macroparticle

$MP_{t,i}$ Total mass of polymer produced in the ith shell in the macroparticle, at time *t*

M_b Bulk monomer concentration around the gallery

$M_p\,(i,t)$ Mass of polymer in the ith element of the gallery at time *t*

$M_{s,i}\,(\mathrm{t})$ Monomer concentration in the ith element of the macroparticle at time *t*

$N_{L,i}$ Number of layers in a single tactoid in the ith shell of the macroparticle

$N_{T,i}$ Number of tactoids in the ith shell of the macroparticle

R Radius of a clay single layer

R_s Radius of the macroparticle at time *t*

R_v Polymerization rate per unit volume in the gallery

V Gallery volume

$V(i,t)$ Volume of the ith element in the gallery, at time *t*

V_L Volume of a clay single layer

V_P Volume of polymer produced in the single gallery

V_{clay} Volume fraction of clay (in percent)

$V_p\,(i,t)$ Volume of polymer in the ith element the gallery at time *t*

$V_{s,i}(\mathrm{t})$	Volume of the ith element in the macroparticle at time *t*
d_{PE}	Density of nascent polyethylene
h_0	Initial interlayer spacing in the gallery
$h(i,t)$	Separation distance between the layers in the ith element in the gallery space, at time *t*
k_p	Propagation rate constant
n	Number of nodal points along the radius of the gallery
n_c	Number of moles of active centers on the surface of individual clay layers
r	Radial position in gallery
r_s	Radial position in the macroparticle
r'	Normalized radial position in the gallery
t	Time
t'	Normalized time
$\Delta r'$	Normalized size of radial element
$\Delta t'$	Normalized time interval
$ø$	Thiele modulus
ε	Macroparticle porosity

Chapter 4

Effect of Organic Treatment on the Effectiveness of Montmorillonite as a Catalyst Support for Metallocenes

4.1 Introduction

A considerable number of papers and patents have been published on in-situ polymerization for the production of polyolefin/clay nanocomposites [59, 61-63, 66, 70-75, 79-81, 90, 91, 96, 110, 111]. In the majority of these publications, the main objective has been either the intercalation of the polymer between the clay layers, or the exfoliation of clay with consequent dispersion of individual clay nanolayers into the polymer matrix.
The two major challenges for preparing polyolefin/clay nanocomposites by in-situ polymerization are related to the clay water content and compatibility mismatch between the clay and the organic phase; these difficulties have been addressed by different approaches, including organic modification of the clay surface with phosphonium [71] and ammonium compounds [63, 66, 74, 75, 79, 96, 111], to make the clay surface less hydrophilic and to increase their interlayer spacing, thus facilitating the intercalation of catalysts, cocatalysts, monomers and solvents. It has been reported that organic modification of clay has a considerable impact on the success of in-situ polymerization [63, 112].
In another technique, water molecules present on Na^+ MMT can be used for the partial hydrolysis of TMA and other alkyl aluminums, making compounds with structures similar to MAO that can activate the polymerization catalyst without requiring the addition of MAO to the reactor [61, 81, 90, 91]. This approach leads to considerably less reactor fouling and improved particle morphology.

In the present study, we compared several commercial organoclays with Na^+ MMT to find the effect of organic modification type on their performance as catalyst supports for ethylene polymerization. We have modified these organoclays and Na^+ MMT with TMA before catalyst impregnation, without using MAO during the supporting stage or during the polymerization. These novel clay-supported metallocenes were tested for ethylene polymerization under fixed polymerization conditions. The criteria we adopted to decide if a given organoclay was adequate as a metallocene support were:

1) High polymerization activity
2) Acceptable polymer morphology
3) Effective intercalation and exfoliation
4) Simple supporting procedure

4.2 Materials& Methods

4.2.1 Materials

Sodium montmorillonite (MMT) and six commercially available MMTs with different organic modifications, called Cloisite 10A, 15A, 20A, 25A, 30B and 93A, were purchased from Southern Clay. These Cloisites are MMTs modified with different types and/or concentrations of ammonium cations. The chemical structures of the clay modifiers and their concentrations are shown in Figure 4.1 and Table 4.1 , respectively. In the case of Na^+ MMT, no surface modifier was used.

Bis-cyclopentadienyl zirconium dichloride (Cp_2ZrCl_2; Aldrich) was used as the metallocene catalyst for all experiments. Toluene and n-hexane (reagent grade; Merck) were dried using molecular sieves 3A and 4A. Freshly distilled toluene was used as diluent in the polymerizations. Trimethyl aluminum (TMA, 2M in toluene), triisobutylaluminum (TIBA, 1M in hexane) and methylaluminoxane (MAO, 10 wt. % in toluene) were also purchased from Aldrich.

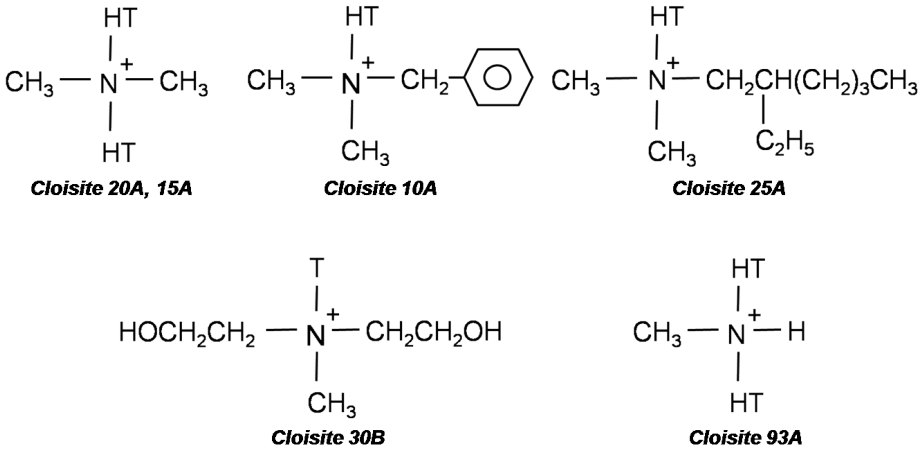

Figure 4.1. Different Cloisite modifiers; T stands for Tallow (~65% C18; ~30% C16; ~5% C14).

Table 4.1. Cloisite specifications provided by Southern Clay.

Cloisite	Modifier Concentration (meq/100g clay)	Ion Pair	Moisture Content (Wt %)	Basal Spacing (Å)
Na^+	92-95	None	4-9%	11.7
10A	125	Chloride	< 2%	19.22
15A	125	Chloride	< 2%	31.5
20A	95	Chloride	< 2%	24.2
25A	95	Methyl Sulfate	< 2%	18.6
30B	90	Chloride	< 2%	18.5
93A	90	HSO_4^-	< 2%	23.6

4.2.2 Catalyst Supporting

One gram of each clay type was suspended in dried solvent inside a Schlenk tube under vacuum for 2 hours. A mass of 2.65 g TMA solution (2.0 M solution in toluene) was added to the Schlenk tube and stirred overnight. The TMA-treated clay was then washed three times with dried toluene before the addition of 1.85 g of Cp_2ZrCl_2 solution (10 μm/g). The Cp_2ZrCl_2/clay system was stirred overnight. The supporting process was completed by washing the slurry three times with dried solvent. Washings were performed by adding fresh solvent, stirring for 5 minutes, and allowing the clay sediment to settle down, followed by removing the supernatant solvent. No drying was performed at the end of the last washing step. The supported catalysts were stored as slurries.

4.2.3 Low-Pressure Polymerization

Catalysts supported on different Cloisites were used to polymerize ethylene at low pressure to find the best organoclay (according to our criteria) for producing polyethylene/clay nanocomposites by in-situ polymerization. In this series of experiments, toluene was used as diluent during the supporting procedure. Polymerizations were performed in approximately 75 mL toluene in the same Schlenk tube used for catalyst supporting for 20 minutes under atmospheric pressure of ethylene, room temperature, and continuous supply of ethylene, with no addition of MAO to the polymerization system.

4.2.4 High-Pressure Polymerizations

High pressure polymerizations were performed to confirm the results from low pressure experiments, to compare Na^+ MMT and Cloisite 93A, and to study the effect of the organic modification on the supporting performance and polymerization activity. High pressure polymerizations were performed for 1 hour in a 300-mL Parr autoclave reactor at 85^{o}C, 5 bar

ethylene pressure, using toluene as diluent, and 0.25 g TIBA solution (1.0 M solution in n-hexane) as scavenger.

The polymerization reactor is equipped with a PI-type temperature controller which controls the temperature by means of a heating jacket around the vessel and a cooling coil inside the reactor. For polymerization, the reactor was heated up to 150°C and subjected to cycles of vacuum and purges with high-purity nitrogen. After purge cycles the reactor was cooled down to about 40°C before the catalyst transfer step. About half of 150 mL diluent was used to transfer the TIBA into the reactor, using a cannula, followed by stirring for 5 minutes to complete the neutralization of the reactor medium. The remaining half of the solvent was transferred to the reactor with the slurry containing the supported catalyst. After all reagents were transferred to the reactor, stirring was restarted and the temperature was allowed to reach its set point. Finally, ethylene was fed to the reactor under a given pressure to start the polymerization reaction. The polymerization was stopped by reducing the ethylene pressure and precipitating the reactor content into acidified ethanol (5 wt. % HCl). The polymer then was further washed with ethanol, filtered and dried in the oven (80°C) for one day.

4.2.5 Material Analysis

Transmission Electron Microscopy (TEM)

TEM imaging was conducted using a Philips CM12 TEM machine at 120kV, with LaB6 Filament, and recorded by Gatan Orius CCD camera. The magnification ranged from 15,000 to 50,000 times. This instruments is located in Brockhouse Institute for Material Research (McMaster University, Hamilton, Canada).

TEM Sample Preparation

The samples in form of powder were dried in the oven at 80°C and atmospheric pressure for 12 hours, then embedded in the ultra low viscosity grade epoxy resin from “Ladd Research”, a combination of dimethylamino ethanol, DER 736, ERL 4221 (a cycloaliphatic epoxide), and n-octenyl succinic anhydride with ratio of 0.2:0.75:5.0:10.5, and cured at 70°C for eight hours. The resin block containing the embedded powder sample was trimmed in the ultramicrotome (Leica EM UC6, located in the Chemical Engineering Department, University of Waterloo), using a trimming diamond knife (DiATOME Cryotrim 45, size 3 with knife angle of 35°) to provide samples with smooth surfaces with dimensions of 0.3 mm by 0.3 mm. The final cut was performed using diamond knife (DiATOME ultra 35°, size 3 with knife angle of 35°), with floating water on top, operated at a speed of 2.5 mm/sec, producing layers with 40-90 nm thickness, which were then collected from the water surface onto TEM cupper grids.

For the TEM analysis of clay or catalyst supported on clay particles, their dilute dispersions (with concentration of about 1.0g/L) were prepared in toluene and dropped onto the TEM cupper grid, and then dried up inside the oven at 80°C for 12 hours.

Scanning Electron Microscopy (SEM)

SEM images were provided with Leo 1530 filed emission SEM (located in Chemistry Department, University of Waterloo) at 15kV using a back scatter detector. For sample preparation, a very small quantity of dried sample was placed on the SEM stage on a double sided adhesive carbon tape and coated with 15-20 nm-thick gold layer using a Denton Deskjet II DC gold sputtering machine. In this technique, images with magnifications between 60 times and 20,000 times were obtained.

X Ray Diffraction Analysis (XRD)

All powder x-ray diffraction measurements were performed using the INEL XRG 3000 powder diffractometer with position sensitive detector and Cu $K\alpha_1$ radiation (located in Chemistry Department, University of Waterloo). This machine gave diffraction pattern from 2.5 to 120 degree (2θ) at once, with resolution of 0.03° 2θ. Powder samples were put on the rotating aluminum plate sample holder and exposed 10 minutes and therefore the exposure time for every position was 10 minutes.

Thermal Gravimetric Analysis (TGA)

Thermal gravimetric analyses were performed using TA Q500 (located in the Chemical Engineering Department, University of Waterloo), at heating rate of 10 °C/min, switching from N_2 to air at 650°C. About 4-6 mg of the sample was placed into the TGA pan. After temperature stabilization at 40 °C and setting N_2 as the atmosphere gas, it was heated up to 650 °C by heating rate of 10 °C/min. At this point, the atmospheric gas was switched to air and heating was continued with the same rate up to 800 °C for elimination of carbonaceous residues, thus obtaining the inorganic content of the sample.

Inductively Coupled Plasma (ICP)

The Zr loading on the clay surface was measured by inductively coupled plasma atomic emission spectroscopy using utilizing a Prodigy high dispersion ICP made by TELEDYNE (located in the Chemical Engineering Department, University of Waterloo). The digestion procedure was first acquired from O.I. Analytical, application note 0631194 and then modified based on the specifications and scale of our system. For sample preparation, about 30 mg of sample were first digested with a combination of $HF/HCl/HNO_3$ with ratio of 3:1:0.5, using a 1200 W Panasonic microwave oven at power level 4 for two rounds of one minute and interval of one minute. The sample in the digestion bomb was then cooled down to room temperature by immersing the whole digestion setup into water for 3 hours. The provided liquor was then diluted to a given volume before being tested in the ICP instrument. Before the measurement, the plasma was geometrically aligned using Mn solution (1000 ppm) and then instrument was calibrated with standard solutions in five concentration levels for each

element of Al, Mg, Si (0, 10, 20, 50 and 100 ppm) and Zr (0, 2, 4, 10, 20 ppm). Measurements were performed 3 times in each sample for calculation of the average.

4.3 Results and Discussion

4.3.1 Preliminary Supporting Procedure and Low-Pressure Polymerizations

Among the clays tested in low pressure polymerization experiments, only Cloisite 93A and Na^+ MMT were active for polymerization. The other clay samples were either inactive or could not be prepared due to the formation of stable colloids in toluene. A summary of supporting and polymerization results is shown in Table 4.2.

Cloisites 10A and 15A formed stable colloids in toluene and could not be washed with toluene effectively. Therefore, they were not tested any further. Cloisite 20A formed a colloid with very long decantation time and was not tested any further. Cloisite 25A also formed a colloid, but a shorter decantation time (approximately 8 hours) was required to achieve good separation from the supernatant; however no activity was observed during the screening polymerizations.

Cloisite 30B did not form a colloid in toluene and the particles sedimented in about 2 hours during the washing steps; however, no noticeable activity was observed during polymerization. Na^+ MMT sedimented quickly in toluene (less than 2 hours) and showed limited polymerization activity. Although Cloisite 93A sedimented more slowly (approximately 24 hours), the supported metallocene had the highest activity of all Cloisite investigated.

Table 4.2. Summary of results for screening ethylene polymerizations.

Clay Sample	Sedimentation Rate	Polymerization Time (min)	Pure Polymer Yield (g/hr)
Na^+ MMT	Quick (< 2 hr)	20	2.61
Cloisite 10A	Very slow	-	-
Cloisite 15A	Very slow	-	-
Cloisite 20A	Slow (>24 hr)	-	-
Cloisite 25A	Moderate(<8hr)	20	-
Cloisite 30B	Quick (≈ 2 hr)	40	very small
Cloisite 93A	Slow (<24 hr)	40	3.21

We can hypothesize that the Cloisites that formed stable colloids in toluene, such as 10A and 15A, had a very large loading of organic modification, compared to the cation exchange capacity of the original Na^+ MMT. Because of the high compatibility between the organic

modification and toluene, sedimentation was extremely slow and they could not be washed with fresh solvent to remove the unsupported catalyst molecules. To compare their sedimentation rates, 2 grams of each Cloisite was dispersed in 150 mL toluene and left for sedimentation. The results of the sedimentation tests after 1 day, and after two weeks, are shown in Figure4.2. Na^+ MMT and Cloisite 30B had the fastest sedimentation rates. Cloisite 25 A and 20A formed colloids that reached partial sedimentation after a long time. Cloisites 10A and 15A did not reach acceptable sedimentation levels to be used for the washing steps even after two weeks. While Cloisites 15A, 20A, 25A and 10A showed gel type- dispersions in toluene, Cloisite 93A, showed a turbid dispersion in toluene and sedimented slowly, but completely, after 2 days.

Sedimentation of Cloisites 15A and 10A (the two that formed stable colloids in toluene) were also tested in n-heptane, which has a lower solubility parameter [δ = 15.3 $(J/cm^3)^{1/2}$] than toluene [δ = 18.3 $(J/cm^3)^{1/2}$]. The sedimentation of these two Cloisites in n-heptane was observed to be much faster. Figure 4.3 shows that after one day, the sedimentation of Cloisites 10A and 15A was complete.

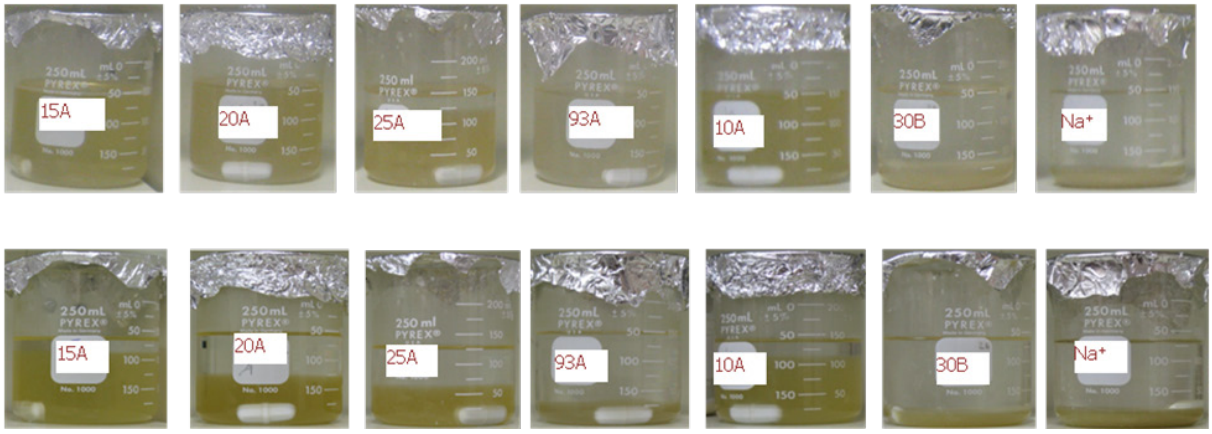

Figure4.2. Comparison between the sedimentation of different Cloisite samples in toluene at room temperature, after one day (top) and after two weeks (bottom).

Figure 4.3. Sedimentation of Cloisites 10A and 15A in heptane after one day.

The dispersion of clays in organic solvents has been reported in the literature. By comparing small angle neutron scattering (SANS) and wide angle neutron scattering (WAXS) profiles of dispersions of Cloisite 15A in different solvents, Ho et al. [113, 114] showed that the quality of dispersion or precipitation of organically-modified clays in the solvent was directly determined by the solubility parameters of the solvent. The Hansen solubility parameter is a tool to predict if a material will dissolve in another material. It is defined by the Equation (4.1)

$$\delta_0^2 = \delta_d^2 + \delta_p^2 + \delta_h^2 \tag{4.1}$$

where dispersive (δ_d), polar (δ_p), and H-bonding (δ_h) forces act together according to Equation (3.1) to determine the overall solubility parameter and final dispersion behavior. The closer the $\delta_0$values of two materials, the more likely they will dissolve in each other. For example, dispersions of Cloisite 15A platelets (δ_0 = 9.35$(cal/cm^3)^{1/2}$ in chloroform δ_0 = 9.21 $(cal/cm^3)^{1/2}$ exhibited scattering characteristic of a fully exfoliated material. Cloisite 15A swells, but retains traces of its tactoid structure in benzene δ_0 = 9.15 $(cal/cm^3)^{1/2}$, toluene δ_0 = 8.91 $(cal/cm^3)^{1/2}$, and p-xylene δ_0 = 8.80 $(cal/cm^3)^{1/2}$, while the platelets aggregate to form large particles in cyclohexane δ_0 = 8.18 $(cal/cm^3)^{1/2}$ and octane δ_0 = 7.62 $(cal/cm^3)^{1/2}$ [114].

4.3.2 High Pressure Polymerization Results

The high pressure polymerization experiments confirmed the results from the screening at low pressure: besides Na^+ MMT, only one type of organoclay, Cloisite 93A, worked as an effective support for the metallocene catalyst. The polymerization conditions and yield with these two clays are summarized in Table 4.3. The activity of Cp_2ZrCl_2 supported onto Cloisite 93A was more than 20 times higher than when it was supported on Na^+ MMT. As it was described before, in this supporting method, the water content on the clay surface is reacted with TMA to produces MAO cocatalyst. Surprisingly, despite its considerably lower moisture

content in comparison to Na^+ MMT, according to Table 4.1, Cloisite 93A was significantly better as a support for Cp_2ZrCl_2.

Table 4.3. Activity of Cp_2ZrCl_2 supported on Na^+ MMT and Cloisite 93A, under constant conditions of *T*=85°C, *P*= 5 bars, TIBA = 2.5 mmol/L; targeted Zr concentration in impregnation = 20 μmol/gram clay.

Support Material	Replicates	Clay (g)	Time (min)	Yield (g)	Average Yield (g/g clay/hr)
Na^+ MMT	NA1	0.4	70	1.9	3.6
	NA2	0.4	70	1.5	
	NA3	0.4	70	1.6	
Cloisite 93A	93A1	0.17	53	11.9	79.5
	93A2	0.17	53	12.1	
	93A3	0.17	53	11.8	

Ineffective Cloisite samples (Cloisites 10A, 15A, 20A, 25A and 30B) were used for catalyst supporting and used in high pressure polymerization experiments in toluene in a 300 mL Parr autoclave reactor at 50°C, 2 to 6 bars of ethylene pressure, and durations of 1 to 3 hours. To complete the supporting procedure in the case of Cloisites 15A and 10A (the samples which showed little sedimentation), hexane was used as solvent during the supporting procedure. No activity was observed during polymerization when Cp_2ZrCl_2 was supported on these clays. For Cloisite 30B, containing hydroxyl groups on the modifier structure (see Figure 4.1), a higher level of TMA (twice as much) was also tried in the supporting step, and a small trace of polymer was made when MAO was used as cocatalyst in the polymerization, but not enough to justify further testing of this system.

The treatment of clay with organic modifiers is expected to increase clay basal spacing and affinity with organic precursors, including alkyl aluminum compounds and metallocene catalysts. Figure 4.4 compares XRD patterns of Na^+ MMT and the modified Cloisites investigated in this work. According to Figure 4.4, and Table 4.1, in some samples such as Cloisite 10A and Cloisite 30B, the organic modifications has led to interlayer expansion and in some cases such as Cloisite 15A, Cloisite 20A, Cloisite 25A and Cloisite 93A it has led to exfoliation and a more disordered clay structure.

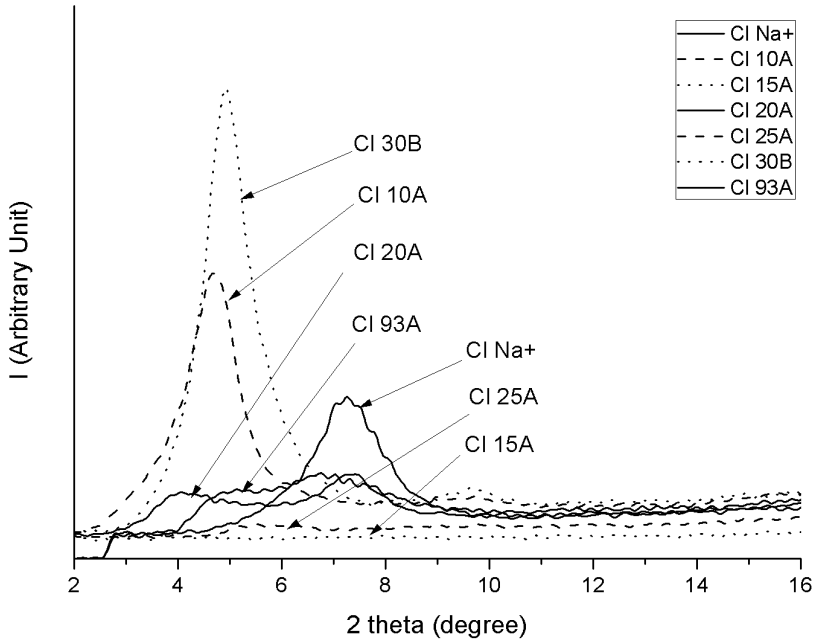

Figure 4.4. X ray diffraction (XRD) patterns for different Cloisites.

Comparing the polymerization activities shown in Table 4.3 for Cp_2ZrCl_2 supported on different clays, it is clear that the stacking structure of the clay is not responsible for its efficiency as a polymerization catalyst support.

As shown in Table 4.2, among all the organoclays studied here, only Cloisite 93A was found to be a good support for Cp_2ZrCl_2. By comparing the structure of the organic modification of Cloisite 93A with those of the other organoclay samples in Figure 4.1, we realize that the main difference between Cloisite 93A and the other organoclays is not the layer spacing, but the type of ammonium cation; unlike the other organoclays investigated herein, which were modified with quaternary ammonium cations, Cloisite 93A is treated with a tertiary ammonium cation.

We may speculate that the difference in types of ammonium cations in the Cloisite samples (tertiary vs. quaternary) determines how well the Cloisite will perform as a catalyst support for the system we are investigating herein.

Unlike primary, secondary, and tertiary ammonium cations, that have Brønsted H^+ able to form H-bonds with oxygen atoms in residual water, hydroxyl groups, or structural oxygen in the silica layer as a proton donor, quaternary ammonium cations are permanently charged and cannot be involved in such bonding [115]. Also it has been shown that it is possible for the tertiary ammonium cation to react with TMA and produce stable amino-alkylaluminum [116-120].

Laubengayer et al. [116] described the reactions of amines ($NH_{3-n}R_n$, with n = 1, 2 or 3, and R representing an alkyl group) and amine hydrohalides (($NH_{3-n}R_n$.HX, with X representing a

halide atom) with alkylaluminum compounds (AlR_3). Reactions with tertiary, secondary and primary amines resulted in R_3N-AlR_3 adducts, $[R_2N\text{-}AlR_2]_2$ dimers, and $[RN\text{-}AlR]_n$ oligomers, respectively. Similarly, amine hydrohalides react with alkylaluminum compounds to give different products. The reactions of $R_3N{\cdot}HX$ with R_3Al and also reaction of R_3N with AlX_3 resulted in the same adduct product R_3N-AlR_2X, known as amino-alanes. In an attempt to modify MAO properties, Sangokoya et al. reported [117, 118] that MAO can react with tertiary ammonium hydride halides to produce tertiary amino aluminoxanes that are more soluble and stable in the organic solvents and, in some cases, increase the catalyst activity when used to activate metallocenes for olefin polymerization. Biswas et al. [119] reported that the reaction between trialkylaluminums and a tertiary ammonium ion resulted in trialkylaluminums adducts that were stable when exposed to air and could be handled outside the glove box (the chamber with inert atmosphere).

Comparing the supporting efficiencies for Cloisite 93A, Cloisite 25A and Na^+ MMT, reveals more information on the effect of the organic modification. The Zr loading for Cloisite 93A, Cloisites 25A, and Na^+ MMT were measured using ICP-AES; the supporting efficiencies are summarized in Table 4.4. Because the concentration of organic modification changes during the catalyst supporting process, the supporting efficiencies were calculated based on the weight fraction of the clay, excluding the non-clay content from the organoclay or clay-catalyst system. According to our definition, the non-clay content is equal to the weight loss from room temperature to 800°C during TGA analysis. The Zr concentration before supporting is the number of moles of Zr that were added to one gram of clay sample, and the Zr concentration after supporting is calculated from ICP-AES data. Table 4.4 shows that Cloisite 93A and Na^+ MMT have considerably higher supporting efficiencies than that of Cloisite 25A.

Table 4.4. Summary of catalyst supporting data for Na^+ MMT, Cloisite 93A, and Cloisite 25A.

Clay Type	Before Supporting			After Supporting			Supporting Efficiency (%)
	Zr/clay (μmol/g)	non-clay content	Zr/pure clay (μmol/g)	Zr/clay (μmol/g)	non-clay content	Zr/pure clay (μmol/g)	
Na^+ MMT	20±2	8±2	30.9±1.9	26.8±2.9	8.5±2	33.9±2.8	**97.3±2.7**
Cloisite 93A	20±2	35.5±2.5	30.9±1.9	23.2±2.5	25.7±2.5	31.1±2.3	**93.9±6.1**
Cloisite 25A	20±2	31.6±2.5	29.2±1.9	2.74±0.2	31.3±2.5	3.7±0.15	**12.7±1.5**

The different supporting efficiencies can be explained by the following mechanism: during the TMA treatment, a major fraction of water content including surface water and hydrating water is reacted to TMA and results in formation of MAO on the clay surface (Equation 4.2). The fuming during this step confirms the release of methane in this reaction.

$$Al(CH_3)_3 + H_2O \rightarrow CH_3[\text{-O-}Al(CH_3)\text{-}]_n + CH_4 \uparrow \quad (4.2)$$

In the next step, the metallocene catalyst can be loaded on the surface via two different mechanisms:

a) Metallocene can react with MAO on the surface for methylation and formation of active sites on the clay surface

$$MAO + Cp_2ZrCl_2 \rightarrow Cp_2Zr(CH_3)Cl + Cp_2Zr(CH_3)^+ {}^-[MAO] \quad (4.3)$$

b) Metallocene can also react with and exchange the Na^+ cation as shown Equation (4.4)

$$\text{--}S^- Na^+ + Cp_2ZrCl_2 \rightarrow \text{--}S\text{-} (Cp_2ZrCl)^+ + NaCl\downarrow \quad (4.4)$$

where, --S^- represents the negatively charged clay surface. Na^+ cation inside the clay gallery is usually accompanied by hydration water molecules. Therefore as a consequence to elimination of Na^+, the water content is decreased inside the gallery. The contact between hydrating water and metallocene, during catalyst impregnation can also explain low polymerization activity of the Cp_2ZrCl_2/Na^+ MMT even when high metallocene supporting efficiency was obtained.

The XRD patterns of Na^+ MMT before supporting and after each step of supporting in Figure 4.5, suggests that the stacking order has been changed during catalyst supporting. The narrower basal peaks at the same time with the basal spacing peak shifted to higher 2θs suggest that two different behaviors can be detected: while a faction of clay has lost their staking order, another part has gained smaller basal spacing. According to XRD patterns of Na^+ MMT Figure 4.5, further structural changes takes place after catalyst impregnation. The structural collapse observed in each step of the catalyst supporting is explained by loss of hydrating water from the surface via reaction to TMA, and by changes in the nature of interlayer cations and therefore their hydration behavior. The tilted d-spacing peak after catalyst supporting steps, indicates a combination of changes including exfoliation, expansion and collapse of layer stacking..

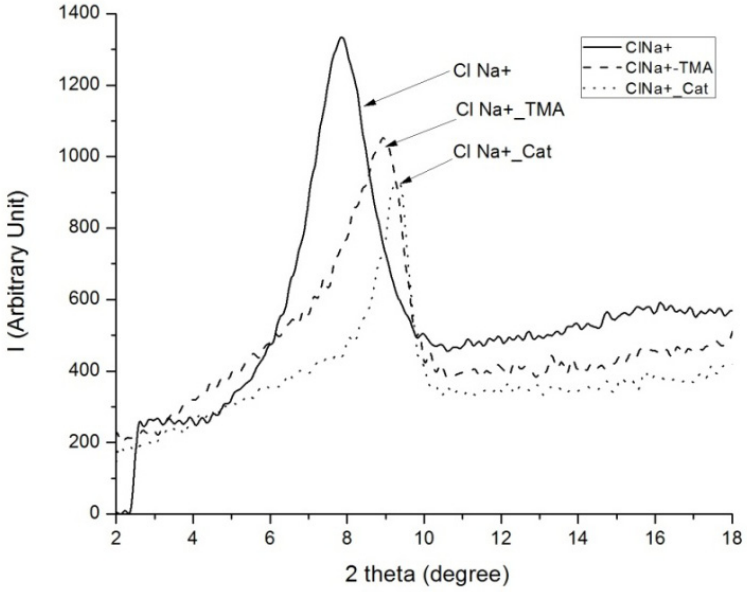

Figure 4.5 XRD spectra for Na^+ MMT after TMA treatment and catalyst impregnation steps

Na^+ MMT samples were tested by thermal gravimetric analysis (TGA) using a heating rate of 10°C/min before and after catalyst supporting (Figure 4.6). The first derivative of the weight loss curves with respect to the temperature (dTG), which determines the rate of weight loss as a function of temperature, are also shown in Figure 4.6. The weight loss in the first dehydration region (< 200°C) can be assigned to water molecules physically absorbed onto the clay surface [121]. The starting weight percent for Na^+ MMT is less than 100%, because water is lost during the initial temperature stabilization step under nitrogen flow in the TGA furnace. In the first dehydration region, the weight loss for Na^+ MMT/catalyst is lower than that of pristine Na^+ MMT. This TGA result supports the proposed hypothesis for the collapsed interlayer spacing after catalyst supporting on Na^+ MMT. In the same time the TGA result proposes that Na^+ MMT has become less hydrophilic after catalyst supporting.

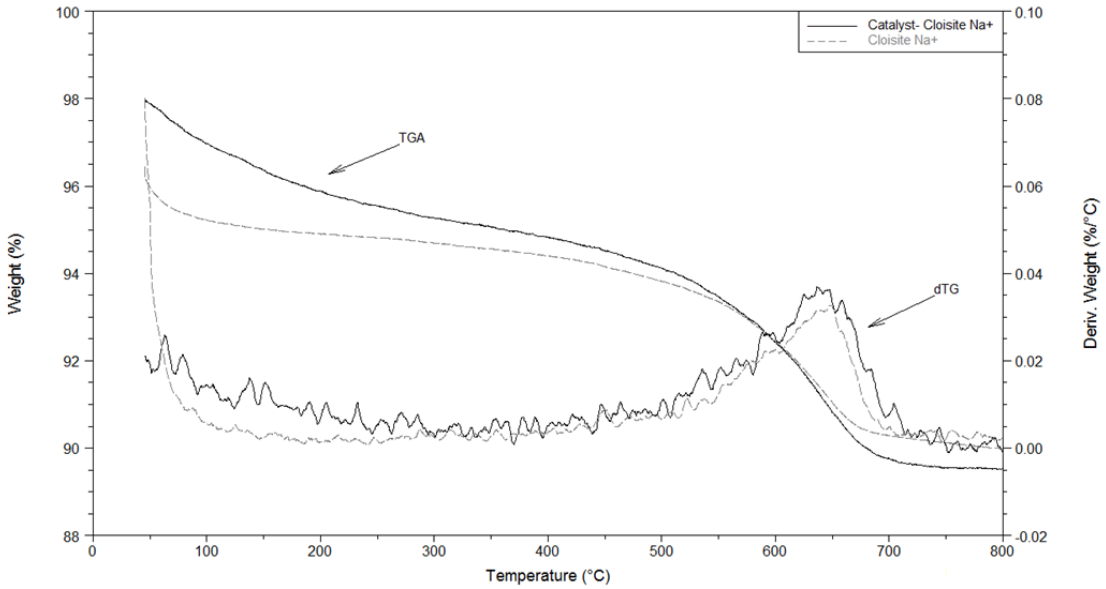

Figure 4.6. TGA results and corresponding dTG (derivative with respect to temperature) for Na^+ MMT before (dashed grey line) and after (solid black line) catalyst supporting (10°C/min heating rate).

According to the suggested mechanism, the considerably lower moisture content in Cloisite 25A (as shown in Table 3.2), has decreased its chance of reaction with TMA and consequently the in-situ formation of MAO. It is possible that the lower MAO content on the surface of Cloisite 25A in turn has resulted in low adsorption of Cp_2ZrCl_2.

According to the second mechanism of metallocene loading, the very weak chance of exchange reaction between the quaternary ammonium cation and metallocene partly explains the low metallocene loading on Cloisite 25A.

Table 4.4 shows that Cloisite 93A showed a high supporting efficiency comparable to that of Na^+ MMT. The higher polymerization activity with Cloisite 93A as supporting material, suggested that Cloisite 93A is a better catalyst support than Na^+ MMT.

The apparent contradiction between high supporting efficiency of Cloisite 93A and its low moisture content, as reported in Table 4.1 may be explained by the presence of other types of water content than physically absorbed water on the surface of Cloisite 93A. As it is known, there are two major types of water on the surface of clay: a) surface absorbed water, which is also known as moisture and can be easily removed by mild thermal treatment and vacuum and b) water that is called hydrating water, which company the cations on the surface and because of their stronger bonding to the surface, will not be removed as easily as moisture. In Cloisite 93A, although the moisture content is low, the water associated with the tertiary amine modifier used in its preparation is a good source of water for in-situ production of MAO.

Generally, for surface modification of clay with quaternary ammonium ions, their salt is dispersed in water and reacted with the clay surface:

$$NR_4^+X^- + --S^- Na^+ + H_2O \rightarrow --S^- {}^+NR_4 + Na^+X^- + H_2O \quad (4.5)$$

But, Cloisite 93A, with tertiary ammonium modification is prepared by treatment of Na^+ MMT with tertiary amine in an acidic medium.

$$NR_3 + H_2O + H^+X^- + --S^- Na^+ \leftrightarrow --S^- NR_3H^+ + --S^- Na^+...H_2O...NR_3 + Na^+ + X^- + OH^- \quad (4.6)$$

The coordination water in Cloisite 93A may react with TMA molecules to produce in-situ MAO,

$$--S^- Na^+...H_2O...NR_3 + Al(CH_3)_3 \rightarrow --S^- Na^+ + MAO + NR_3\downarrow + CH_4\uparrow \quad (4.7)$$

and at the same time

$$--S^- NR_3H^+ + MAO \rightarrow --S^- {}^+NR_3{}^-[MAO] + CH_4\uparrow \quad (4.8)$$

The $^+NR_3{}^-$[MAO] species is now a new interlayer cation that is connected to the surface via ionic interactions. These species have been reported to be able to methylate the zirconocene dichloride and outperform the regular MAO [117, 118].
When preparing Cloisite 93A, Na^+ MMT is treated with a tertiary amine in an aqueous acidic system; a fraction of tertiary amines are only bridged to the clay surface via hydrating water molecules [57, 115]. As a result, this type of water promotes partial hydroxylation of TMA in a controlled manner to produce useful in-situ MAO that enhances catalyst loading and polymerization activity.
The TGA plots and their corresponding dTG plots for Cloisite 93A after different catalyst supporting steps in Figure 4.7 and Figure 4.8 show that the extraction of the organic modification happens mainly during the TMA treatment step. Higher rates of dehydration, in the first dehydration region for Cloisite 93A after TMA treatment confirm the extraction of a part of the organic modification and consequent increase in hydrophilicity.
The shoulder that appeared in the peak located in the 200-450°C region (in Figure 4.8), which disappeared after TMA treatment, can be assigned to a fraction of organic modification in Cloisite 93A that was removed in the TMA treatment step. The discontinuity in TGA and related sharp peak (dTG) at around 650°C is due to switching from nitrogen to air for complete thermal oxidation degradation in order to determine the final clay content.

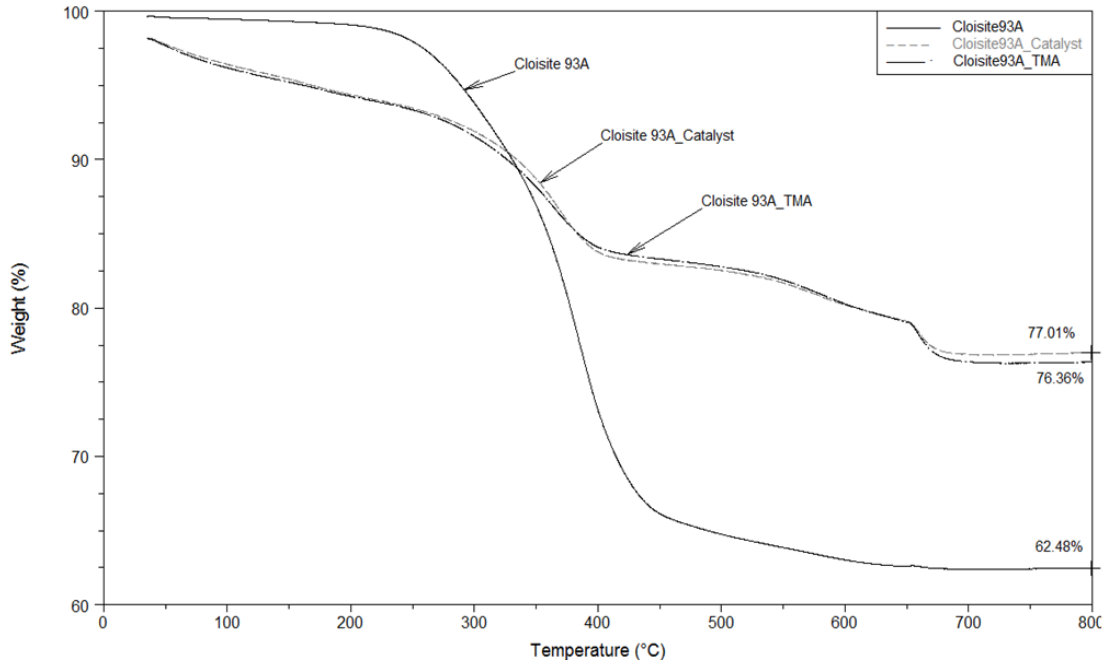

Figure 4.7. TGA results for original Cloisite 93A (solid black line), after TMA treatment (black dash-dotted line) and after catalyst supporting (grey dashed line) (10°C/min heating rate).

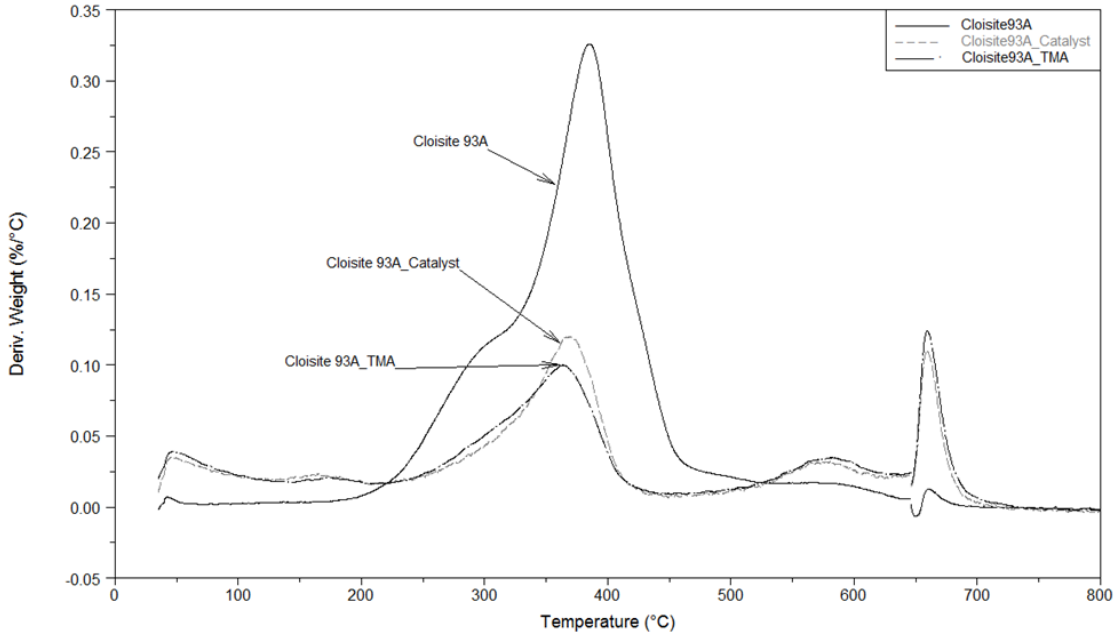

Figure 4.8. Corresponding dTG plots (derivative with respect to temperature) for the TGA results depicted in Figure 4.7 for Cloisite 93A (10°C/min heating rate).

The loss of organic modification in Cloisite 93A during supporting may be explained by two mechanisms: i) simple interaction between organic modification and organic solvent and ii) reaction with the supporting reagents. The solvent used during catalyst supporting may be able to extract a fraction of the organic modification from the clay galleries. To test this hypothesis, 1.0 g of Cloisite 93A was washed with 100 mL toluene five times and then dried. Comparing TGA results of Cloisite 93A before and after washing with toluene in Figure 4.10 it appears that washing with toluene decreased the total weight loss, or non clay content, from 37.15 to 32.77 wt%. Comparing the loss of non-clay content due to simple washing (Figure 4.9) with the non-clay loss due to catalyst supporting reaction (Figure 4.6) it is suggested that a higher fraction of organic modification is removed solely because of chemical reaction in the catalyst supporting.

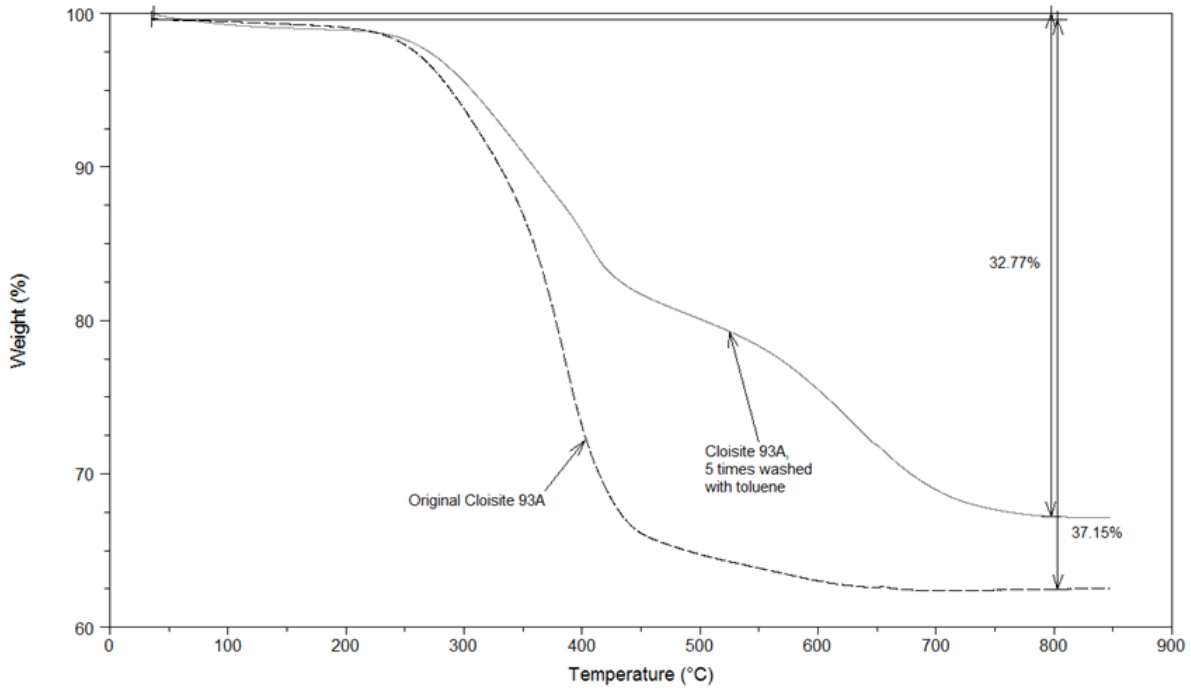

Figure 4.9. Role of interaction with toluene on the extraction of organic modification in Cloisite 93A

The XRD patterns for Cloisite 93A after different catalyst supporting stages are compared in Figure 4.10. The XRD spectrum of pristine Cloisite 93A shows a dual basal spacing peak ($2\theta_1$= 5.0°, $2\theta_2$= 7.0°) that is likely caused by a non-homogeneous ion exchange treatment. It appears that the main structural change happened during TMA treatment. The first peak remains at approximately the same 2θ position (5.0°) but with higher diffraction intensity, indicating increased tactoids arrangement order after TMA treatment. The second peak shifts to a higher 2θ positions (9.5°), but has small intensity, indicating removal of the organic modification and collapsed of the clay galleries. After catalyst impregnation, the first basal spacing shifts slightly to a higher 2θ position (5.5° vs. 5.0°), but has higher intensity that would be indication of slightly higher stacking order after catalyst impregnation.

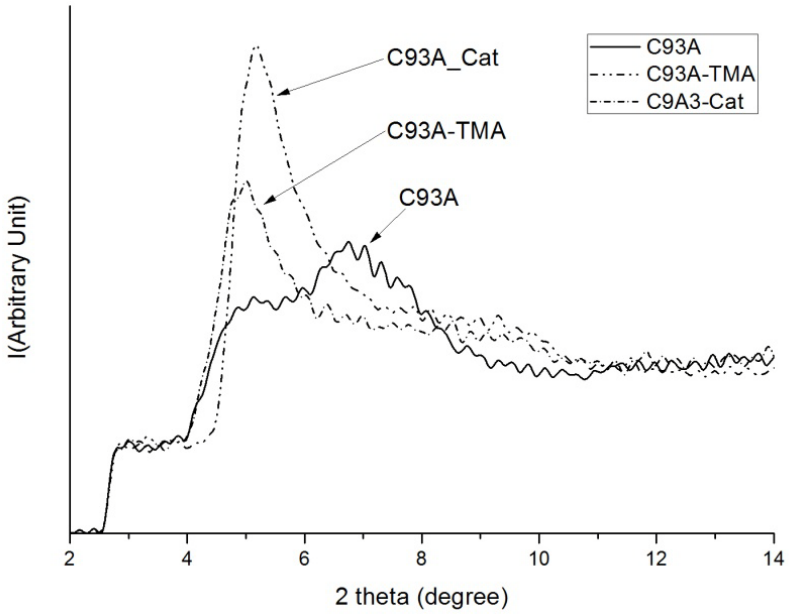

Figure 4.10. Changes in the layer stacking for Cloisite 93A during the supporting steps using toluene as a solvent.

The TEM image of Cp_2ZrCl_2/cloisite 93A is depicted in Figure 4.11, showing disorder in the orientation of clay thin tactoids without an overall regular arrangement.

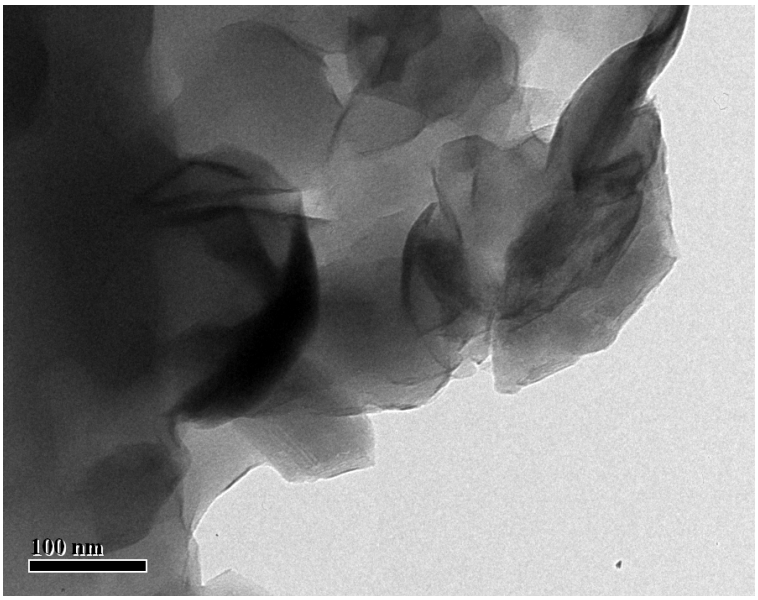

Figure 4.11. TEM image of Cp_2ZrCl_2/cloisite 93A.

It appears that loss of organic modification is in direct relationship with catalyst loading on the surface of organically modified clay support. Cloisite 25A, that showed very poor catalyst loading, as seen in Figure 4.12, it barely showed any loss of organic modification during the supporting procedure. Lee et al. [63] reported that Cloisite 25A lost about 90 percent of its organic modification content when it reacted with modified MAO (MMAO). They explained the removal of organic modification from the surface of Cloisite 25A as result of reaction between oxygen atoms in MMAO and reduction of quaternary ammonium ion and consequent change into tertiary amine that easily leaves the clay surface. Comparing organic modification losses of Cloisite 25A in reaction with TMA and MMAO, suggests higher reactivity of organic modification in organically modified clay with alumoxanes. According to this hypothesis, primarily in reaction with TMA, MAO is produced on the surface of Cloisite 93A and consequently during impregnation metallocene catalyst is bound to the clay surface via reaction to in-situ produced MAO.

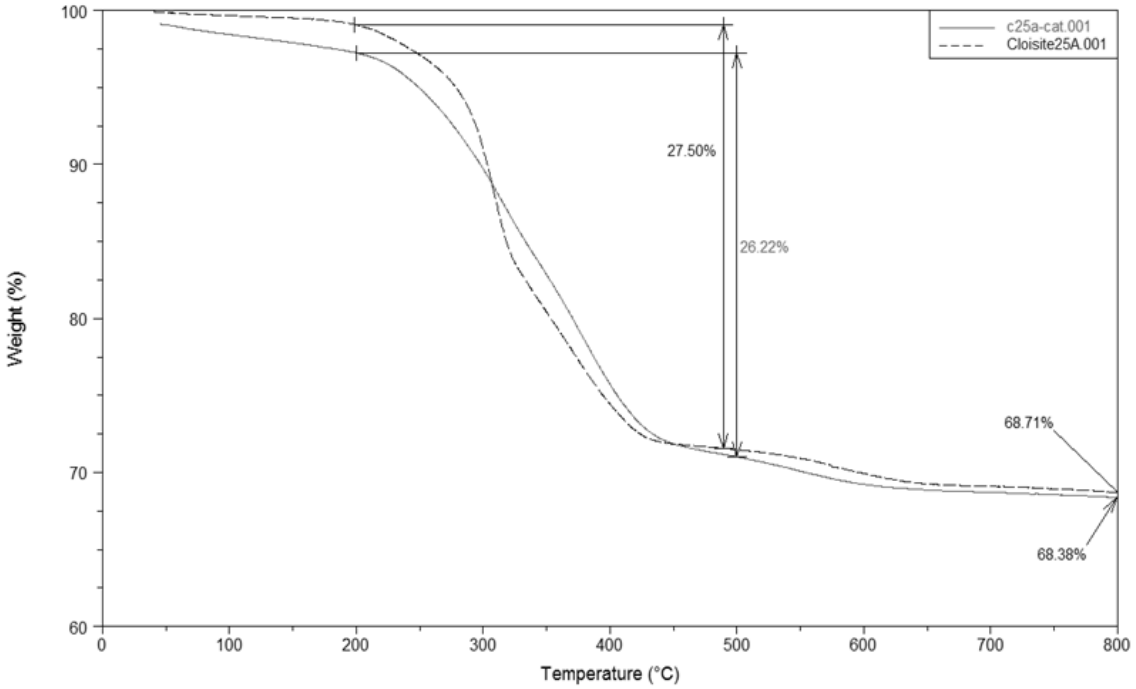

Figure 4.12. Changes in organic modification content of Cloisite 25A due to catalyst supporting

As an experimental observation, during the TMA treatment of Na^+ MMT, more intense fuming was observed than for Cloisite 93A. Regarding all observations above, the different fuming behaviors can be interpreted as different type of water sources available in TMA treatment step: as Na^+ MMT has a low surface compatibility to toluene, the major source of water should be moisture type, while for Cloisite 93A the ionically bonded water behaves similarly to crystal water that is released in a more controlled manner. The way TMA reacts with water influences the structure of produced MAO and consequently polymerization

activity of the metallocene catalyst [9]. This can partly explain the higher polymerization activity of Cp_2ZrCl_2/Cloisite 93A compared to Cp_2ZrCl_2/ Na^+ MMT.

4.3.3 Microstructural Studies of Polymer-Clay Nanocomposite Particles

The effect of catalyst supporting on the clay microstructure was investigated using scanning electron microscopy. SEM pictures of Na^+ MMT before and after catalyst supporting are shown in Figure 4.13 and Figure 4.14, respectively. By comparing these images, we can conclude that porosity and surface area decrease after catalyst supporting.

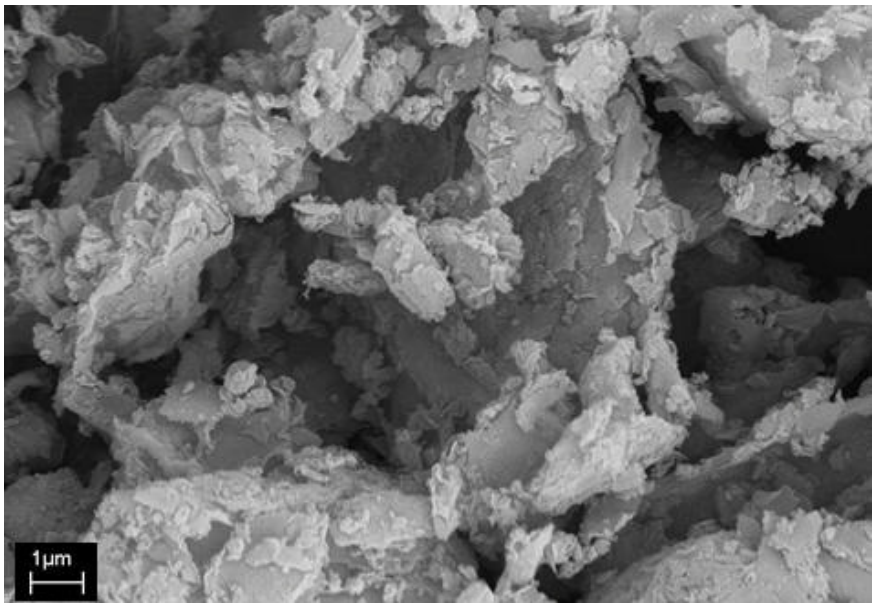

Figure 4.13. SEM picture of pristine Na^+ MMT before catalyst supporting.

On the other hand, SEM images for Cloisite 93A (Figure 4.15) and Cp_2ZrCl_2/Cloisite 93A (Figure 4.16) show that the particles have a more exfoliated appearance after catalyst supporting.

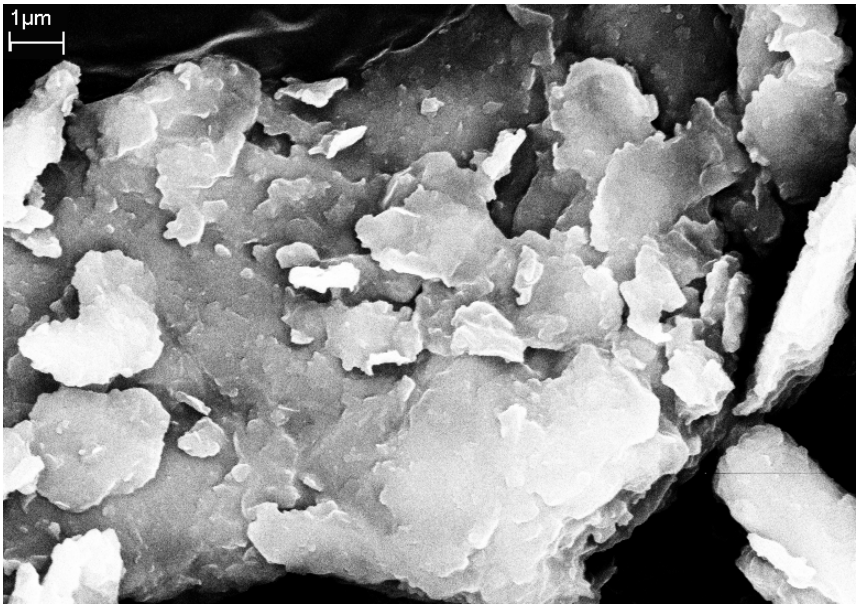

Figure 4.14. SEM picture of Cp_2ZrCl_2/Na^+ MMT.

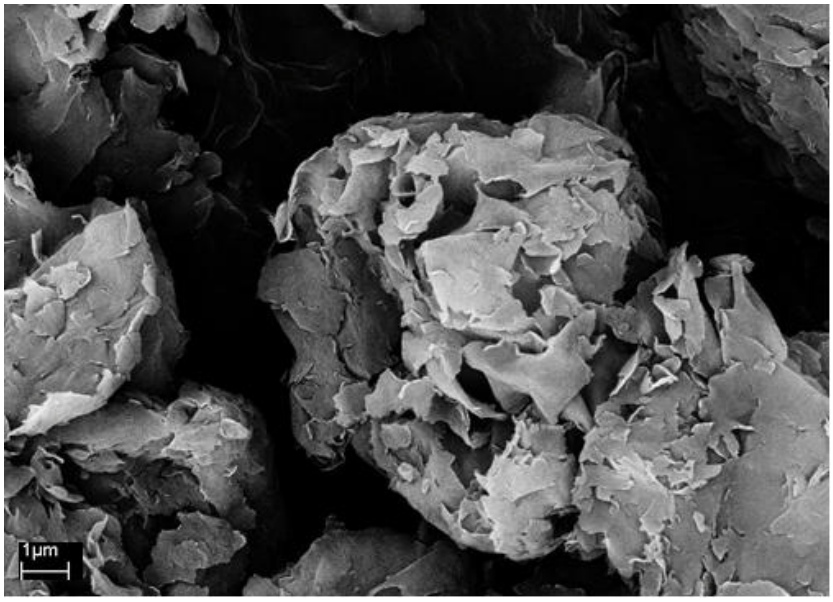

Figure 4.15. SEM picture of Cloisite 93A before catalyst supporting.

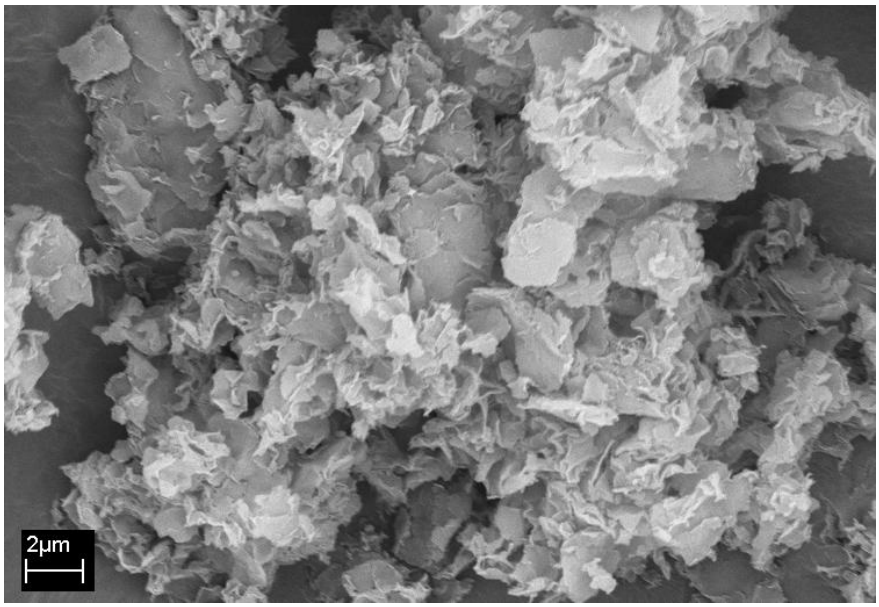

Figure 4.16. SEM picture of Cp_2ZrCl_2/Cloisite 93A.

The effect of the organic modification, after the supporting process, can be observed by comparing the SEM micrograph for Cp_2ZrCl_2/Na^+ MMT (Figure 4.14) and Cp_2ZrCl_2/Cloisite 93A (Figure 4.16). For Cp_2ZrCl_2/Cloisite 93A, (apparently) weakly agglomerated smaller particles (mainly irregular flaky particles with distorted edges that may provide additional surface area for catalyst supporting) form larger macroparticles with high porosity and surface area. On the other hand, the Cp_2ZrCl_2/Na^+ MMT macroparticles seem to be denser and to have a lower surface area. Differences in the morphologies of these two clay samples can partly explain the considerably higher polymerization activity of Cp_2ZrCl_2/Cloisite 93A. Different particle morphologies after catalyst supporting are believed to be direct result of surface modification.

To confirm this hypothesis, original samples of Cloisite 93A and Na^+ MMT were washed with toluene and their microscopic structures were investigated. Comparing the particle morphologies of Na^+ MMT and Cloisite 93A after washing with toluene in Figure 4.17 and Figure 4.18 shows that the organic modification on the surface of Cloisite 93A plays an important role to enhance the interaction between clay surface and the organic solvent that carries the reactants during the catalyst supporting.

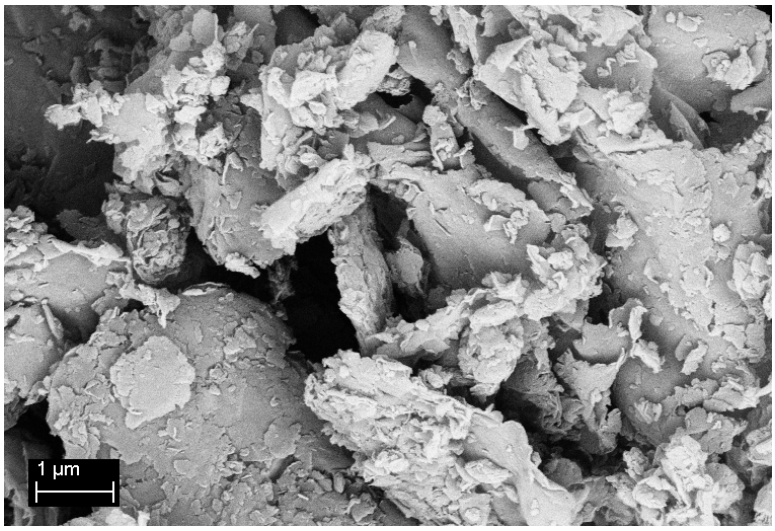

Figure 4.17. Particle morphology of Na^+ MMT after washing in toluene.

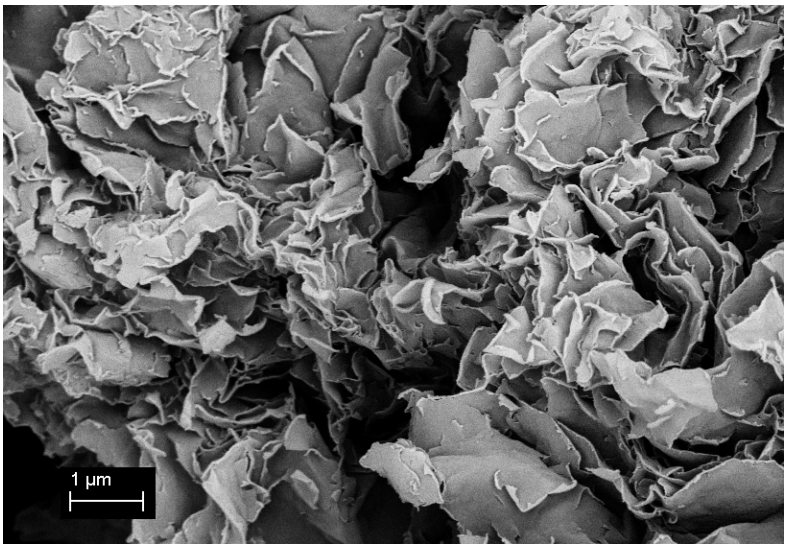

Figure 4.18. Particle morphology of cloisite 93A after washing in toluene.

A typical SEM image of a polyethylene-clay nanocomposite made with Cp_2ZrCl_2/Na^+ MMT is presented in Figure 4.19, showing particles with non-uniform morphology. Despite the relatively long polymerization time (70 minutes), the clay content was 26.6 wt % because of the low polymerization activity. Polymer-rich to clay-rich regions were detected using chemical analysis by energy dispersive x-ray spectroscopy (EDX), as shown in Figure 4.20. The brighter areas in Figure 4.19 have higher polymer contents than the darker regions. In the area labeled 1, no considerable particle break up has happened; therefore, it has the lowest C/Si weight ratio of 3.2. The brighter regions, labeled as 2 and 3, have C/Si weight ratios of

11.3 and 11.8, respectively. Finally, region 4 shows partial particle break up and a C/Si weight ratio of 7.0.

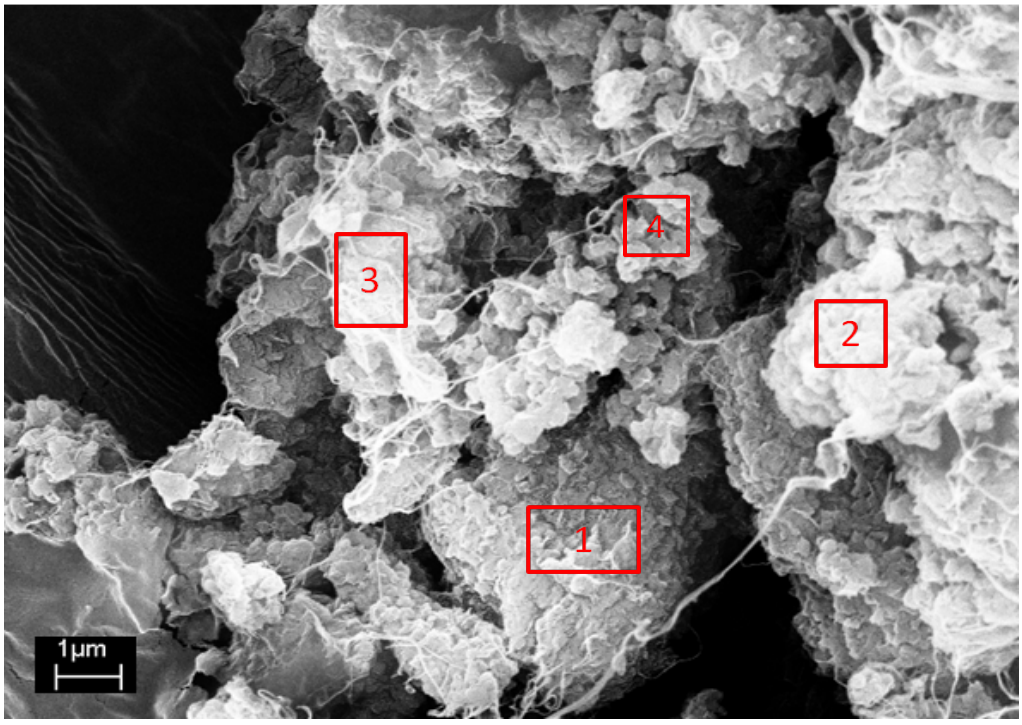

Figure 4.19. Morphology of polyethylene particles made with Na^+ MMT/ Cp_2ZrCl_2 (Clay content: 26.6 wt. %); *T* = 85°C, *P* = 5 bar, *t* = 70 minutes.

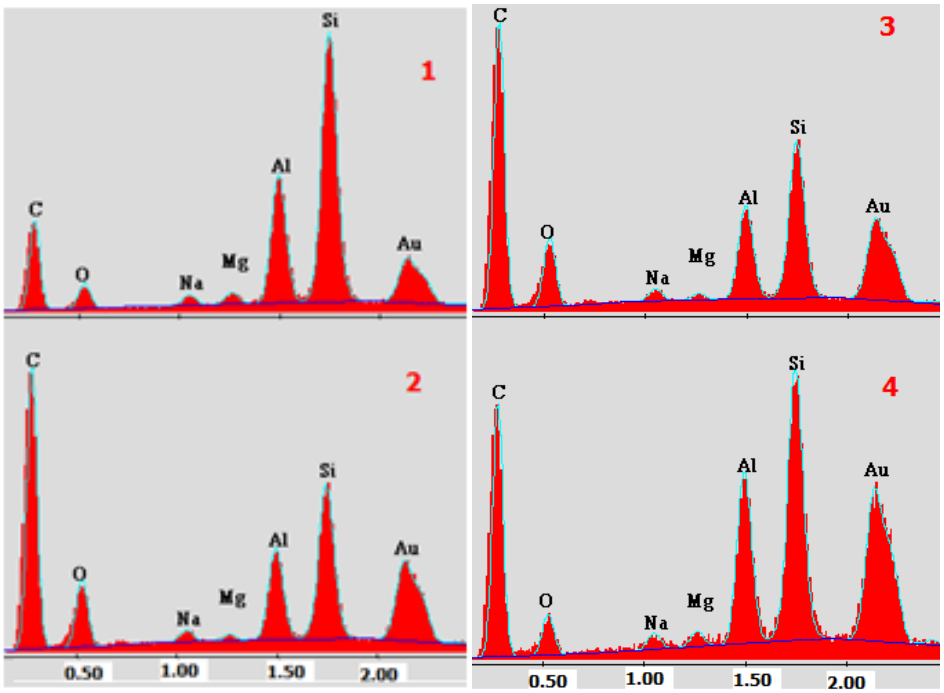

Figure 4.20. Corresponding EDX results for C/Si weight ratio for the locations shown in Figure **4.19**: 1) 3.2; 2) 11.3; 3) 11.8; and 4) 7.0.

The XRD pattern of the same Na^+ MMT/polyethylene sample is compared with those of Na^+ MMT before and after catalyst supporting in Figure 4.21. Appearance of the basal spacing peaks, nearly in the same location after polymerization indicates that catalyst supporting and in-situ polymerization has not increased the layer separation for Na^+ MMT and therefore, effective exfoliation has not been achieved.

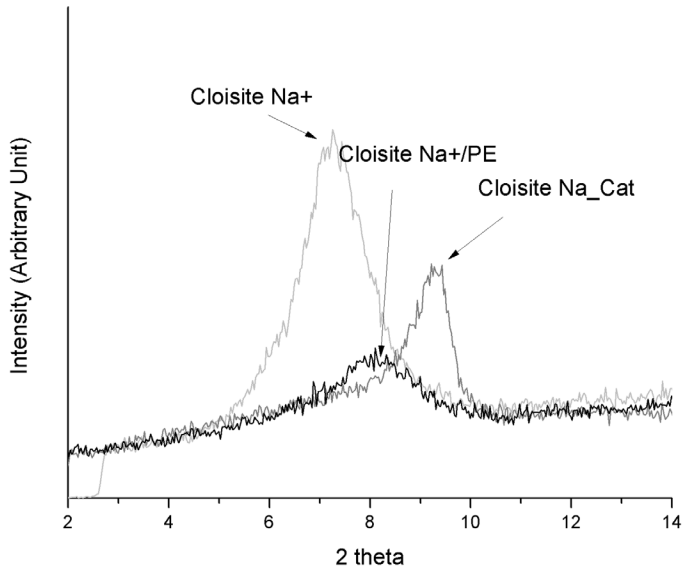

Figure 4.21. XRD diffraction patterns for Na+ MMT, Cp2ZrCl2/Na+ MMT, and polyethylene/Na+ MMT nanocomposite with clay content of 26.6 wt. %; Polymerization conditions: T=85°C and P=5 bar (Table 4.3).

A TEM image of the same polyethylene/Na^+ MMT is shown in Figure 4.22. A non homogeneous dispersion of clay particles in the form of tactoids with different thicknesses are observed in the polyethylene matrix. The TEM images in Figure 3.23 together with the XRD diffraction in Figure 3.22 indicate inefficient in-situ polymerization when Cp_2ZrCl_2/Na^+ MMT was used as polymerization catalyst. The poor quality of exfoliation, despite high supporting efficiency for Na^+ MMT, suggests deactivation of a major fraction of active centers when they are in contact with the clay surface. One plausible hypothesis is that deactivation of these active centers was caused by ineffective reaction between TMA and the surface water, perhaps due to the poor interaction between organic solvent used to dissolve TMA and the clay internal surfaces.

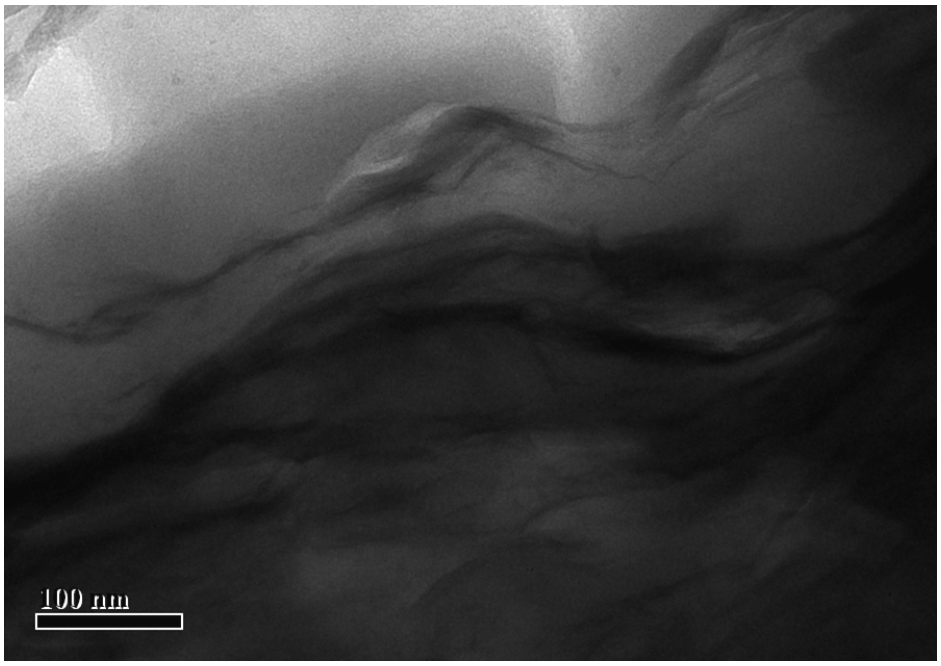

Figure 4.22 TEM image of polyethylene particles made with Cp_2ZrCl_2/ Na^+ MMT (Clay content: 26.6 wt. %); *T* = 85^{o}C, *P* = 5 bar and *t* = 70 minutes.

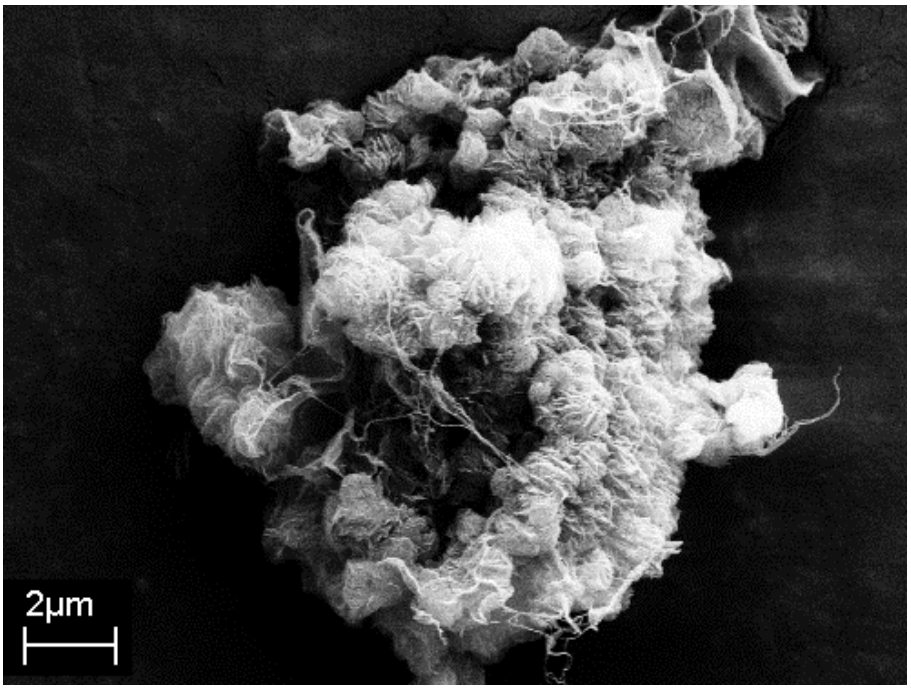

Figure 4.23 Morphology of polyethylene particles made with Cp_2ZrCl_2/cloisite 93A (1.5wt %). *T*= 85°C; *P*=5 bar; *t*= 53 min.

The morphology of polyethylene/Cloisite 93A nanocomposite particles with 1.5 wt% of clay made with Cp_2ZrCl_2/Cloisite 93A is shown in Figure 4.23. Macroparticles formed by several microparticles with a few hundred nanometers of diameter (comparable to the theoretical dimensions of the clay tactoids or individual layers) are observed. The particle morphology of polyethylene made by Cp_2ZrCl_2/Cloisite 93A seems to be much more uniform than what was made with Cp_2ZrCl_2/Na^+ MMT. This can be interpreted as a result of enhanced distribution of active sites on the surface of Cloisite 93A.

As it was discussed, under the same polymerization conditions (85°C, 5 bar, 53 minutes - Table 4.3), Cp_2ZrCl_2/Cloisite 93A had much higher polymerization activity than Cp_2ZrCl_2/Na^+ MMT. As a result, much lower clay contents were observed (1.5 wt% for Cloisite 93A and 26.6 wt. % for Na^+ MMT). The low clay concentration in the polyethylene/Cloisite 93A nanocomposite makes the investigation of clay exfoliation by XRD unfeasible. In Figure 4.24, the XRD pattern for a polyethylene nanocomposite made with Cp_2ZrCl_2/Cloisite 93A is compared with that of a homogeneously-made polyethylene. Even for the homogeneous polyethylene, a shoulder is detected in the basal spacing region ($2° < 2\theta < 10°$) that cannot be related to the presence of clay. Therefore no stacking arrangement was detected for the Cloisite 93A/polyethylene nanocomposite. The clay dispersion in the polyethylene nanocomposite made with Cp_2ZrCl_2/Cloisite 93A is apparent in the TEM image for a sample with a clay content of 7.2 wt. % (Figure 4.25). The clay nanolayers are dispersed more homogeneously in the polyethylene matrix, forming single layers and thin tactoids.

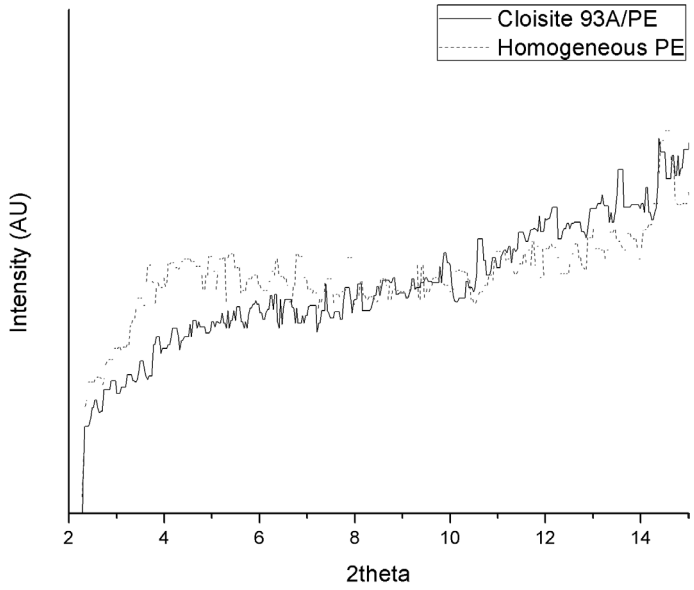

Figure 4.24 Comparison of XRD patterns for Cloisite 93A/polyethylene and homogeneous polyethylene in the basal space region; (Clay content: 1.5 wt. %); *T* = 85°C, *P* = 5 bar, *t*= 53 minutes.

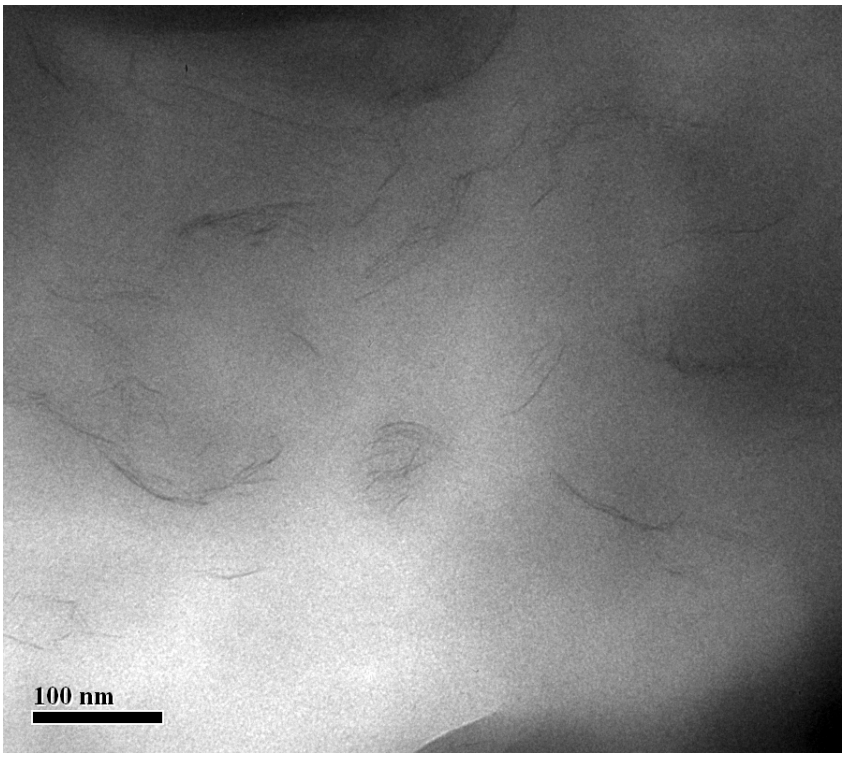

Figure 4.25 TEM image of polyethylene particles made with Cp_2ZrCl_2/ Cloisite 93A (Clay content: 7.2 wt. %); *T* = 55°C, *P* = 5 bar, *t* = 60 minutes.

4.4 Conclusions

We used a novel procedure to support Cp_2ZrCl_2 onto the surface of Na^+ MMT and several commercially available organoclays. We observed that the type of ammonium cation used during the clay organic modification is crucial to the success of the supporting method. It was observed that, for the same supporting conditions, Cloisite 93A (modified with tertiary ammonium cations) generates a catalyst with very high polymerization activity without application of MAO while the other Cloisites (modified with quaternary ammonium cations) led to poorly supported catalysts that were completely inactive for polymerization.

Despite the high supporting efficiencies for both Cp_2ZrCl_2/Na^+ MMT and Cp_2ZrCl_2/93A, the higher catalyst activity of Cloisite Cp_2ZrCl_2/93A a the same time with more uniform powder morphology of produced polymer is explained to be a direct result of organic modification in Cloisite 93A.

It is concluded from the experimental results that in Cloisite 93A a coordination type of water content is responsible for reaction with TMA. Due to slower release of this type of water, because of its stronger bonding to the surface, it is speculated that the MAO quality is enhanced compared to that in Na^+ MMT.

The abundant water content on the surface of Na^+ MMT is not able to efficiently react with TMA due to lack of compatibility between the clay surface and the carrier solvent. Two catalyst supporting mechanisms were considered for Na^+ MMT as a support material. In the first mechanism metallocene reacts with in-situ formed MAO and indirectly supported to the surface. And in the second mechanism, it is proposed that Cp_2ZrCl_2 is supported to the surface by reaction to Na^+ cation. In this mechanism Na^+ is exchanged by the metallocenium cation and NaCl is released. The catalyst supported on the clay surface with the second mechanism is mostly deactivated due to reaction with hydrating water remaining with Na^+ cation due to inefficient TMA treatment. In Cloisite 93A, higher interaction between organic solvent and clay surface, results in more efficient reaction of water to TMA and therefore lower catalyst deactivation rates are expected. The proposed adducts of MAO with tertiary ammonium cation is speculated to even more enhanced the in-situ made cocatalyst.

Further studies on the role of different parameters on the course of in-situ polymerization, and some studies on the evolution of nanocomposite morphology, will be reported in the next chapters of this thesis.

Chapter 5

Effect of Polymerization Conditions on the Morphology of Polyethylene/Clay Nanocomposites

5.1 Introduction

In Chapter 4, an in-situ ethylene polymerization method was introduced in which good clay exfoliation was obtained using Cp_2ZrCl_2 supported on Cloisite 93A. It was shown that the tertiary ammonium modifier on the clay surface considerably enhanced the polymerization activity of the supported catalyst. To better understand this heterogeneous catalyst, its response towards changes on different polymerization conditions is studied in this chapter.

5.2 Materials& Methods

5.2.1 Materials

Cloisite 93A was purchased from Southern Clay. Bis-cyclopentadienyl zirconium dichloride (Cp_2ZrCl_2, Aldrich) was used as the catalyst for all experiments. Toluene and hexane (reagent grade, Merck) were dried using molecular sieves 3A and 4A. Freshly distilled toluene was used as diluent in the polymerizations. Trimethyl aluminum (TMA, 2M in toluene), triisobutylaluminum (TIBA, 1M in hexane) and methylaluminoxane (MAO, 10 wt. % in toluene) were also purchased from Aldrich.

5.2.2 Catalyst Supporting

5.2.2.1 TMA Treatment

The same procedure described in Chapter 4 was used to support the metallocene catalyst onto Cloisite 93A surface. A fraction of TMA-treated Cloisite 93A (Cl93-TMA), without added metallocene, was saved for the in-situ supporting experiments described later in this chapter.

5.2.2.2 Catalyst Supporting

Catalyst was supported onCl93-TMA by adding either 2.0 g (B20) or 1.0 g (B10) of a solution of Cp_2ZrCl_2 in toluene (10 μm/g) per gram of Cloisite 93A in the Schlenk tube. The Cp_2ZrCl_2/Cloisite 93A system was stirred at room temperature overnight. The supporting procedure was completed by washing the support three times with dried toluene. No drying was performed at the end of the last washing step. The Cloisite 93A-supported metallocene (Cl93-Cat) was kept as a slurry, ready for polymerization. Keeping the catalyst as slurry has

the advantage of avoiding clay collapse and promotes better exfoliation during the polymerization step. On the other hand, catalyst aging and deactivation is more likely to happen when the catalyst is kept as slurry than when it is stored as a dry powder. This creates a limitation on the time elapsed between polymerization runs for a designed series of experiment. Therefore, we tried to study the effect of individual polymerization parameters in separate series of experiments within a short time interval using different batches of supported catalysts.

5.2.2.3 Polymerization with supported catalyst

High pressure polymerizations using Cp_2ZrCl_2 supported on Cloisite 93A (B10 and B20) were performed in a 300 mL Parr autoclave reactor with toluene as diluent, according to the procedure described in Chapter 4.

5.2.2.4 Polymerization with in-situ supported catalyst

To investigate the effect of the supporting technique on the in-situ polymerization of ethylene, a simpler supporting technique was also used, called in-situ supporting. In this method, Cloisite 93A was treated with TMA (Cl93-TMA), as for our standard supporting technique, but no catalyst was added to Cl93-TMA before the polymerization. Instead, a given quantity of homogeneous Cp_2ZrCl_2 was introduced into the reactor after the addition of Cl93-TMA. Since the only source of cocatalyst was on the surface of Cl93-TMA, active sites can only be generated in-situ on the support surface before polymerization can take place. This method has the advantage of being more flexible than our standard procedure, since a separate catalyst supporting step is not required, allowing for easier variation of catalyst concentration and type.

5.3 Material Analysis

Material Characterization and analysis was performed according to procedures explained in Chapter 4.

Gel Permeation Chromatography (GPC)

The polymer molecular weight averages and molecular weight distribution (MWD) were measured by Polymer Char high temperature gel permeation chromatography (GPC, located in the Chemical Engineering Department, University of Waterloo). The samples were dissolved to a concentration of 2 mg/mL at 145 °C with 1,2,4-trichlorobenzene and passed with flow rate of 1mL/min through three linear “Polymer Laboratories” columns which were calibrated with polystyrene standard.

5.4 Results and Discussion

The loading of zirconium on B20 and B10 was measured with inductively coupled plasma-atomic emission spectroscopy (*ICP-AES*). The results are shown in Table 5.1. As the concentration of organic modification changes during catalyst supporting (since part of the modifier is extracted from the support, as shown in Chapter 4), the calculations for supporting efficiencies were based on the weight of the clay fraction, excluding the non-clay content from the organoclay or clay-catalyst system. The non-clay content is measured by the weight loss from room temperature to 800°C during TGA analysis. These amounts are reported in Table 5.1 as non-clay content. The Zr concentration before supporting is the number of moles of Zr that we added to one gram of Cloisite 93A and after supporting (the Zr concentration obtained from ICP-AES analysis). Table 5.1 show that when the number of moles catalyst added to Cloisite 93A is decreased by 50% (from B20 to B10), the Zr loading on the clay surface was also reduced by 50%. For both cases, the supporting efficiency is very high, nearing 100%.

Table 5.1. Supporting efficiencies for the two supporting series

Clay Type	Before Supporting			After Supporting			Supporting Efficiency (%)
	Zr/clay (µmol/g)	non-clay content	Zr/pure clay (µmol/g)	Zr/clay (µmol/g)	non-clay content	Zr/pure clay (µmol/g)	
B10	10±1	35.5±2.5	15.5±1.0	13.5±1.3	25.7±2.5	16.4±1.2	**96.3±2.7**
B20	20±2	35.5±2.5	30.9±1.9	26.5±2.6	25.7±2.5	31.1±2.3	**93.9±6.1**

Table 5.2 lists the operation conditions, catalyst activities and corresponding clay contents for several polymerization runs. The ethylene concentration in hexane and toluene were calculated from T_{xy} diagrams created by Peng-Robinson equation of state in Aspen Plus® library.

Peng-Robinson equation of state was shown [122] to best fit the solubility of ethylene in toluene. Under any given condition, the mole fraction of ethylene in the ethylene-toluene binary system, $X_{1,}$ is extracted. Then the concentration ethylene in toluene, $[C_1]$, is calculated from Equation 4.1.

$$[C_1] = \frac{X_1}{(1 - X_1) \cdot M_{w,2} \cdot \rho_2} \tag{5.1}$$

where, $M_{w,2}$ and ρ_2 are molecular weight and density of toluene, respectively. The ethylene concentrations under different temperatures at 2 and 5 bar ethylene pressures are shown in Figure 5.1.

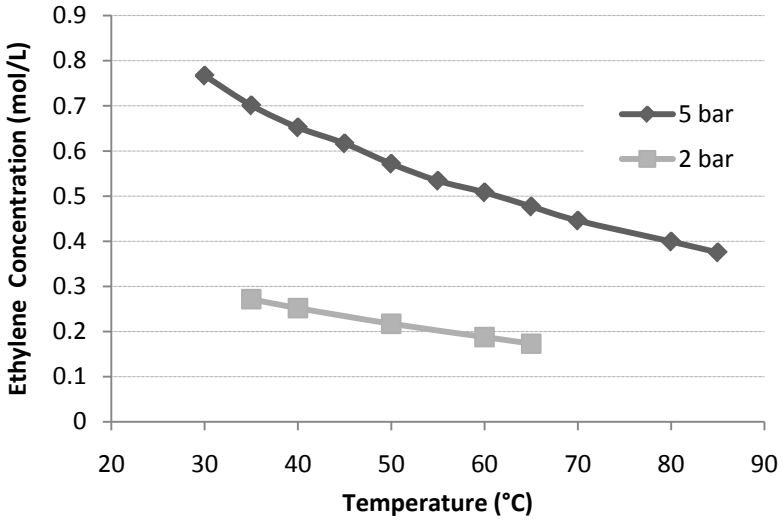

Figure 5.1. Ethylene concentration in toluene under different polymerization conditions produced by Peng-Robinson estimation

5.4.1 Role of TIBA

Table 5.2 shows that different Al/Zr ratios, from 27 to 2,133, resulted in active polymerization runs. The Al content reported in Table 5.2 refers to Al in TIBA (or MAO, in the case of homogeneous polymerizations) used in the polymerization reactor.

The effect of Al/Zr on the polymerization activities from the two supporting series, B10 and B20, are investigated in Figure 5.3. Figure 5.3 shows that there is an Al/Zr ratio that corresponds to a maximum polymerization activity for both B10 and B20, but that the locations of these maxima are not the same. Generally, B20 series resulted in higher polymerization activities. It is also observed that the maximum polymerization activity for B20 is reached in at a lower Al/Zr ratio (58) than for B10 (356 -711).

A more interesting result is obtained when we plot polymerization activity as a function of the number of moles of Al added to the reactor as TIBA, as illustrated in Figure 5.3.Regardless of Zr loading on the clay surface (B10 or B20), the maximum polymerization activity is reached at a certain TIBA concentration. If the concentration of TIBA is further increased, the polymerization rate is reduced. This seems to indicate that TIBA acts initially as an impurity scavenger. But, at the same time it changes the catalytic properties of the supported catalyst. For the B10 polymerization series, the reactor was rinsed with 0.2 g TIBA solution (1.0 M in hexane) prior to polymerization to neutralize reactor contaminants, but no polymerization activity was detected without the addition of TIBA into polymerization reactor (run 219 in Table 5.2).

Table 5.2. Summary of polymerization conditions.

Run No	Supporting Series	Zr Content (µmol/L)	P (bar)	T (°C)	C93-Zr (mg)	TIBA (µmol/L)	Al/Zr	Time (min)	Activity (kg/(mol Zr.hr.[C_2]))	Clay content (wt.%)
84	B20	4.7	5	50	28	960	204	30	19,305	0.72
113	B20	21.7	2	35	123	1,920	88	120	3,131	2.3
114	B20	23.9	2	65	135	1,920	80	80	6,722	2.4
117	B20	25.6	2	50	145	1,920	75	120	3,906	2.2
153	B20	35.3	4	50	200	3,840	109	29	5,903	3
157	B20	35.3	1	50	200	3,840	109	160	3,320	4.5
168	B20	17.7	2	50	100	480	27	27	11,054	3.4
169	B20	17.7	2	50	100	7,670	433	53	5,303	3.6
170	B20	17.7	2	50	100	3,840	217	44	6,684	3.4
171	B20	17.7	2	50	100	960	54	21	15,468	3.1
200	Homo.	2	5	50	0	3,450*	1,725	5	229,030	0
203	Cl93-TMA	1	5	50	100**	1,920	1,920	20	104,944	3.3
204	Cl93-TMA	2	5	50	100**	1,920	960	20	75,083	2.3
205	Cl93-TMA	l.0	5	80	100**	1,920	1,920	20	132,631	3.9
219	B10	2.7	5	50	30	0	0	90	611	-
221	B10	2.7	5	50	30	3,840	1,422	90	3,495	1.5
222	B10	2.7	5	50	30	5,760	2,133	90	2,628	2.9
228	B10	2.7	5	50	30	1,920	711	90	4,290	2
234	B10	2.7	5	60	30	1,920	711	90	7,537	1.35
235	B10	2.7	5	40	30	1,920	711	90	2,074	3.64
236	B10	2.7	5	80	30	1,920	711	60	12,281	1.54
239	B10	2.7	5	50	30	960	400	60	4,006	3.2
242	B10	2.7	5	50	30	1,920	800	90	4,461	1.9
243	B10	2.7	5	50	30	480	200	70	1,279	8.6

*MAO used as cocatalyst; **Cl93-TMA has no Zr loading

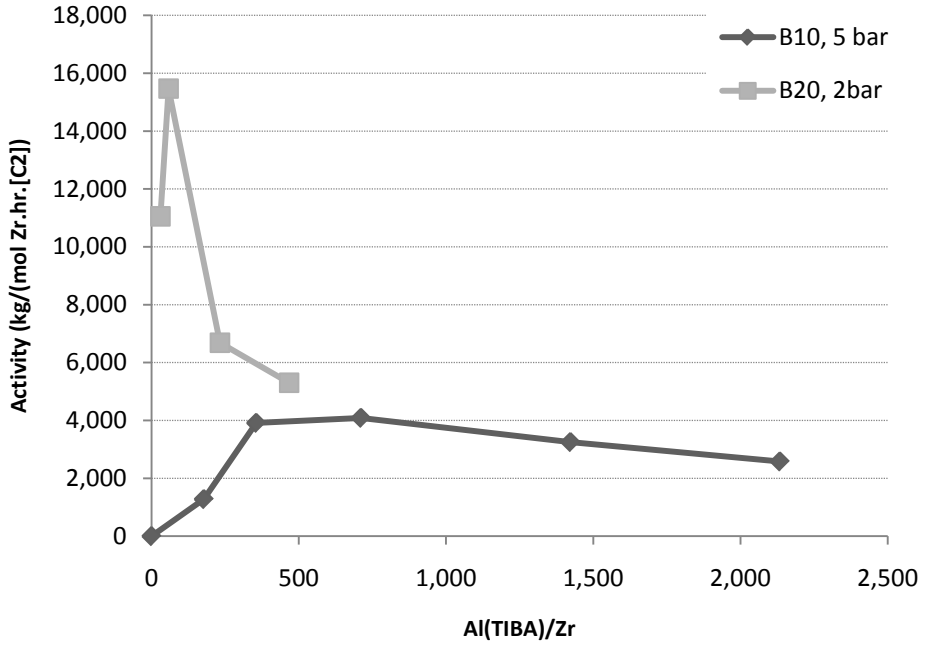

Figure 5.2. Effect of Al/Zr on polymerization activity (polymerization temperature= 50^{o}C, *P*=5 bar for B10; and *P*= 2 bar for B20).

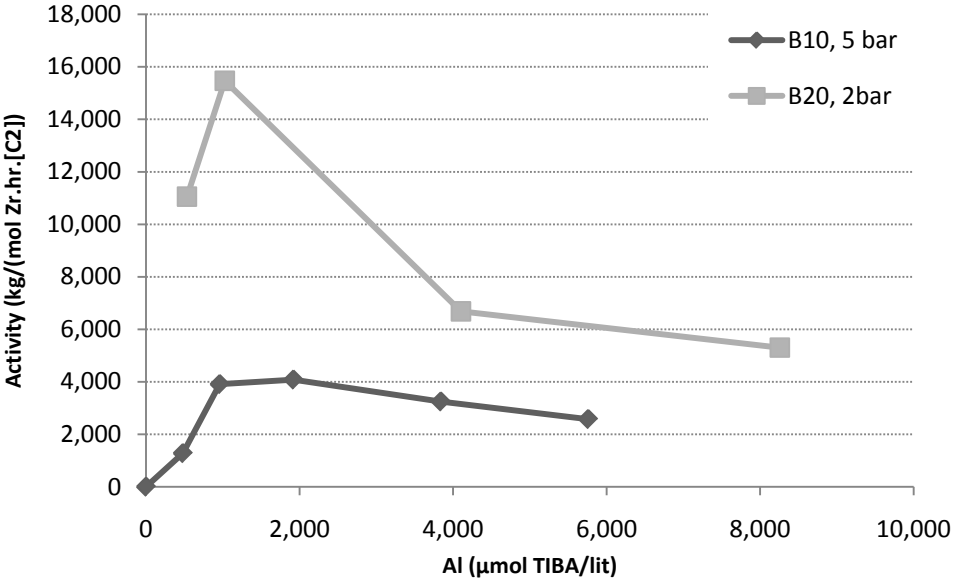

Figure 5.3. Effect of TIBA concentration on catalyst activity (polymerization temperature= 50^{o}C, *P*=5 bar for B10 and *P*=2 bar for B20).

The ethylene consumption profiles for B20 and B10 with varying TIBA concentrations are shown in Figure 5.4 and Figure 5.5, respectively. The trends in the two figures show how

increase TIBA concentration affects ethylene polymerization behavior The monomer uptake profiles for B20 are more sensitive to TIBA concentration. The considerably low Al/Zr ratio by which the maximum polymerization activity was achieved when B20 was used, and considering that both B10 and B20 reached maximum activity in the presence of the same TIBA concentration, suggests that the in-situ made MAO is active during polymerization, but TIBA is needed as impurity scavenger.

In Figure 5.4, it is observed that run 168 (480 μmol/L TIBA) initially had higher ethylene consumption, but a higher deactivation rate than run 171 (960 μmol/L TIBA). Increasing the Al content after this "optimum" value drastically lowered the ethylene uptake profile, as shown in runs 170 (3,840 μmol/L TIBA) and 169 (7,670 μmol/L TIBA).

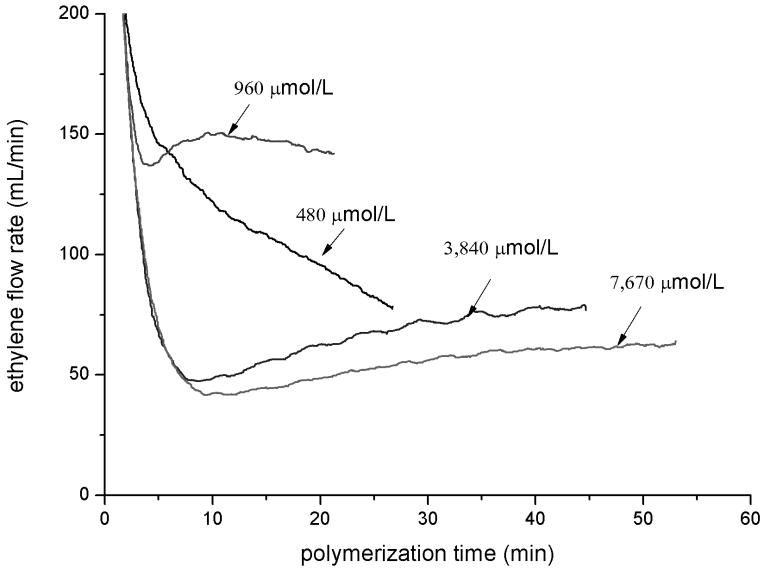

Figure 5.4. Ethylene reactor flow rate profiles in the presence of different TIBA concentrations for B20 (P = 2 bar, T = 50°C); TIBA concentration varies from 0 to 7,670 μmol/L.

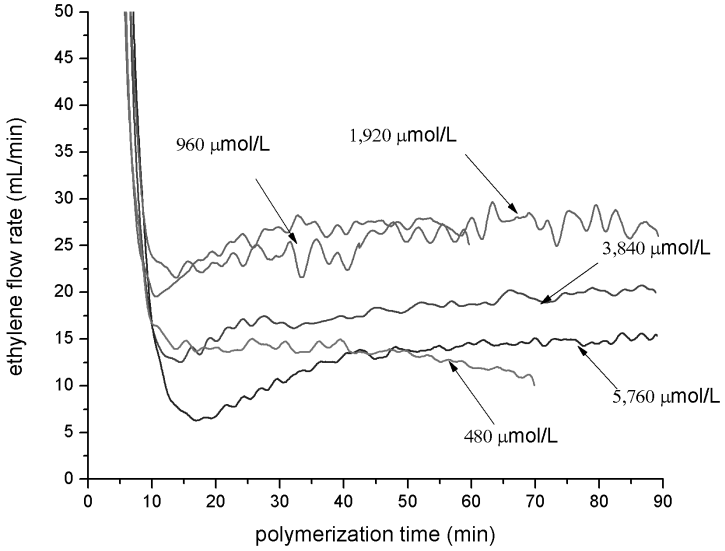

Figure 5.5. Ethylene reactor flow rate profiles in the presence of different TIBA concentrations for B10 (P = 5 bar, T = 50°C).

According to Figure 5.5, almost the same trend is observed for the B10 series at different TIBA concentrations; however, the effect of TIBA concentration on polymerization activity seems to be less significant with B10.

The effect of TIBA concentration on the molecular weight of polymers made with B20 is shown in Table 5.3 and Figure 5.6. Sample 168 (480 μmol/L TIBA) has the highest molecular weight (M_w = 387 kg/mol) and narrowest molecular weight distribution (M_w/M_n = 2.03). By increasing TIBA concentration to 3,840 μmol/L, the molecular weight distribution is extended from the lower end, but the upper limit remains the same. Therefore, M_w becomes 332 kg/mol and M_w/M_n increases to 3.05. Further increase in the TIBA concentration to 7,670 μmol/L shifts the MWD to lower values. M_w decreases to 248 kg/mol, and the MWD becomes slightly narrower.

Table 5.3. Effect of TIBA on the molecular weight averages of polymers made with B20 at T=50°C and P= 2bar.

Run No	TIBA mmo/L	Clay loading (mg)	Al/Zr	M_n (kg/mol)	M_w (kg/mol)	M_w/M_n
168	480	27	27	190.8	387.5	2.03
169	7,670	433	53	88.2	248.4	2.82
170	3,840	217	44	109.0	332.7	3.05
171	960	54	21	-	-	-

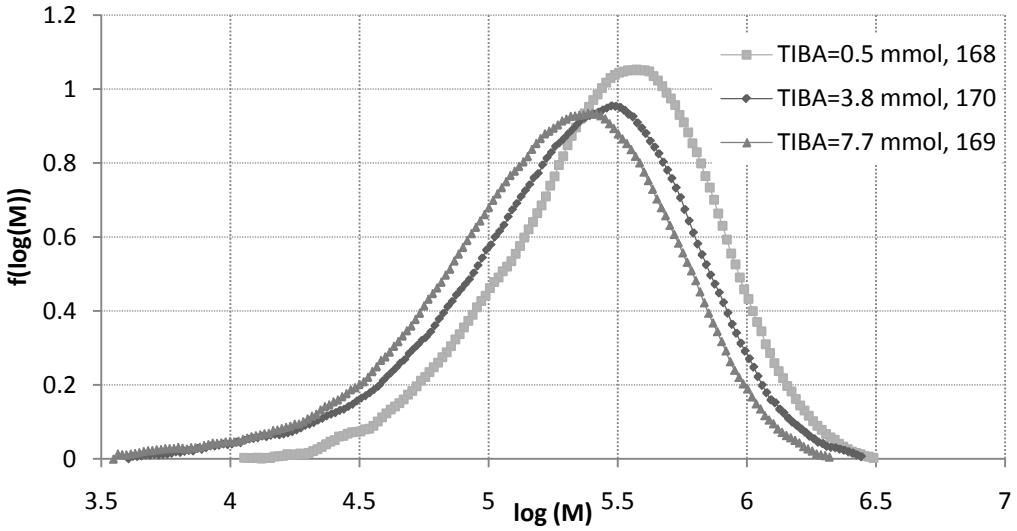

Figure 5.6. Effect of TIBA concentration on the GPC results of polymers made with B20, under *P* =2 bar and *T*=50°C.

The lower polymerization activity with B10 than with B20 was explained by partial deactivation of polymerization catalyst in prolonged contact with the clay surface. Assuming a constant contamination level for the clay surface, B10 with lower catalyst loading would have a larger fraction of deactivated catalyst. To test this hypothesis, we performed polymerization with in-situ supported catalyst, as explained in the Experimental section. The reaction conditions for in-situ supported polymerizations are summarized in Table 5.4. The in-situ supported polymerization runs (203, 204 and 205) had considerably higher activities, more than one order of magnitude, than B10 and B20 catalysts.

Table 5.4. In-situ supported polymerization experiments

Run No	C93-TMA (mg)	TIBA (μ mol/L)	T (°C)	Zr (μ mol/L)	Al/Zr	Activity (kg/(mol Zr.hr.[C_2]))	M_n (kg/mol)	M_w (kg/mol)	M_w/M_n
200	0	3,450*	50	2.0	1,725	229,030	34	173	5.05**
203	100	1,920	50	1.0	1,920	104,944	145	369	2.54
204	100	1,920	50	2.0	960	75,083	169	376	2.22
205	100	1,920	80	1.0	1,920	132,631	108	233	2.16

* MAO is used as cocatalyst

**Broad MWD may be caused by simultaneous polymerization and saturation at the beginning of the polymerization (variable ethylene concentration)

The higher polymerization activities obtained for the in-situ supported catalysts supports the hypothesis of metallocene deactivation due to longer contact times between metallocene and clay in standard supporting technique, assuming that the remaining polar groups or impurities on the clay surface were responsible for deactivating some of the catalysts supported in the B10 and B20 series.

5.4.2 Effect of Polymerization Temperature

The effect of polymerization temperature on ethylene reactor flow rates using the B10 and B20 catalyst series is shown in Figure 5.7 and Figure 5.8, respectively. The kinetics of polymerization with both catalyst batches follows classic acceleration/decay profiles for coordination catalysts. An approximately steady-state rate is reached after the acceleration period for lower temperatures but, for higher temperatures, constant rate decay is observed.

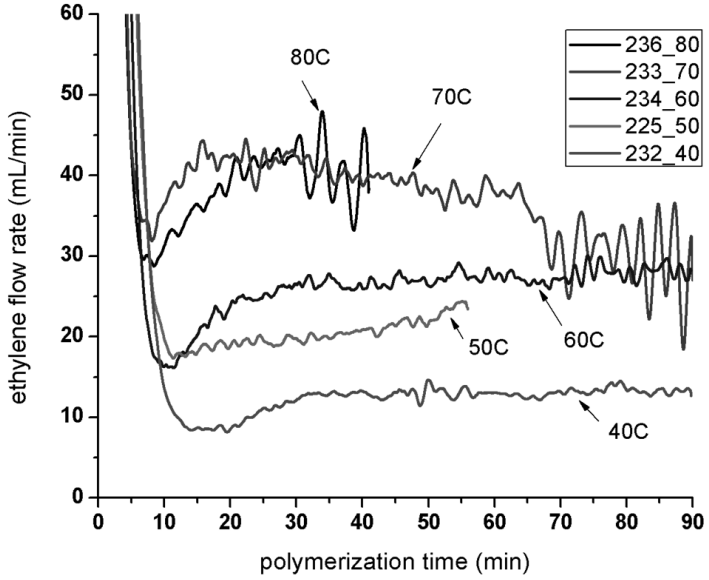

Figure 5.7. Effect of polymerization temperature on the ethylene uptake profiles using catalyst series B10; *P*=5 bar.

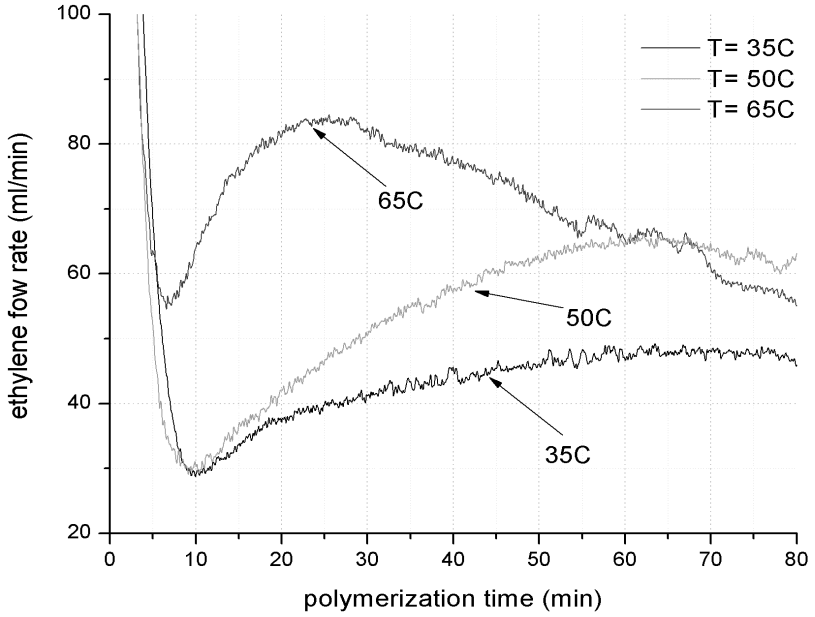

Figure 5.8. Effect of polymerization temperature on the ethylene uptake profiles using catalyst series B20; *P*=2 bar.

The rate acceleration period has been commonly associated with catalyst particle breakup and exposure of active sites for polymerization, while the rate decay behaviour at higher temperatures is related to the thermal degradation of the catalyst sites. In the present case, the acceleration period for the ethylene consumption may be an indication of clay agglomeration break up and exfoliation. As shown in Figure 5.7, polymerizations performed at 70°C and 80°C have poor temperature control at higher polymerization times, which results in polymers with broader MWD (Table 5.5). The effect of polymerization temperature on the molecular weights of polymers made with B20 and B10 are shown in Figure 5.9 and Figure 5.10, respectively, and summarized in Table 5.5.

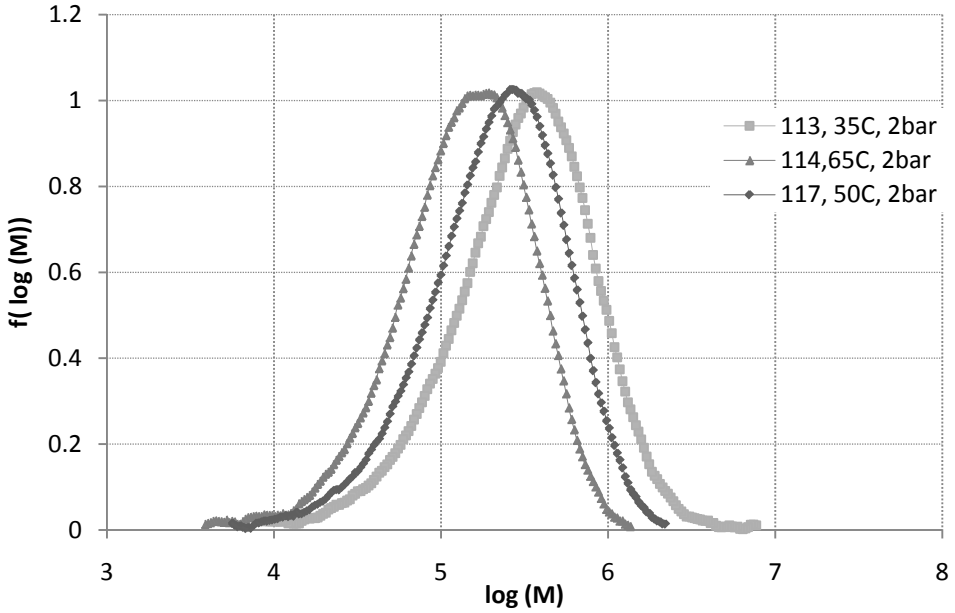

Figure 5.9. Effect of polymerization temperature on the MWD of polymers made with B20 at 2 bar.

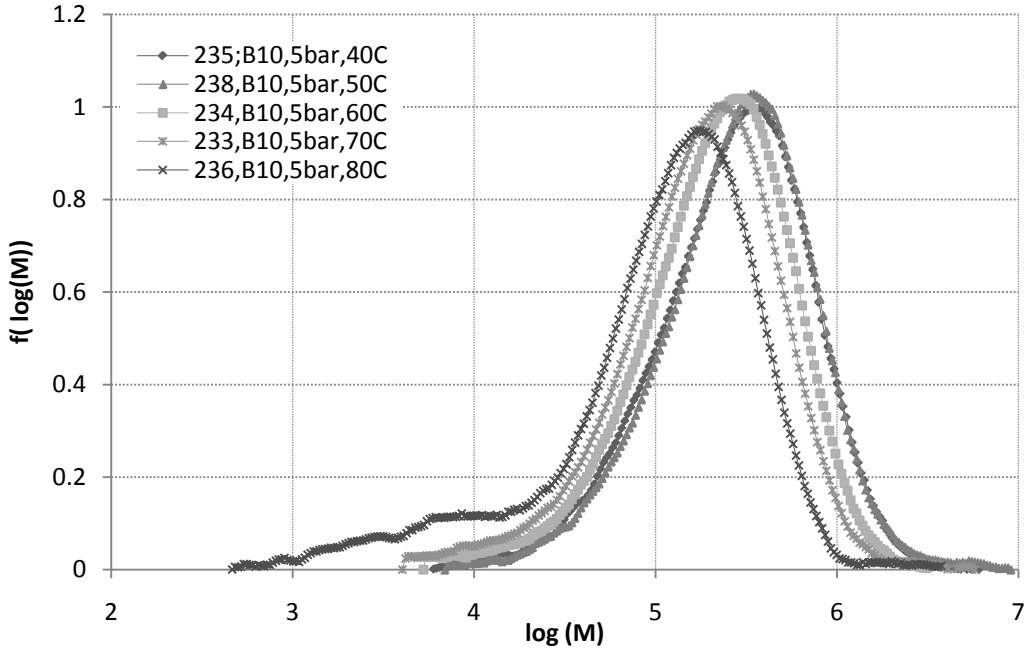

Figure 5.10. Effect of polymerization temperature on the MWD of polymers made with B10 at *P*=5 bar.

Table 5.5. Effect of reaction temperature on polymer properties.

Run No	*T* (°C)	*P* (bar)	Catalyst	Clay loading (mg)	TIBA (mmol/L)	M_n (kg/mol)	M_w (kg/mol)	M_w/M_n
113	35	2	B20	123	1.92	173.6	474.2	2.73
117	50	2	B20	145	1.92	125.3	297.8	2.38
84	50	5	B20	28	0.96	169.4	421.8	2.49
114	65	2	B20	135	1.92	82.2	191.6	2.33
235	40	5	B10	27	1.92	152.1	379.0	2.49
238	50	5	B10	27	0.69	162.0	436.8	2.70
234	60	5	B10	27	1.92	115.6	307.6	2.66
233	70	5	B10	27	1.92	90.0	271.0	3.01
236	80	5	B10	27	1.92	26.3	188.8	7.19

For both catalysts, B10 and B20, usually, increasing the polymerization temperature lowered the polymer molecular weight, but it is noticed from Table 5.5 that in B10 series, sample 235 (T= 40°C, TIBA=0.96mmol/L), resulted in lower molecular weight compared to 238(T=50°C, TIBA =0.69 mmol/L). This indicates that TIBA concentration in the polymerization reactor has a significant effect on the molecular weights. Molecular weight of three samples made with B10 and B20, under different pressures are shown in Figure 5.11. It can be noticed that the Zr loading on the clay support has no significant effect on the molecular weight of polyethylene, but lower polymerization pressures results in lower molecular weights, as expected.

As shown in Figure 5.12, the in-situ supported polymerization series, showed different shapes of ethylene uptake profiles. The ethylene uptake profiles showed higher rates of active site deactivation, while they had still higher rates of ethylene polymerization.

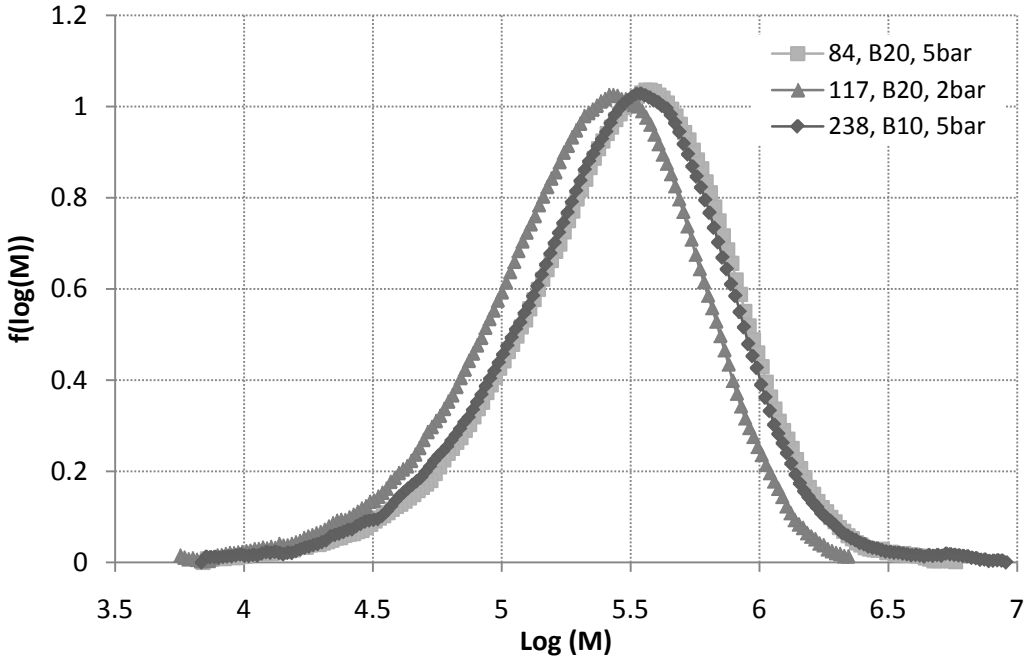

Figure 5.11. Effect of catalyst loading and polymerization pressure on polymer MWD.

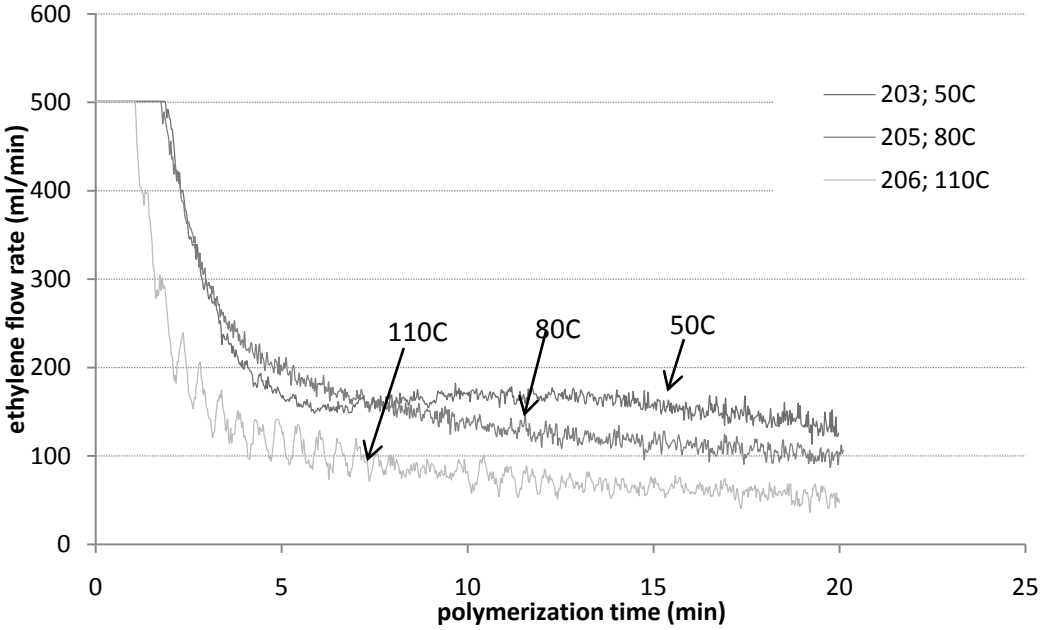

Figure 5.12. Effect of polymerization temperature on the ethylene consumption profiles for polymerization runs using in-situ supported catalyst; catalyst concentration: 1.0µmol/L, *P*=5bars; *T*= 50°C (run 203), 8°0C (run 205) and 110°C (run 206)

5.4.3 SEM Imaging

Scanning electron microscopy (SEM) images of nascent polymer particles from the B10 series are shown in Figure 5.13. Samples prepared at lower temperatures consist of large porous particles made by the agglomeration of primary particles with dimensions varying from 100 to 200 nm, connected by polymer nanofibrils. Particles made at higher temperatures have lower porosity and fewer nanofibrils.

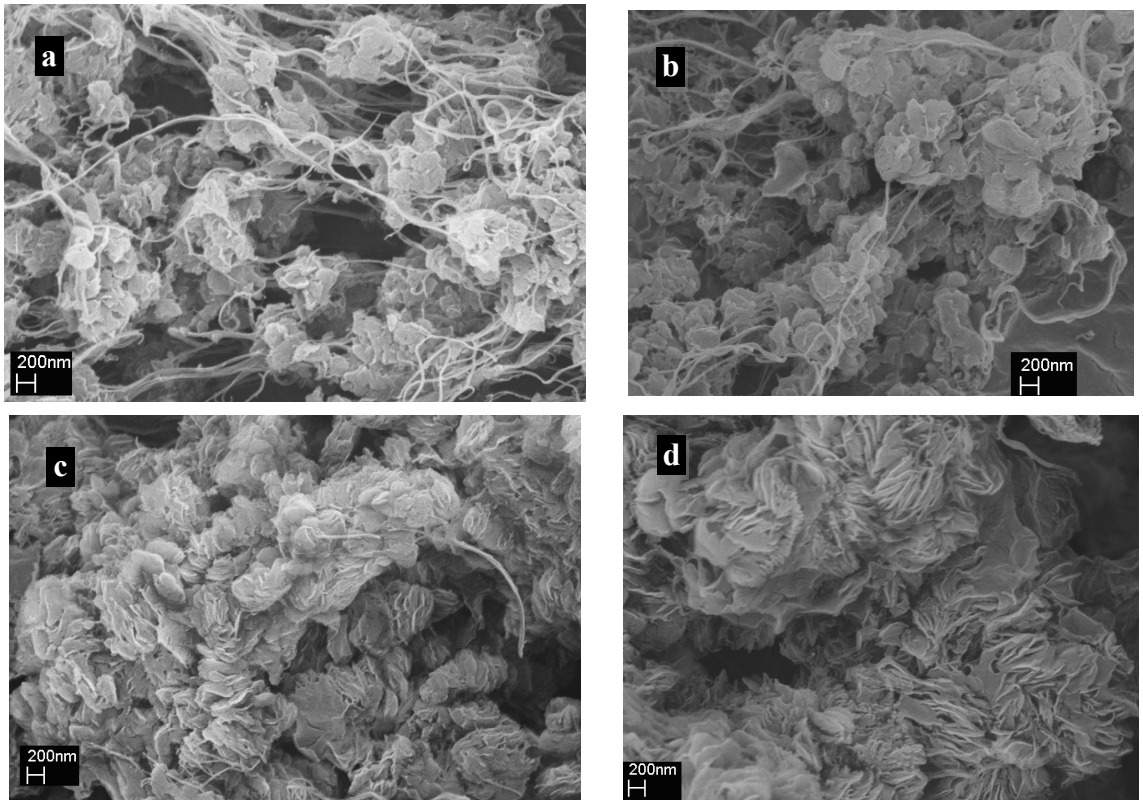

Figure 5.13. Effect of polymerization temperature on the particle morphology of samples made with B10: (a) sample 232, *T* = 40°C, (b) sample 234, *T* = 60°C, (c) sample 233, *T* = 70°C, and (d) sample 236, *T* = 80°C; *P*=5 bar.

SEM images for samples made with the B20 series are shown in Figure 5.14. The powder morphology for polymer made with series B20 does not show a high population of nanofibrils between the primary particle aggregates.

Formation of fibrils is classical for bulk-crystallized high molecular weight polyethylene with the usual folded-chain texture when stretched beyond its yield point [123-125]. In the beginning of heterogeneous polymerization, a thin layer of polymer is formed on the external surfaces of the support via inter-globular cocrystallization which occurs far from the hot polymerization centers. The cocrystallization process depends on the ease of heat removal from the polymerization front and on the relative rates of polymerization and crystallization

[126]. Under conditions of identical polymerization and crystallization rates, a simultaneous polymerization and crystallization mechanism is expected, giving rise to fibrillar morphology with extended-chain macroconformation. Based on this concept and according to the SEM images of polymers made at different temperatures, it seems that at lower polymerization temperatures, the rate of polymerization and crystallization are similar for our system.

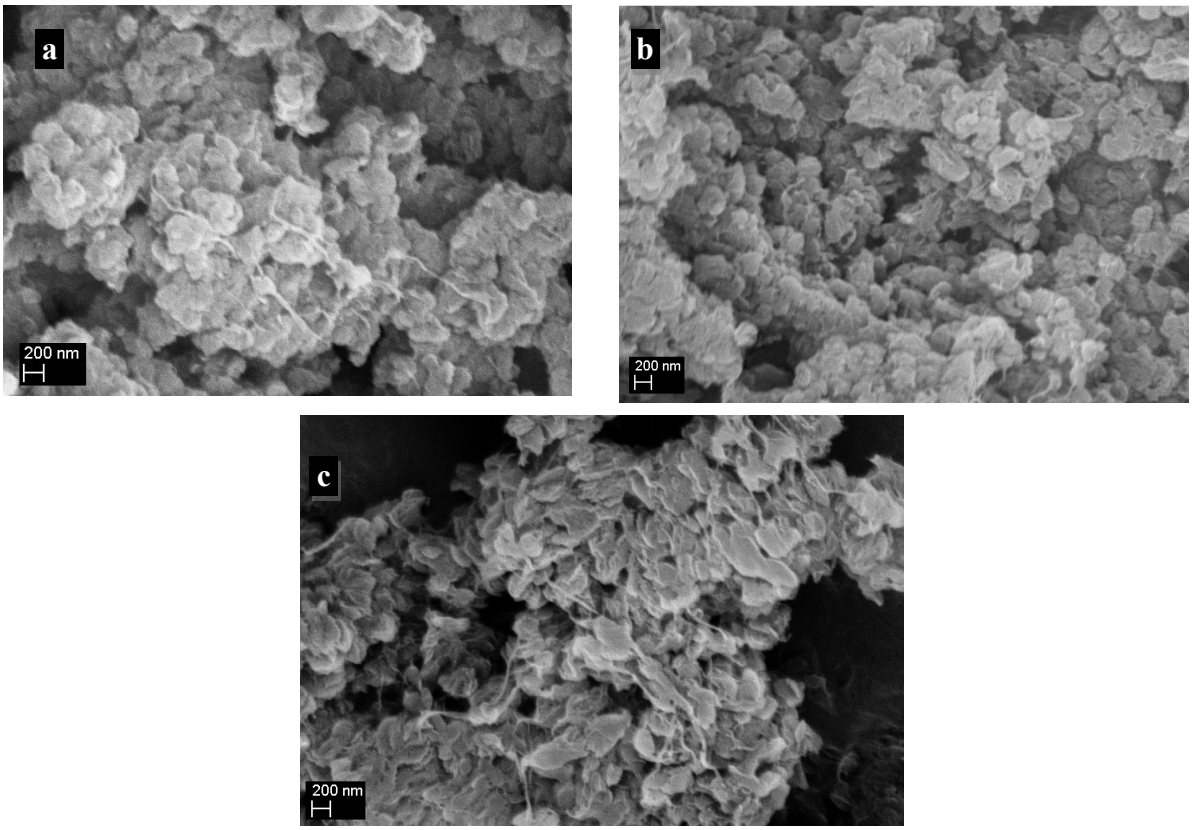

Figure 5.14. Effect of polymerization temperature on the particle morphology of samples made with B20: (a) sample 113, *T*=35°C, (b) sample 117 *T*=50°C, and (c) sample 114, *T*=65°C; *P*=2 bar.

The SEM images for polymers made with B10 and B20 show that as the polymerization temperature increases, the polymer particle morphology transitions from globular to "flatter" particles and finally to leaf-like shapes.
Similar morphological changes are observed for polymers made with in-situ supported catalysts, as shown in Figure 5.15 for polymerization at 50 to 80°C; at 110°C, extraction of active sites and encapsulation of clay particles with homogeneously-made polyethylene seems to take place.

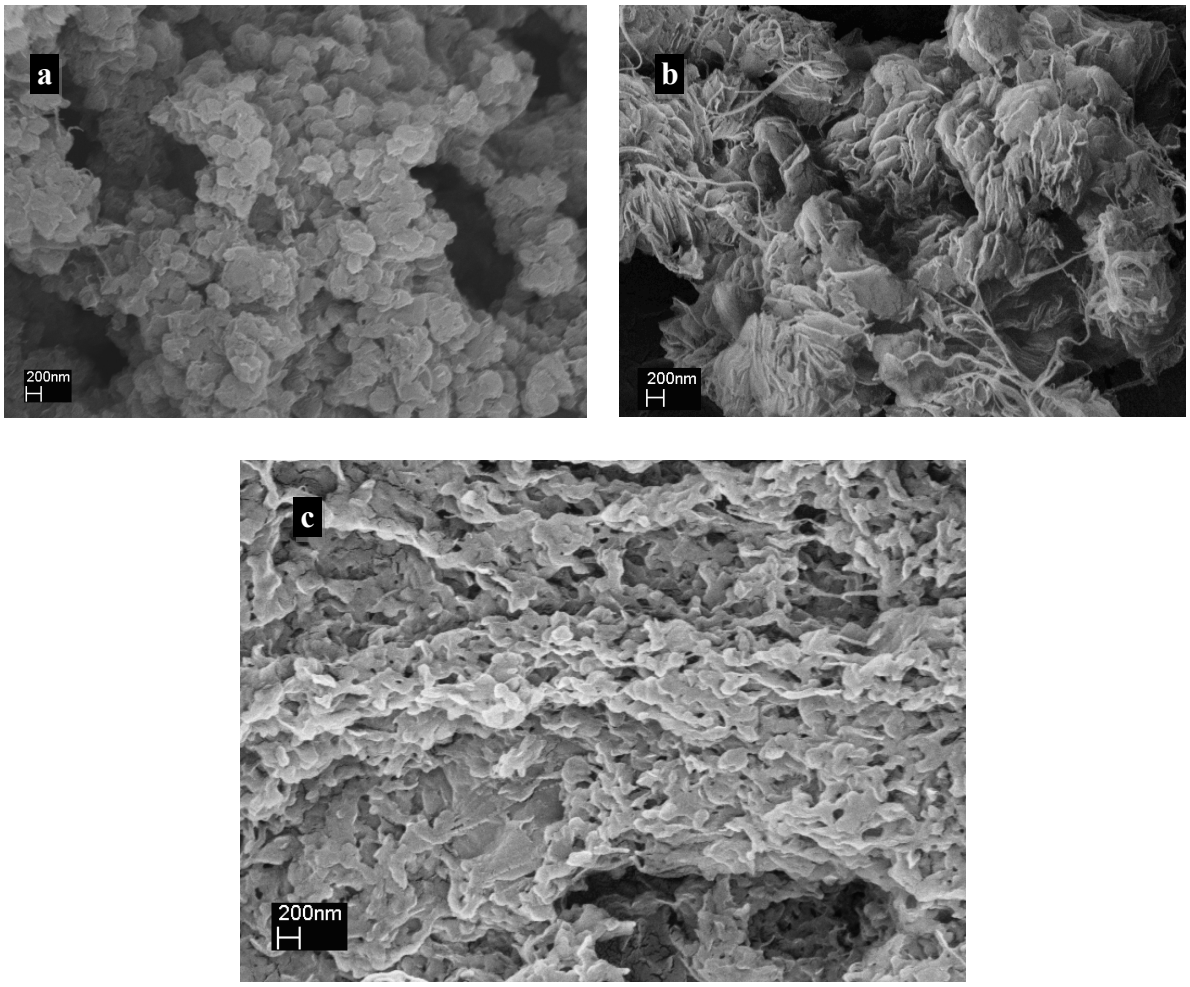

Figure 5.15. Effect of polymerization temperature on the morphology of samples made with in-situ supported catalyst using 1.0 µmol/L Cp_2ZrCl_2: temperatures: (a) 50°C, (b) 80°C, and (c) 110°C; *P*=5bar.

The acceptable morphology of polymers made with the in-situ supported catalyst, and at the same time providing stable and high activity (as 40% high as its homogeneous counterpart, compared to the polymerization activity of run 200 in Table 5.2) polymerization runs and making polymer with higher molecular weights, suggest that TMA-treated C93A is able to act as a cocatalyst and can substitute the conventional MAO cocatalyst.

5.4.4 TEM Imaging

TEM images of two samples produced with B10 at different temperatures, 50°C (run 228) and 80°C (run 236), are shown in Figure 5.16 and Figure 5.17, respectively. The optimum TIBA concentration, 1,920 µmol/L was used to make these samples. Figure 5.16 shows that the particles for the sample made at 50°C are well dispersed in the polymer matrix and no large

clay agglomerates are observed. However, as indicated in location (a), some small clay aggregates are observed.

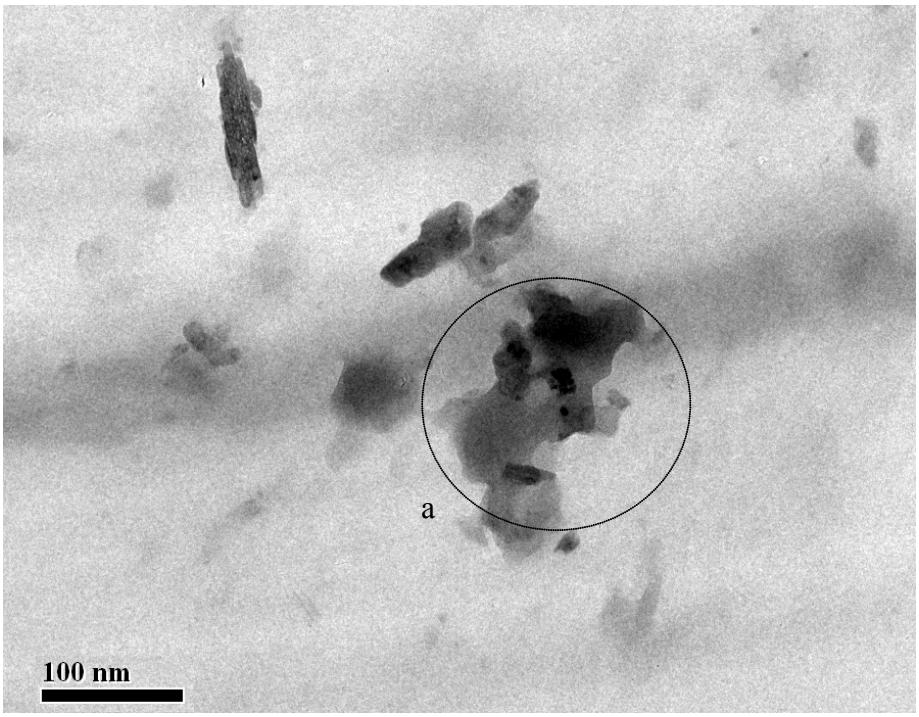

Figure 5.16. TEM image of sample 228, *T*=50°C, B10, TIBA=1920 µmol/L; clay content 2.0 wt.%.

For the sample made at 80°C, Figure 5.17, three different regions (a) aggregation, (b) partial exfoliation, and (c) complete exfoliation, are observed. The sizes of the clay aggregates made at 80°C are larger than those made at 50°C. Remembering that the polymerization at 80°C had poor temperature stability and produced polymer with broad MWD, it is possible that some of the active sites were extracted during the polymerization, leading to incomplete clay exfoliation.

The TEM micrographs of nanocomposites made with the B20 catalyst are shown in Figure 5.18 to Figure 5.21. The TEM images show the effect of TIBA concentration on clay exfoliation. Figure 5.18 shows that the clay layers for sample 168 with minimum TIBA concentration (480µmol/L) are well exfoliated. On the other hand, the TEM images for sample 169 with TIBA concentration of 7,670µmol/L in Figure 5.19 indicate incomplete exfoliation. The dark grey regions in Figure 5.19-a indicate stacking of the clay layers from face view. Figure 5.19-b present a side view of stacked clay layers. The remaining stacking structures in Figure 5.19 suggest that the extra TIBA content favors polymerization in outer surfaces, which are normally in competition with inner surfaces and therefore postpones exposure of inner fixed active centers.

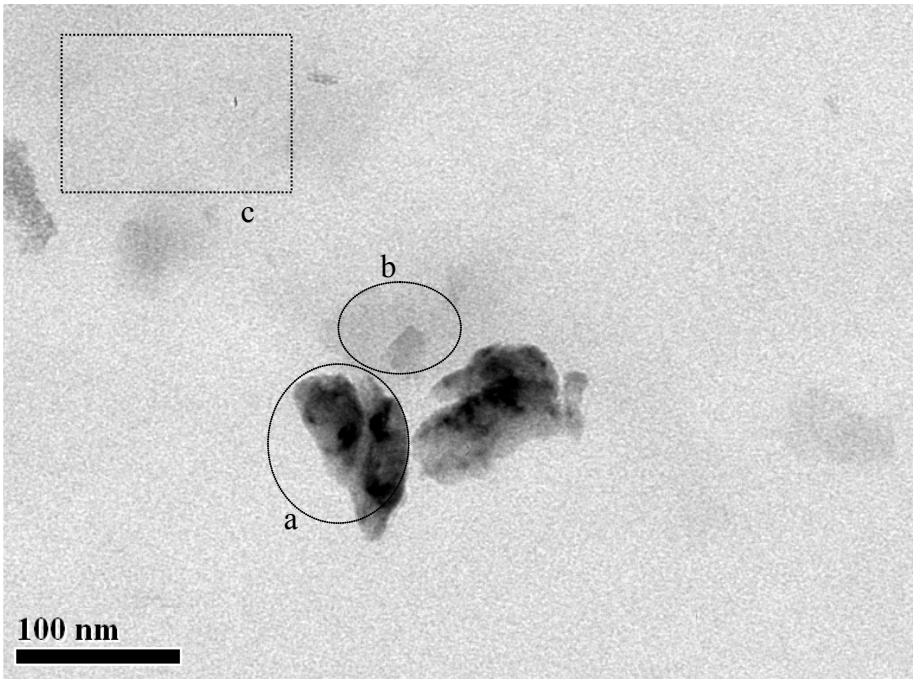

Figure 5.17. TEM image of sample 236, *T*=80°C, TIBA = 1,920 µmol/L; clay content 1.5 wt. %; different morphologies are observed: (a) aggregation, (b) partial exfoliation and (c) complete exfoliation.

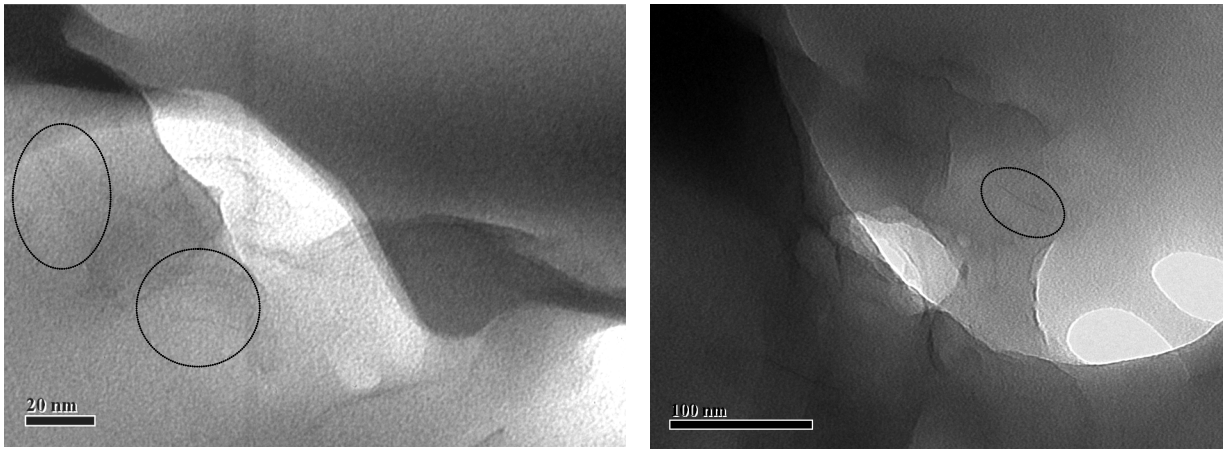

Figure 5.18. TEM image of sample 168, B20, TIBA=480 µmol/L, *T*=50°C; clay content: 3.4 wt.%.

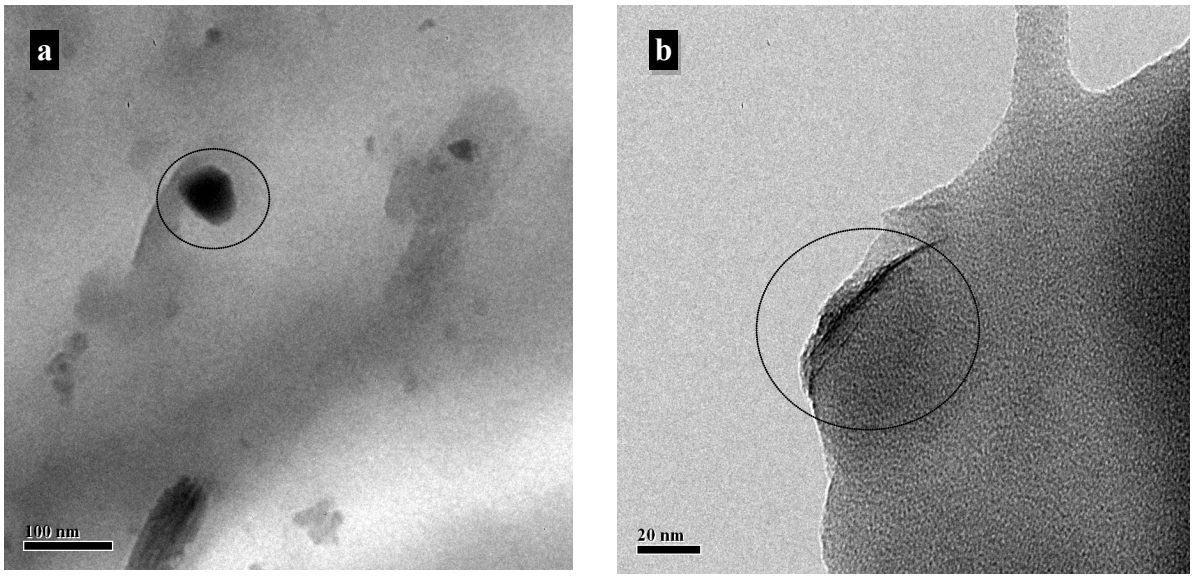

Figure 5.19. TEM images of sample 169, B20, TIBA=7,670 µmol/L, *T*=50°C; clay content: 3.6 wt.% showing incomplete exfoliation; (a) face view and (b) side view.

The effect of temperature on clay exfoliation for nanocomposites made with the B20 catalyst at 35 and 65°C, in presence of 1,920 µmol/L TIBA, was investigated by comparing their TEM images in Figure 5.20 and Figure 5.21. The sample made at the 65°C (sample 114, Figure 5.21) was better exfoliated than the one prepared at 35°C (sample 113, Figure 5.20). It is also interesting to notice that the monomer uptake profile for sample 114 (Figure 5.8) shows a fast acceleration period, achieving the highest polymerization activity among the other samples, which can be linked to its extensive particle break-up and exposure of active sites during polymerization.

The comparison between TEM images within the two catalyst supporting series, B10 and B20, suggests that considering temperature limits at which active sites are extracted from the clay surface, the exfoliation quality is enhanced by increasing the temperature. For samples made with B10, it was shown that a better separation happened upon at higher polymerization temperatures. At the same time, the powder morphologies for samples made with B10 at higher temperatures (70°C and 80°C) are better than those produced at lower temperatures (40°C or 50°C). All polymer-clay nanocomposites made with B20 showed fine powder morphologies and better exfoliation was detected by TEM. By putting together the powder morphologies and TEM images, it can be concluded that the powder morphology is connected to the quality of exfoliation: samples with acceptable exfoliation, appear to have fine powder morphology.

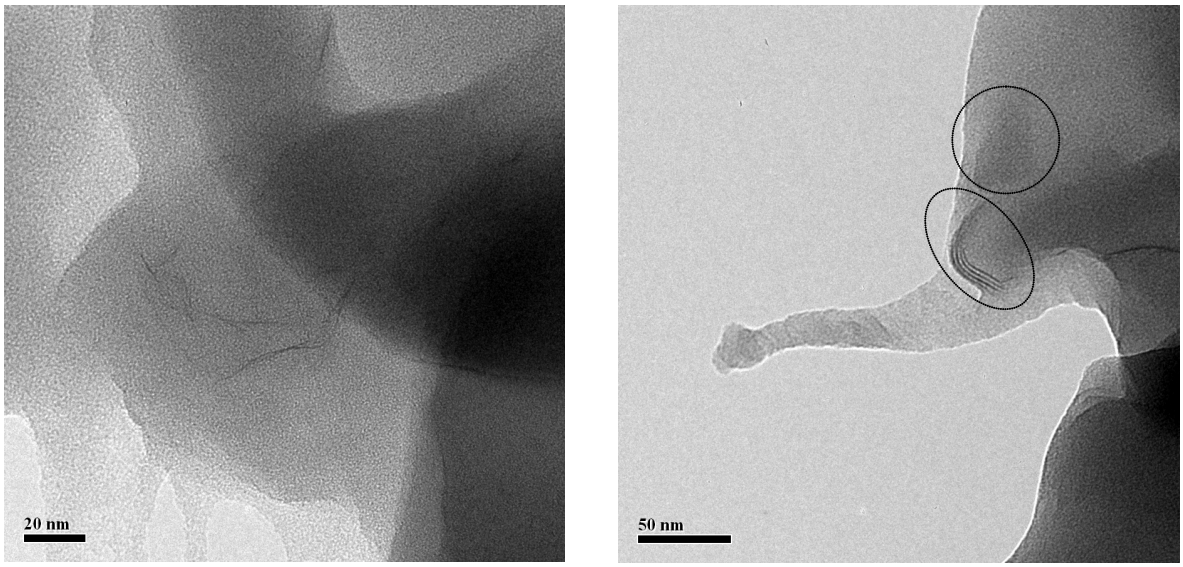

Figure 5.20. TEM images of sample 113, B20 series, *T*=35°C, *P*= 2bars, TIBA concentration = 1,920µmol/L; clay content 2.3 wt.%.

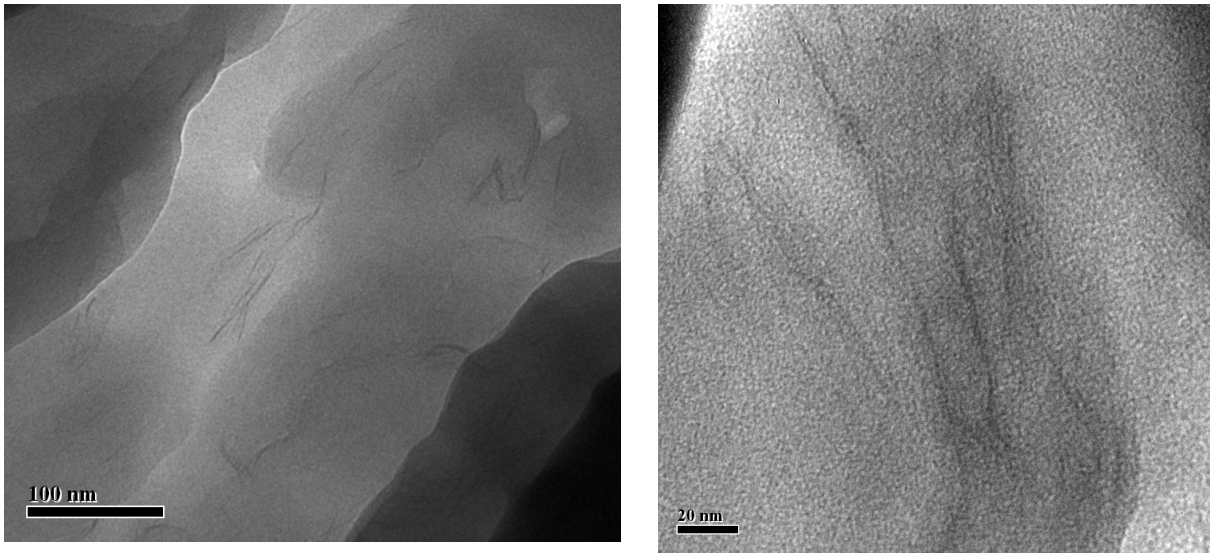

Figure 5.21. TEM image of sample 114; B20, *T*=65°C, *P*=2 bars, TIBA concentration = 1,920µmol/lit; clay content 2.4 wt. %.

By comparing the TEM results for the two series of samples, it can be concluded that before any parameter, the catalyst loading has a key impact on the quality of exfoliation.

A TEM image of sample 203, prepared with in-situ supporting method at 50°C and 5 bars and using 1.0 µmol/L Cp_2ZrCl_2, is shown in Figure 5.22. In this TEM image, no sign of aggregation was found, only traces of impurities from the initial Cloisite 93A.

Comparing TEM images of the nanocomposites made by B10 and B20 to the TEM images of B20 (Figure 5.23) and B10 (Figure 5.24), it can be realized that most of the in-situ polymerization runs resulted in noticeable destruction of the initial clay stacking.

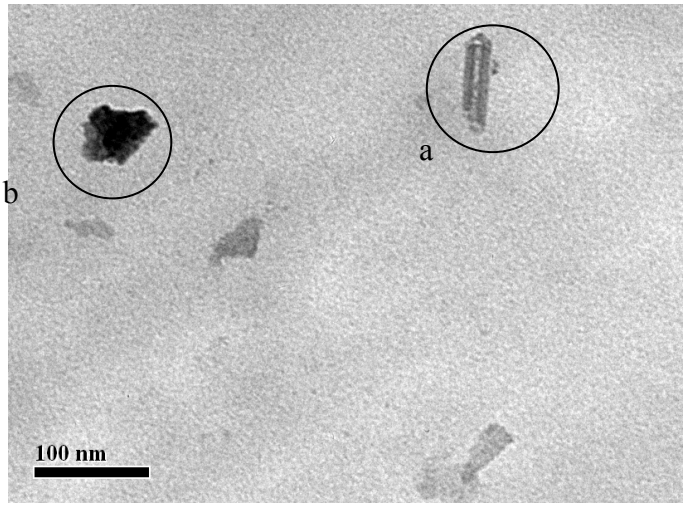

Figure 5.22. TEM image of sample 203, prepared by in-situ supporting method under 50°C and 5 bar polymerization conditions; Clay content: 3.3 wt.%; locations (a) and (b) shows a non-clay impurity remaining in the polyethylene matrix.

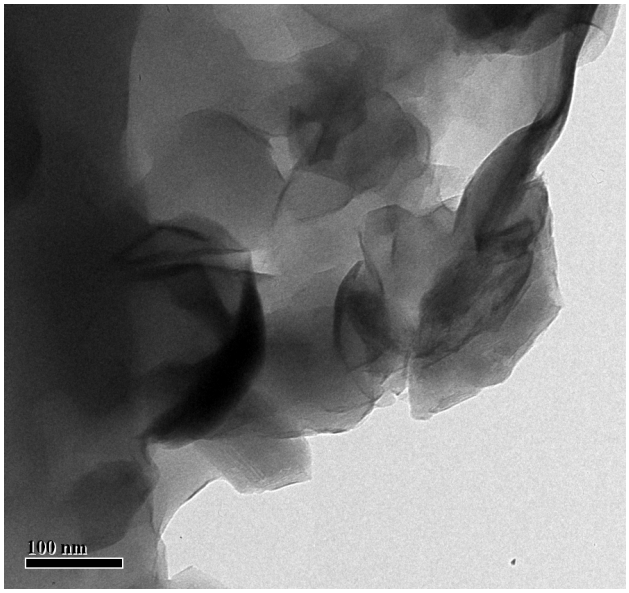

Figure 5.23. TEM image of B20 particles, embedded in epoxy resin for ultra-microtome.

Figure 5.24. TEM image of B10 particles embedded in epoxy resin for ultra-microtome.

5.5 Conclusions

Two series of clay-supported (Cp_2ZrCl_2), with different zirconium loadings, were prepared according to the method described in Chapter 4, and the effect of different polymerization parameters on the quality of nanolayer dispersion, polymerization activity, exfoliation quality and powder morphology were studied.

The similarly high supporting efficiencies for the two supporting series, B10 and B20, suggests that the capacity of clay surface for supporting Zr catalyst is still bigger than catalyst concentrations applied during catalyst supporting. The ability of clay surface to load more catalyst gives more chance for enhancement of the exfoliation quality, as the concentration of catalyst added to the clay support showed to have a major effect on the final properties of the nanocomposite. Higher Zr loading on the surface of Cloisite 93A resulted in higher polymerization activities, better exfoliation quality, and more sensitivity towards other parameters, such as TIBA concentration and temperature.

From the polymerization results it is concluded that the MAO-like compound produced on the clay surface, resulting from the reaction of TMA and water on the clay surface, is able to activate the and stabilize the catalyst; high polymerization activity was obtained in presence of small Al/Zr ratios (with Al from TIBA) and the main role of TIBA in polymerization was shown to be as an impurity scavenger. However, extra TIBA concentration has a negative effect on the polymerization rate and quality of the exfoliation. TIBA also showed significantly negative effect on the molecular weights of polyethylene.

Comparing the polymerization activities using B10 and B20 catalysts with those used as in-situ supported catalyst suggests that a big fraction of active sites are deactivated due to prolonged contact between active site and clay surface in the slurry state. The in-situ supporting method also provided acceptable powder morphologies, high molecular weights and narrow molecular distribution, indicating uniform polymerization on the clay support. Therefore it can be an appropriate alternative method for in-situ polymerization technique.

Increasing the polymerization temperature was shown to favour clay exfoliation and dispersion within the polyethylene matrix. However beyond a certain temperature, polymer or active site extraction and polymerization instability may be resulted.

Chapter 6

Effect of Solvent Type

6.1 Introduction

In Chapter 4, the importance of a proper organic modification of clay surface was shown on the efficiency of in-situ polymerization and quality of clay exfoliation in polyethylene/clay nanocomposites. Considering the mutual effect of solvent – surface modification, question may be raised on the effect of solvent type during catalyst supporting and polymerization on the success of in-situ polymerization.

Principally, the success of in-situ polymerization depends on how easily the catalysts and cocatalyst interact with the clay surface, and how the monomer intercalates into the clay galleries and is polymerized by the supported catalyst. These phenomena should also be influenced by the type of solvent used during clay treatment, catalyst supporting, and polymerization.

It has been shown that during clay modification with organic modifiers, the solvent type influences the intercalation of bulky ammonium cations [51, 57]. Ho et al. [113, 114] showed that the dispersion of organically modified clays in different solvents (ranging from precipitation to intercalation and complete exfoliation) depended on the interaction between the solvent and surface modification on the clay surface.

In this chapter, we compare how replacing toluene (used in Chapters 4 and 5) with hexane influences the behavior of the in-situ polymerization method developed in this thesis.

6.2 Materials& Methods

6.2.1 Materials

The materials used in this chapter are described in Chapter 4. Hexane (reagent grade) was obtained from Merck and dried using molecular sieves 3A and 4A.

6.2.2 Catalyst Supporting

Catalyst supporting on the clay samples was performed using toluene or hexane, according to the procedure described in Chapter 4.

6.2.3 Polymerization Procedure

High pressure ethylene polymerizations were performed using metallocene supported on Cloisite 93A (Cl93Zr-H) according to the procedure described in Chapter 4.

6.3 Materials Analysis

Material Characterization and analysis was performed according to procedures explained in Chapter 4. Gel permeation chromatography (GPC), was performed according to procedure explained in Chapter 5

6.4 Results and Discussion

The dispersion behavior of Cloisite 93A in hexane or toluene is rather different. Cloisite 93A forms a pale pink dispersion in hexane that precipitates faster (in approximately 1 hour), while its dispersion in toluene is pale green, and took longer to precipitate (approximately 1 day) for the same slurry concentration (Figure 5.1).

As discussed in Chapter 4, XRD results showed that when toluene was added to Cloisite 93A, the clay *d*-spacing peaks (for layer stacking) disappear. Ray and Bousmina [127] calculated that the solubility parameter for the organic modification of Cloisite 93A was δ =17.7 $(J/cm^3)^{1/2}$. Since the solubility parameter of toluene (δ = 18.3 $(J/cm^3)^{1/2}$) is closer to δ =17.7 $(J/cm^3)^{1/2}$ than that for hexane (δ = 14.9 $(J/cm^3)^{1/2}$), Cloisite 93A dispersion in toluene are expected to be more stable than in hexane, which would explain the observed longer precipitation times.

Figure 6.1. Dispersion of Cloisite 93A in toluene (right) and hexane (left) (the picture was taken during stirring).

The color of a dispersion of the clay in hydrocarbon solvents can be a measure of its ability for dispersion in polyolefins in production of polyolefin-clay nanocomposites [128]. For clays such as montmorillonite which contain iron in their crystal lattice, a white opaque dispersion is

indication of poor organoclay solvation while a clear green color indicates good solvation. The color development in montmorillonites is caused by presence of Fe^{2+} /Fe^{3+} color centers in the clay crystal lattice[128]. Ferrous (Fe^{2+}) containing aluminosilicates are generally colorless to blue, while ferric (Fe^{3+}) containing aluminosilicates are yellow to tan. A combination of oxidation states give rise to a mixture of blue and yellow color centers which produces an overall green coloration. The ratio of the iron oxidation state affects the color, and the degree of particle surface wetting affects the color intensity. For organoclays, increased solvation quality by means of increased hydrocarbon chain length would be denoted by changed dispersion color. Dispersing an organoclay prepared from a Wyoming montmorillonite which contains iron in the crystal lattice of the clay (e.g., Cloisite 20A) produces a white opaque dispersion in hexane because of poor wetting of the organoclay surface [128]. Similarly in our dispersion experiments, the green dispersion of Cloisite 93A in toluene compared to its pale pink (white) dispersion in hexane is translated to better dispersion of Cloisite 93A in toluene.

The organic modification contents and degradation behavior of Cl93Zr-T (using toluene during the supporting step) and Cl93Zr-H (using hexane during the supporting step) were compared using thermal gravimetric analysis (TGA). The weight loss between 200°C and 800°C was assigned to degradation of the clay organic modification, but it must be kept in mind that clay dehydroxylation (from 450°C to 700°C) falls in this range. Figure 6.2 shows that the initial organic modification content of Cloisite 93A was 36.6 wt%, while it decreased to 17.6 wt% when toluene was used, and to 21.6 wt% when hexane was used.

The initial weight loss, from 40°C to 200°C, can be assigned to the removal of surface absorbed water. When compared to the water content in Cloisite 93A, it becomes a measure of the clay hydrophilicity upon removal of part of the organic modification that takes place during catalyst supporting. Cl93Zr-T, with 6.1 wt% water, has become more hydrophilic than Cl93Zr-H, with 3.4 wt. % water. The initial water content for Cloisite 93A was measured to be 0.6 wt. %. Hence, comparing the water content of Cl93Zr-T and Cl93Zr-H also confirms that a higher fraction of the organic modification was removed from the surface of Cloisite 93A when catalyst supporting was performed in toluene.

To understand the role of solvent interaction on the extraction of the surface modification, Cloisite 93A was washed with hexane and toluene several times, and the modification content was measured using TGA after some washing steps. Figure 6.3 shows that, unlike toluene, hexane is not able to extract the organic modifier from the clay surface. Higher extraction rate of organic modification in toluene compared to hexane explains the different levels of organic modification losses during catalyst supporting in hexane and toluene.

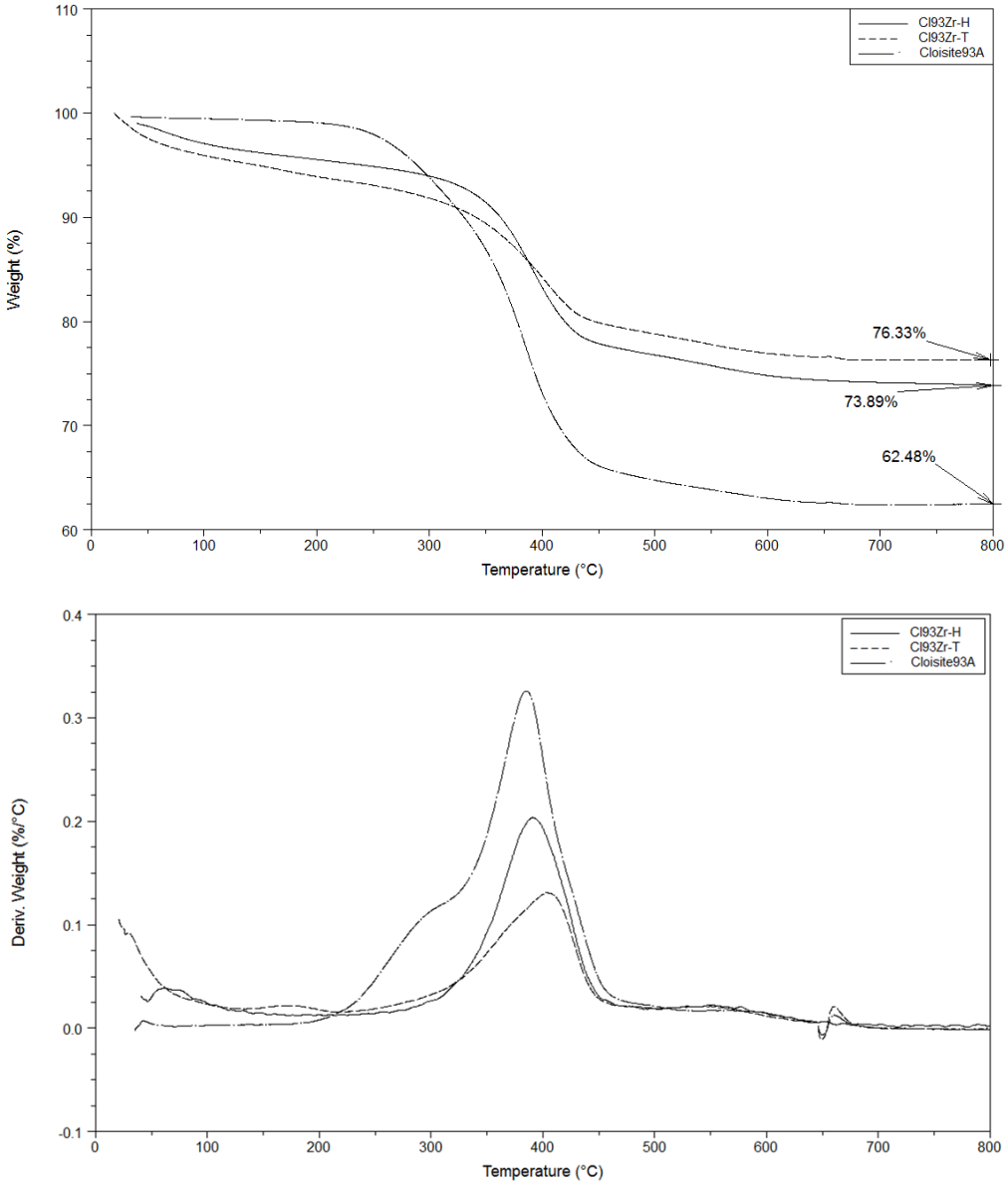

Figure 6.2. TGA (top) and dTG (bottom) results for C93Zr-H, C93Zr-T and Cloisite 93A (reference case).

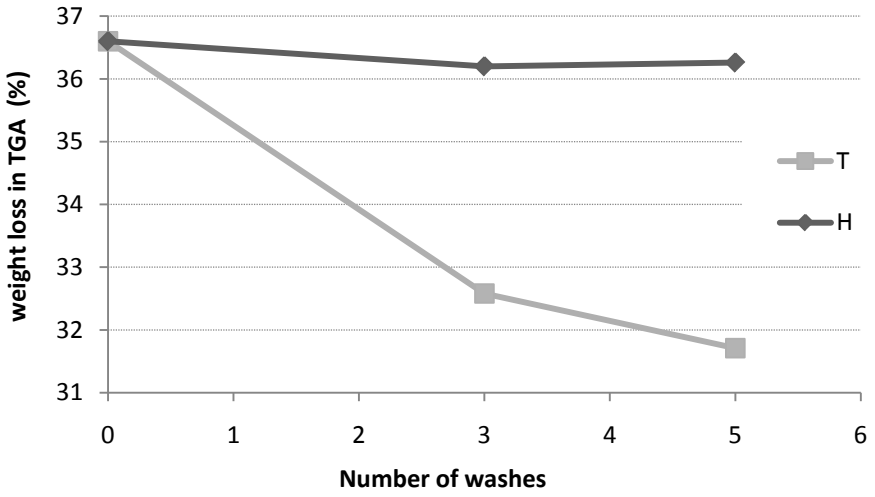

Figure 6.3. Changes in organic modification content of Cloisite 93A by successive washing with (H) hexane and (T) toluene.

Comparing the extents of surface modification losses in blank and TMA reaction modes, it appears that the type of solvent has significantly influenced the extent of physical extraction of the surface modification during the washing steps and the reaction of TMA and other reactant on the surface of Cloisite 93A should not be changed noticeably. It was explained in Chapter 4 that during clay surface modification with tertiary amine to produce tertiary ammonium cation, due to inability of tertiary amine to remove water molecule or exchange the Na^+, some part of tertiary amine remains unreacted and some is bridged to the surface via hydrating water molecules on the clay surface. It was also explained that during TMA treatment, TMA can react with the hydrating water molecules that has bridged the free amine to Na^+ on the clay surface, and therefore leave them with no bonding to the clay surface. It can be speculated that during catalyst supporting in hexane, the free tertiary amine cannot be removed from the clay surface due to poor interaction of hexane with tertiary amine and clay surface.

Comparing the XRD diffraction patterns after the different supporting steps in toluene (Figure 6.4) and hexane (Figure 6.5,) the clay stacking structure has been partly retrieved during catalyst supporting in toluene, due to the loss of organic modification. However in hexane the small remaining stacking structure seems vanish after catalyst supporting.

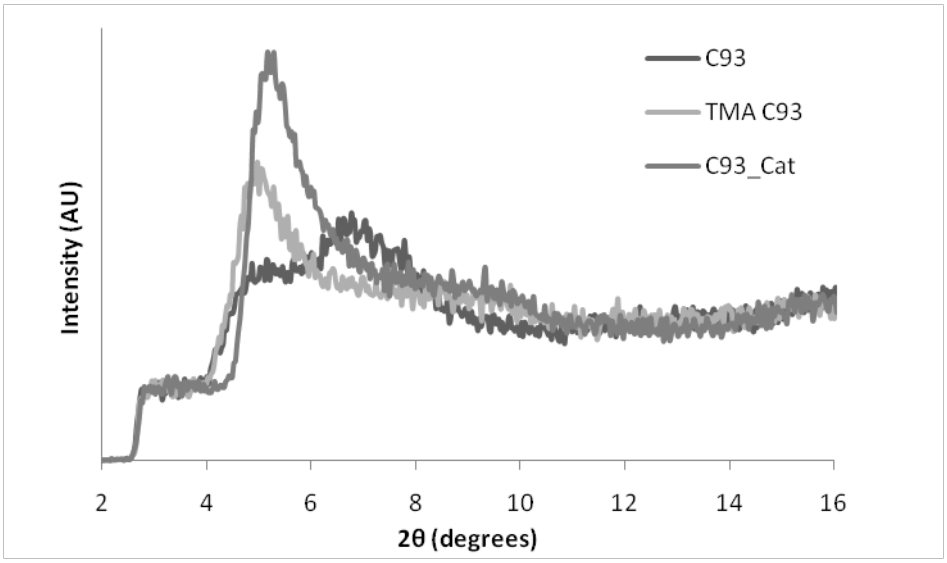

Figure 6.4. XRD diffraction patterns for Cloisite 93A after different supporting steps using toluene as a diluent.

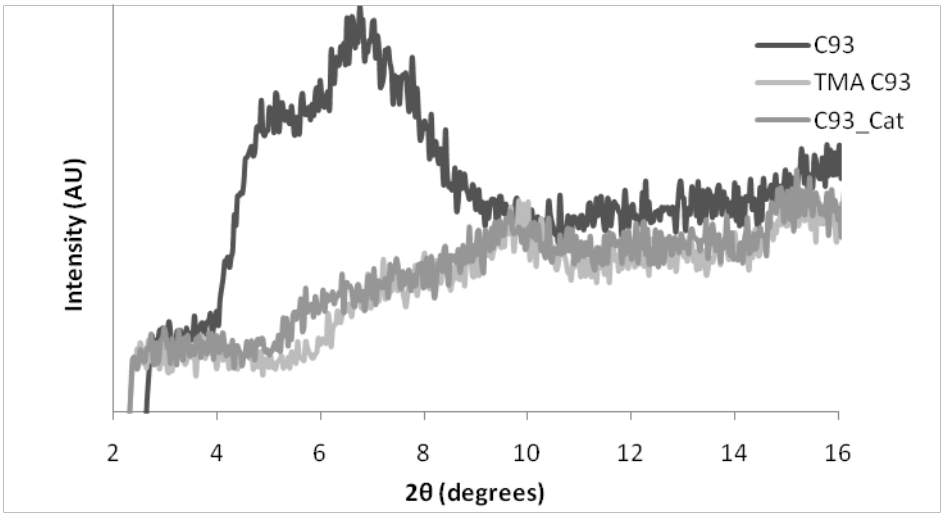

Figure 6.5. XRD diffraction patterns for Cloisite 93A after different supporting steps using hexane as a diluent.

A TEM image of Cl93Zr-H in Figure 6.6 shows that tactoids with different numbers of clay layers are randomly distributed in the embedding resin. While the XRD results indicate complete loss of basal spacing, the TEM images show the layer stacking in Cloisite 93A after catalyst supporting. This TEM results indicates that using XRD results alone is not reliable to quantify clay exfoliation after catalyst supporting. Local stacking orders are observed for Cl93Zr-T in Figure 6.7.

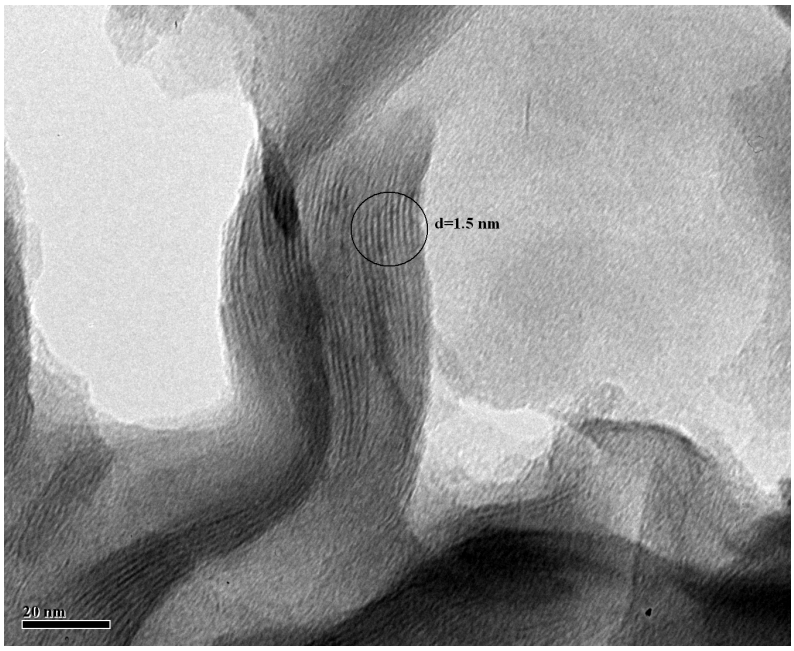

Figure 6.6. TEM image of Cl93Zr-H microstructure.

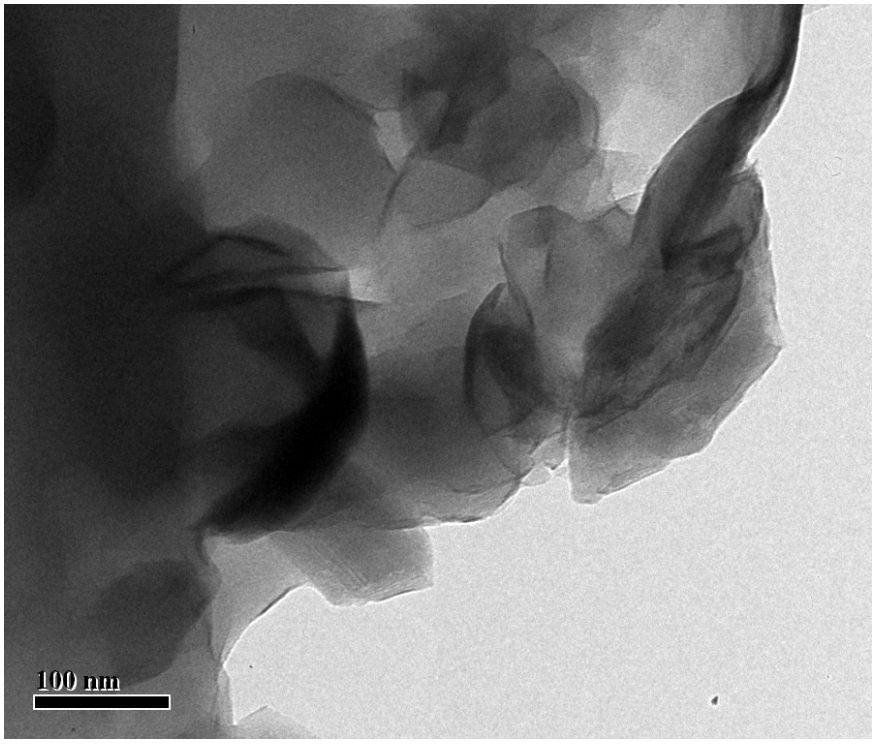

Figure 6.7. TEM image of Cl93Zr-T microstructure.

The Zr loading for Cl93Zr-T and Cl93Zr-H were measured using ICP-AES and the supporting efficiencies are summarized in Table 6.1. Catalyst supporting efficiencies were calculated as explained in Chapter 4. Despite the fact that the solubility parameter of toluene is closer to that of the organic modification of Cloisite 93A, catalyst supporting in hexane and toluene are practically the same, close to 100 percents.

Table 6.1. Supporting efficiencies using hexane and toluene as solvents.

Catalyst	Before Supporting			After Supporting			Supporting Efficiency (%)
	Zr/Cl93A (µmol/g)	non-clay content	Zr/pure clay (µmol/g)	Zr/Cl93Zr (µmol/g)	non-clay content	Zr/pure clay (µmol/g)	
Cl93Zr-T	20±2	35.5±2.5	30.9±1.9	26.8±2.9	21±2	33.9±2.8	**97.3±2.7**
Cl93Zr-H	20±2	35.5±2.5	30.9±1.9	23.2±2.5	25.7±2.5	31.1±2.3	**93.9±6.1**

Theoretically, the maximum catalyst loading on the clay surface would be the cation exchange capacity of the clay support. For Cloisite 93A, the cation exchange capacity of the original clay is about 0.95 mmol or 950 µmol per gram of pure clay. Comparing this theoretical capacity with the quantity of catalyst used per gram of pure clay in these supporting processes (30.9 grams per pure clay) suggests that only a small fraction of catalyst loading capacity of the clay support has been used; therefore, in this level of catalyst loading the type of solvent had no effect on the supporting efficiency. The 100 percent supporting efficiency on the clay surface has been reported previously [70]. In supporting late transition catalyst (2,6-bis[1-(2,6-diisopropylphenylimino)ethyl] pyridine iron(II) dichloride) on the surface of organoclay, Ray et al [70] reported that almost all Zr resided on the clay surface.

The results from polymerizations using Cl93Zr-H under different conditions are summarized in Table 5.2, and compared with a single polymerization run with Cl93Zr-T, knowing from Chapter 5 that in this in-situ polymerization technique, TIBA merely plays the role of scavenger. All polymerization runs (except run 268, using 480 µmol/L TIBA) were performed in the presence of 960 µmol/L TIBA, as a characteristic concentration for this polymerization reactor.

Under the same polymerization conditions, the polymerization run 268 with 480 µmol/L TIBA showed a considerably lower activity than run 267, with 960 µmol/L TIBA (43,358 vs. 69,223 kg/(mol Zr.hr.[C_2])). The decreased polymerization activity in response to increased TIBA concentration is similar to what was observed when Cl93Zr-T was used as polymerization catalyst. Therefore the same function is concluded for TIBA in polymerization using Cl93Zr-H.

In presence of a constant TIBA concentration, different loadings of Cl93Zr-H (runs 264 and 265) and therefore different Al/Zr ratios had no significant effect on the polymerization activity (compared to variations between replicates 265 and 267).

Table 6.2. Summary of polymerization conditions using C93Zr-H and C93Zr-T (as a reference point for comparisons) at *P*=5 bar ethylene pressure

Run No	*T* (°C)	Catalyst	TIBA (μmol/L)	Al/Zr	Diluent	Activity kg/(mol Zr.hr.[C_2])	Clay wt. in reactor (mg/L)	Time (min)	Clay content (wt%)
84	50	C93Zr-T	960	204	Toluene	19,305	187	30	0.72
259	50	C93Zr-H	960	264	Hexane	15,368	147	30	0.92
260	30	C93Zr-H	960	264	Hexane	3,404	147	40	2.20
262	20	C93Zr-H	960	264	Hexane	1,097	147	60	4.00
264	50	C93Zr-H	960	264	Toluene	70,233	147	20	0.30
265	50	C93Zr-H	960	528	Toluene	73,081	73	20	0.29
266	40	C93Zr-H	960	528	Toluene	25,163	73	60	0.24
267	50	C93Zr-H	960	528	Toluene	69,223	73	30	0.20
268	50	C93Zr-H	480	264	Toluene	43,358	73	45	0.21

The polymerization activity of a run performed by Cl93Zr-H (run 264), was compared to one performed under the same conditions but using Cl93Zr-T (run 84 as a single point acquired from other sets of experiments) had a higher activity by a factor of 3.6. This proposes a great improvement in the supporting success upon change of the solvent in the supporting process.

Generally, under the same conditions, polymerization with Cl93Zr-H in toluene yielded significantly higher activities than polymerization in hexane. For example, polymerization activity of run 244 (50°C, TIBA= 960 μmol/L, in toluene) was 4.5 times higher than polymerization activity in run 259 (50°C, TIBA= 960 μmol/L, in hexane).

The ethylene consumption profiles of polymerization runs using Cl93Zr-H in toluene in Figure 6.8 show continuously decreasing rates. This is unlike the observation in Chapter 5 for polymerization runs using Cl93Zr-T that showed initial accelerating ethylene consumption rates. The initial increasing rate may be associated with particle break-up [129], and therefore it can be assigned to the intercalative polymerization and exfoliation. The absences of this accelerating period, suggests absence of significant particle break up during polymerization with Cl93Zr-H in toluene. The higher polymerization activities with Cl93Zr-H, compared to those with Cl93Zr-T, also indicates a significant effect of the solvent type on the catalyst supporting efficiency, catalyst activity and particle break up behavior.

The comparatively high polymerization activity using Cl93Zr-H, indicates that a major fraction of water content on the surface of clay has been consumed to produce MAO with higher quality; as a result of poor interaction between hexane and the clay surface in Cloisite 93A, the rate at which hydrating water reacts with TMA is expected to be considerably lower, than supporting in toluene. The milder reaction between TMA and hydrating water on the clay surface would result in more active MAO.

The poor interaction between hexane and surface modification in Cloisite 93A also resulted in smaller extraction of non bonding tertiary amine from surface of Cl93Zr-H. During ethylene polymerization with Cl93Zr-H in toluene, the remaining tertiary amine on the clay surface enhances the interaction between toluene and catalyst active sites. Therefore, Cl93Zr-H can be exfoliated upon contact with toluene, before polymerization started. Consequently, individual layers are exposed to monomer from the beginning of the polymerization. This mechanism can explain the absence of the initial acceleration period during polymerization.

Unlike polymerization in toluene, ethylene polymerization using C93Zr-H in hexane, as shown in Figure 6.9, has an initially accelerating ethylene uptake profile, regardless of the polymerization temperature. This behavior may result from the poor interaction between hexane and the remainder of the organic modification on the surface of Cl93Zr-H.

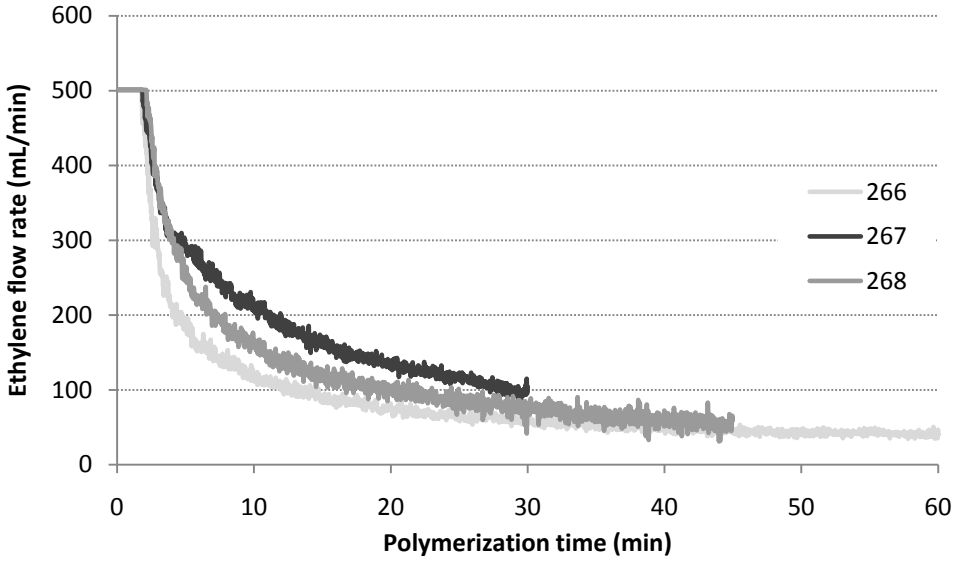

Figure 6.8. Ethylene uptake profiles for polymerization runs using C93Zr-H in toluene slurry under 75 psi ethylene pressure and (266) 40°C and TIBA =960 µmol/L, (267) 50°C and TIBA = 960 µmol/L and (268)50°C and TIBA =480 µmol/L

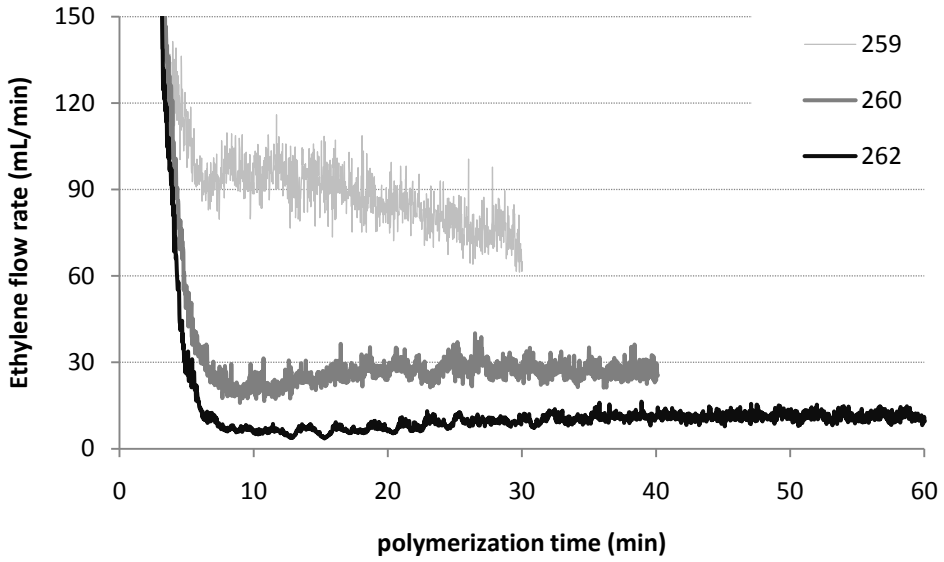

Figure 6.9. Ethylene uptake profiles for polymerization runs using C93Zr-H in hexane as diluent; polymerization conditions: TIBA =960 µmol/L, *P*=75 psi and *T*=(259) 50°C, (260) 30°C and (262) 20°C

Different ethylene uptake profile shapes in polymerization with C93Zr-H in different solvents suggests that C93Zr-H agglomerates break up depends on the type of polymerization solvent. The significantly lower polymerization activities in hexane, suggests that the concentration of accessible active sites in ethylene polymerization in hexane is much lower than that in toluene.

6.4.1 Polymer Microstructure and Morphology

The molecular weight distributions (MWD) of polyethylene produced with Cl93Zr-H was determined by gel permeation chromatography (GPC) and summarized in Table 6.3. As a reference for comparison, the GPC results for one sample made by C93Zr-T (Run 84) is also shown in Table 6.3. Comparing results for samples made at 75 psi and 50°C, in the presence of 960 µmol/L TIBA, using Cl93Zr-H (samples 265 and 267 as replicates) and Cl93Zr-T (sample 84) shows that samples made with Cl93Zr-H had higher molecular weights (M_w =524.7 kg/mol for run 265 vs. M_w = 421 kg/mol for run 84). The corresponding molecular weight distributions for samples 84 (made by Cl93Zr-T) and 265 (made by Cl93Zr-H) are shown in Figure 6.10.

Table 6.3. Molecular weight measurements for polyethylene made by C93Zr-H under 75 psi ethylene pressure

Run No	T (°C)	Catalyst	Clay wt. (mg)	TIBA (µmol/L)	Activity kg/(mol zr.hr.[C_2])	M_n (kg/mol)	M_w (kg/mol)	M_n/M_w
84	50	C93Zr-T	28	960	19,305	169.4	421.8	2.5
265	50	C93Zr-H	11	960	73,081	209.0	524.7	2.5
266	40	C93Zr-H	11	960	25,163	227.7	594.3	2.6
267	50	C93Zr-H	11	960	69,223	192.0	497.0	2.6
268	50	C93Zr-H	11	480	43,358	190.1	518.2	2.7

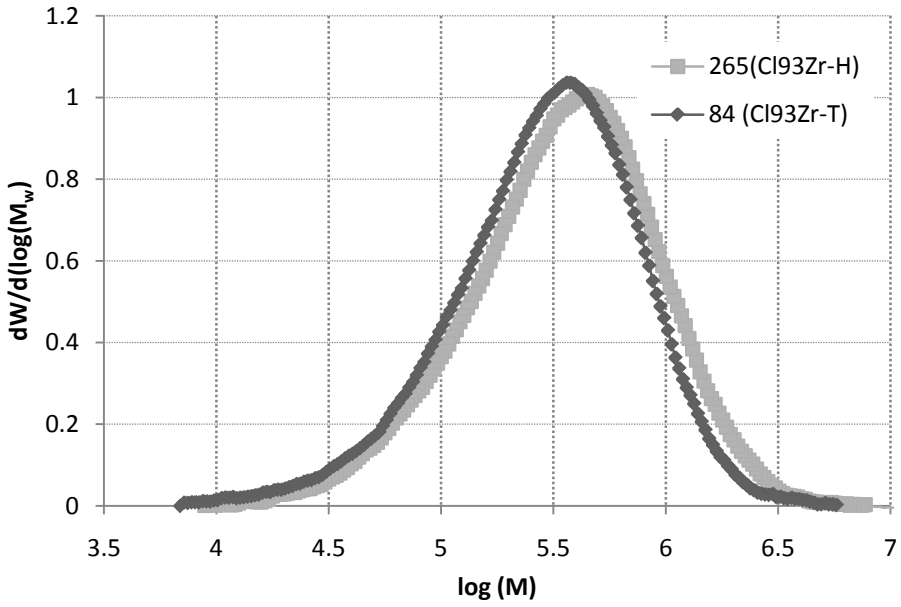

Figure 6.10. Molecular weight distributions of polyethylenes made with different catalyst systems at *P*= 75 psi, and *T*= 50°C in presence of 960 µmol/L TIBA, (84) C93Zr-T and (265) C93Zr-H.

The morphology of nascent particle was studied by SEM. The micrographs of sample 267 prepared with Cl93Zr-H are shown in Figure 6.11. The particle morphology of these samples is similar to those made with Cl93Zr-T. The SEM images of the powder particles and the submicron dimensions of the primary particles suggest a fine dispersion of clay layers.

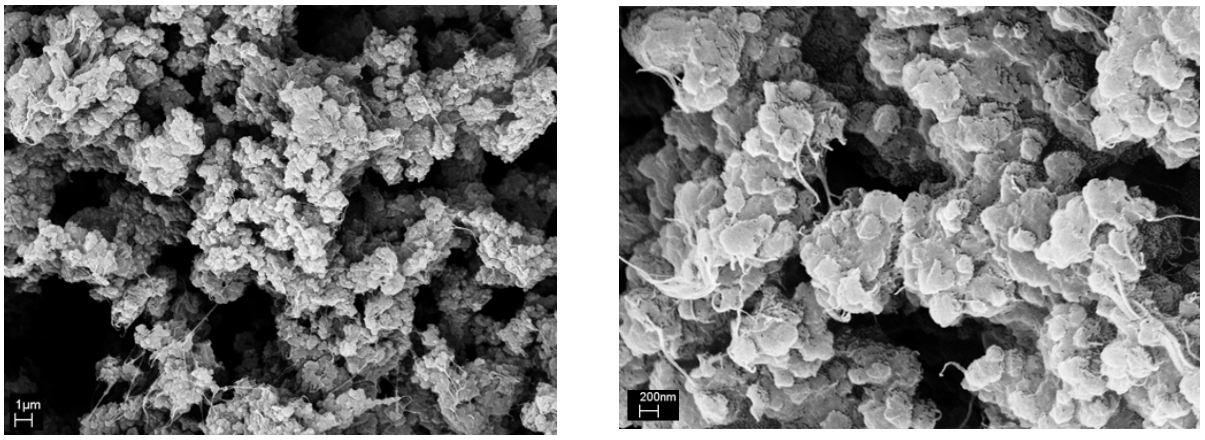

Figure 6.11. SEM micrograph for sample 267 made using C93Zr-H (Polymerization temperature = 50°C, *P*=75 psi, TIBA = 960µmol/L); final clay content= 0.2 wt. %.

The exfoliation and dispersion of clay in the polyethylene was studied by TEM. The micrographs of samples made with C93Zr-H in hexane (262) and toluene (267) under different conditions are shown in Figure 6.12 and Figure 6.13, respectively. According to the TEM images, no sign of layer stacking or agglomeration is observed. However, traces of individual layers and some impurities can be observed.

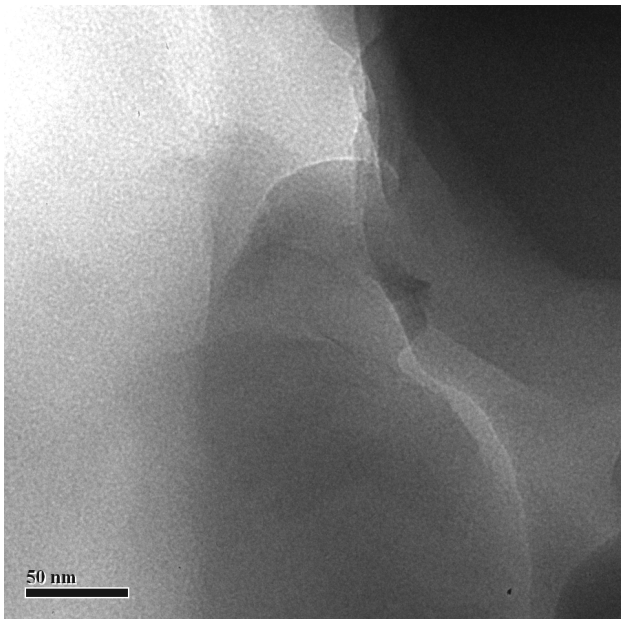

Figure 6.12. TEM image of sample (262) made using C93Zr-H, (Polymerization temperature = 20°C, *P*=75 psi, TIBA = 960µmol/L) in hexane, clay content = 4 wt.%.

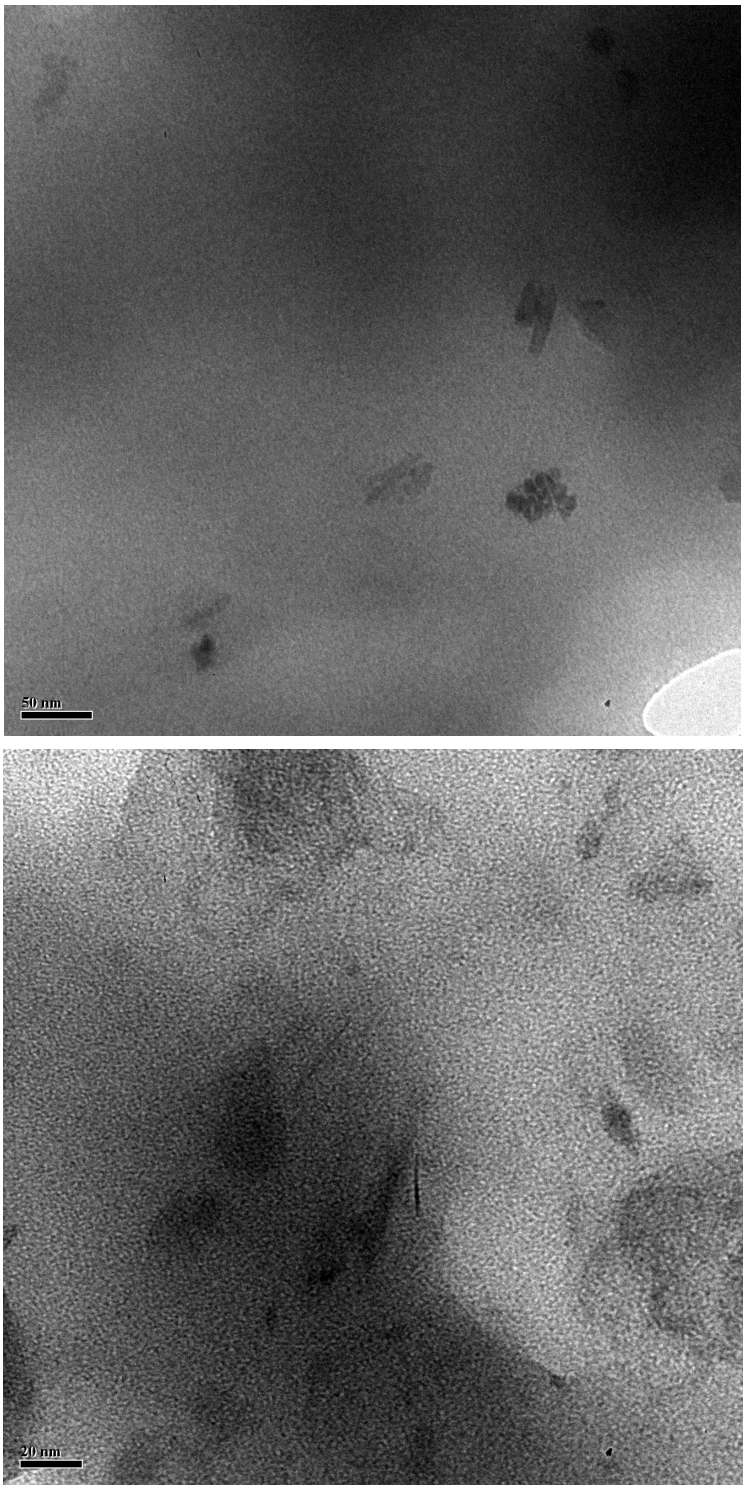

Figure 6.13. TEM images of sample (267) made using C93Zr-H (Polymerization temperature = 50°C, *P*=75 psi, TIBA = 960µmol/L), in toluene; final clay content= 0.2 wt. %.

6.5 Conclusion

Cp_2ZrCl_2 was supported on the surface of Cloisite 93A using our novel supporting technique in hexane as solvent. It was found that the type of solvent had an undeniable effect on the overall behavior of the in situ polymerization, from supporting efficiency to polymerization and polymer microstructure.

It was found that despite a decreased interaction between surface modification and solvent, high supporting efficiency were obtained, together with acceptable particle morphology after polymerization. The TEM images and the ethylene uptake profiles, when polymerization was performed in toluene suggest better exfoliation of the clay layers before onset of polymerization, due to compatibility between toluene and clay surface, after supporting in hexane (C93Zr-H).

Lower polymerization activities, even after normalization to monomer concentration in hexane, indicate the importance of compatibility between organic surface modification and the carrier solvent.

Concerning theoretically high supporting capacity of Cloisite 93A (900 μmol/g pure clay), compared to the level of catalyst loading used in our experiments (30 μmol/g pure clay), it is not possible to make any conclusions on the effect of solvent on the supporting efficiency with low catalyst loading in this work. In order to be able to more clearly acknowledge the effect solvent, higher catalyst loadings are recommended.

Chapter 7

Overall Conclusions

A diffusion-reaction model for olefin polymerization with catalyst supported on the spaces between the clay layers was developed and used to study the effect of intraparticle monomer mass transfer limitations. It was shown that due to the small clay nanolayers dimensions, interlayer polymerization was not diffusion controlled. Therefore, assuming a uniform distribution of active sites on the clay surfaces, a uniform monomer concentration distribution and clay layer expansion rate are expected.

A novel catalyst supporting method was developed for the immobilization of metallocene catalyst onto the clay interlayer surface. This method had only been previously reported to support catalysts onto unmodified sodium montmorillonite clays which contain considerable amount of surface water to react with trimethylaluminum, producing in-situ MAO on the clay surface that is needed to active the catalyst. We extended this methodology to clay samples with different types of organic modification. Among the six different organoclays studied, only the one modified with a tertiary ammonium salt (Cloisite 93A) produced an effective catalyst for ethylene polymerization. The other five clays, modified with quaternary ammonium salts, led to poorly active or completely inactive catalysts.

It was concluded that the tertiary ammonium modification of the clay surface not only facilitates the supporting process via enhanced solvent-surface compatibility, but also is involved in the supporting reactions and enhances the quality of the resulting active sites. The use of Cloisite 93A for catalyst supporting was shown to considerably enhance the polymerization activity, exfoliation quality, and the final polymer powder morphology. In addition, the supporting efficiency for this procedure was close to 100%, which practically eliminates catalyst waste during the supporting step.

The effect of different polymerization conditions, such as polymerization temperature, tri-isobuthylaluminum (TIBA) concentration, and Zr loading on clay were also extensively investigated. Catalyst loading had a large positive impact on clay exfoliation quality, polymerization activity, and final powder morphology. Increasing the polymerization temperature was also shown to enhance the extent of clay exfoliation; however, it increased the risk of polymer/active site extraction from the clay surface and therefore the risk of reactor fouling and deteriorated polymer particle morphology. TIBA, which was initially used as scavenger, was shown to provide a maximum polymerization activity at a given concentration in the reactor. Excessive TIBA concentrations led low polymerization activity, to polymers with lower molecular weights, broader molecular weight distribution, and poorly exfoliated clay particles in the nanocomposite.

An in-situ supporting technique, where the catalyst was supported on the clay directly in the reactor, was also briefly studied. The in-reactor catalyst supporting led to catalysts with higher polymerization activities and acceptable clay exfoliation. It has been proposed that the shorter

contact times between clay surface and catalyst used in the in-situ supporting technique may be responsible for lower catalytic deactivation and, consequently, higher polymerization rates.

The effect of solvent type (toluene and hexane) on supporting efficiency and polymerization behavior was also studied. Catalyst supporting using a solvent that is less compatible with the clay organic modification (hexane, H-type) resulted in considerably higher polymerization activities and higher molecular weights. Unlike polymerizations with catalysts supported in toluene (T-type) that showed an initial acceleration period in the ethylene consumption profile, the constantly deceasing monomer consumption profiles seen for ethylene polymerization with H-type catalysts indicates that H-type catalysts are already considerably exfoliated even before the polymerization begins. In addition, the tertiary amine molecules remaining on the surface of H-type catalysts is likely to affect the polymerization behavior of this catalyst.

Overall, this thesis helped clarify some important aspects of polyethylene-clay nanocomposite production by in-situ polymerization. A new and efficient organoclay-supported metallocene catalyst was developed. Model results have shown that for a given set of assumptions the rate limiting step is the catalyst activity and not the monomer mass transfer. It was also shown that several polymerization conditions can be used to affect polymerization rates and the quality of nanocomposites made with this catalytic system.

Chapter 8
Contributions and Future Work

8.1 Contributions

The main contributions to polymer science and engineering in this thesis are:

1) *A novel mathematical model for clay exfoliation and break up during in-situ polymerization:*

We developed a particle break up model for olefin polymerization with clay-supported metallocenes which featured interlayer polymerization and gallery expansion during particle growth. With this model we found that, to have acceptable dispersion of clay nanolayers within a limited polymerization time and a desired clay content, the catalyst active sites should be homogenously distributed within the clay nanolayers.

2) *A novel metallocene supporting technique:*

For the experimental study of the particle break up and morphology development, we applied a novel supporting technique, in which the clay water content was reacted with TMA to produce MAO on the clay surface. We have also tested the effect of organic modification on the success of in-situ polymerization, and found that the type of ammonium modification has a determining influence on the success of metallocene supporting on the clay surface. Quaternary ammonium modifications were found to be inadequate, whereas the tertiary ammonium modification enhanced the supporting efficiency, polymerization activity and stability. Very fine dispersions of clay nanolayers on the polyethylene matrix were obtained as a result of ethylene polymerization only on the clay surface using this method.

Interestingly, this novel polymerization system was active in the absence of free MAO, which usually causes active site leaching and reactor fouling. The TIBA quantity that was used during high pressure polymerizations was shown to function solely as impurity scavenger. It was also shown that higher catalyst loadings resulted in higher polymerization activity, better exfoliation, and good powder morphology.

3) *Influence of solvent compatibility with the surface modifier on the organoclay during catalyst supporting:*

The higher polymerization activities and higher molecular weights resulted with the metallocene supported in hexane compared to those supported in toluene, proposed better quality of MAO produced upon reaction of TMA on the surface of Cloisite 93A. This is plausible because it has been reported that gentle reaction of TMA with water results in more efficient MAO structures. In our system the poor interaction between hexane and clay surface retarded the water supply for reaction to TMA and consequently better MAO was produced.

4) *Different Mechanisms for Particle Break up and Exfoliation:*

By changing the organic solvent during catalyst supporting, and comparing the ethylene uptake profiles during polymerization with different solvents at different temperatures, it was realized that the compatibility between clay surface and the organic solvent during ethylene polymerization plays an important role on particle break up and exfoliation. Depending on the compatibility between clay surface and the organic solvent in the polymerization reactor, a combination of two mechanisms explains the particle break up in in-situ polymerization.

The first mechanism is intercalation of ethylene monomer into clay interlayers and polymerization and exfoliation. This mechanism is applicable when no good compatibility is available between clay surface and the organic solvent (due to loss of organic modification, or solvent incompatibility or low temperature). The second mechanism is exfoliation before polymerization that can enhance the dispersion of clay in polymer matrix. This mechanism is applicable when good interaction between clay surface modification and the organic solvent is available in the polymerization conditions. This mechanism was more observed when catalyst supporting was performed in hexane on the Cloisite 93A (Cl93Zr-H) and polymerization was performed in toluene in moderate temperatures.

8.2 Future Work

In this thesis we did a systematic investigation of the factors affecting the in-situ polymerization of ethylene with a metallocene catalyst supported on different clay types using a novel supporting technique. Although a good deal of understanding about these systems was acquired, some important topics need further investigation, as suggested below:

1) *Use of shorter polymerization times:*

Shorter polymerizations should be used to investigate the initial stages of particle break up, a critical step for the production of polyolefin clay nanocomposites with the proposed in-situ polymerization technique.

2) *Use of methylated catalysts*:

In our polymerizations, we supported Cl_2ZrCl_2 on the clay surface and used TIBA, together with in-situ formed MAO, as the methylation agent to activate the catalyst. However, our experimental results indicate that TIBA plays solely the role of impurity scavenger. To prove this hypothesis, we need to design experiments with an already methylated metallocene and study the effect of TIBA on its activity.

3) *Use of higher catalyst loadings:*

We observed that almost all added catalyst was supported on the clay surface. We also observed that the type of solvent and organic modification (Cloisite 93A compared to Na^+ MMT) did not affect the catalyst supporting efficiency, in which was always close to 100%. We speculated that the clay surface capacity for catalyst loading is as high as its cation exchange capacity. Therefore, in order to study the effect of parameters such as supporting conditions, organic modification, and the solvent type, higher catalysts concentrations should be tested for better differentiation. We also observed that increased catalyst loading on the Cloisite 93A surface increased the polymerization activity and led to a better powder morphology.

4) *Multiple catalyst supporting:*

The TMA treated Cloisite 93A used in the in-situ supporting approach is a very versatile way for the production of polyolefins with two or more metallocene catalysts, because a separate supporting step is not required. Therefore, the relative amounts of polymer made by each metallocene type is easily controlled by varying the amount of catalysts added to the polymerization reactor, similarly to what would be done in a solution polymerization process. This property can be used to designing new polyolefins with complex molecular weight and chemical composition distributions.

5) *Ethylene/a-olefin copolymerizations:*

The main application of the polyethylene-clay nanocomposites are in the packaging sector due to their enhanced barrier properties. Studying the effect of clay support on the comonomer incorporation for different metallocenes would be beneficial to develop films with improved barrier properties. Furthermore, due to the reduced crystallinity of ethylene/α-olefin copolymers, the inclusion of α-olefin comonomers in the polymer is likely to affect particle break-up and perhaps open a new way to enhance powder morphology.

6) *Propylene polymerization:*

Polypropylene is one of the most important commodity polymers today. Clay-polypropylene nanocomposites are potentially important products and the technique developed in this thesis could also be applied to these systems. It would be particularly interesting to study the effect of clay/organic modifier/catalyst interaction of the stereo- and regioselectivity of these catalysts for propylene polymerization.

References

1. White, J.L. and D.D. Choi, *Polyolefins - Processing, Structure Development, and Properties.. Hanser Publishers*. 2005: Hanser Publishers.
2. Bochmann, M., *Kinetic and mechanistic aspects of metallocene polymerisation catalysts.* Journal of Organometallic Chemistry, 2004. **689**(24): p. 3982-3998.
3. Fink, G., R. Mulhaupt, and H.H. Brintzinger, *Ziegler catalysts: recent scientific innovations and technological improvements*. 1995, Berlin ; New York: Springer-Verlag.
4. Reddy, S.S., G. Shashidhar, and S. Sivaram, *Role of trimethylaluminum on the zirconocene-methylaluminoxane-catalyzed polymerization of ethylene.* Macromolecules, 1993. **26**(5): p. 1180-1182.
5. Mason, M.R., et al., *Hydrolysis of tri-tert-butylaluminum: the first structural characterization of alkylalumoxanes $[(R_2Al)_2O]_n$ and $(RAlO)_n$.* Journal of the American Chemical Society, 1993. **115**(12): p. 4971-4984.
6. Ystenes, M., et al., *Experimental and theoretical investigations of the structure of methylaluminoxane (MAO) cocatalysts for olefin polymerization.* Journal of Polymer Science Part A: Polymer Chemistry, 2000. **38**(17): p. 3106-3127.
7. Kaminsky, W., *Metallocene-catalysed Polymerisation*. 2000: Rapra Technology Ltd.
8. Long, N.J., *Metallocenes : an introduction to sandwich complexes*. 1998, Blackwell Science: Malden, MA, USA. p. 230.
9. Reddy, S.S. and S. Sivaram, *Homogeneous metallocene-methylaluminoxane catalyst systems for ethylene polymerization.* Progress in Polymer Science, 1995. **20**(2): p. 309-367.
10. Reddy, S.S., K. Radhakrishnan, and S. Sivaram, *Methylaluminoxane: synthesis, characterization and catalysis of ethylene polymerization.* Polymer Bulletin, 1996. **36**(2): p. 165-171.
11. Giannetti, E., G.M. Nicoletti, and R. Mazzocchi, *Homogeneous Ziegler-Natta catalysis. II. Ethylene polymerization by IVB transition metal complexes/methyl aluminoxane catalyst systems.* Journal of Polymer Science: Polymer Chemistry Edition, 1985. **23**(8): p. 2117-2134.
12. Sinn, H., et al., *In Transition Metals and Organometallics as Catalysts for Olefin Polymerization*, W. Kaminsky and H. Sinn, Editors. 1988, Springer: New York. p. 257.
13. Cam, D. and U. Giannini, *Concerning the reaction of zirconocene dichloride and methylalumoxane: Homogeneous Ziegler-Natta catalytic system for olefin polymerization.* Die Makromolekulare Chemie, 1992. **193**(5): p. 1049-1055.
14. McDaniel, M.P., et al., *Metallocene Activation by Solid Acids*, in *Tailor-Made Polymers Via Immobilization of Alpha-Olefin Polymerization Catalysts*, J.R. Severn and J.C. Chadwick, Editors. 2008, Wiley-VCH: Weinheim, Germany. p. 171-210.
15. Tritto, I., M.C. Sacchi, and S. Li, *NMR study of the reactions in $Cp_2TiMeCl/AlMe_3$ and $Cp_2TiMeCl$/methylalumoxane systems, catalysts for olefin polymerization.* Macromolecular Rapid Communications, 1994. **15**(3): p. 217-223.
16. Pédeutour, J.-N., et al., *Use of "TMA-depleted" MAO for the activation of zirconocenes in olefin polymerization.* Journal of Molecular Catalysis A: Chemical, 2002. **185**(1-2): p. 119-125.
17. Chien, J., *Supported metallocene polymerization catalysis.* Topics in Catalysis, 1999. **7**(1): p. 23-36.
18. Sinn, H.W.H., DE), Kaminsky, Walter O. (Pinneberg, DE), Vollmer, Hans-jurgen C. (Hamburg, DE), Woldt, Rudiger O. H. H. (Luneberg, DE), *Preparing ethylene polymers using Ziegler*

catalyst comprising cyclodienyl compound of zirconium. 1983, BASF Aktiengesellschaft (DE): United States.

19. Kaminsky, W.P., DE), Hahnsen, Heinrich (Delingsdorf, DE), Kulper, Klaus (Hamburg, DE), Woldt, Rudiger (Luneburg, DE), *Process for the preparation of polyolefins*. 1985, Hoechst Aktiengesellschaft (DE): United States.
20. Ribeiro, M.R., A. Deffieux, and M.F. Portela, *Supported Metallocene Complexes for Ethylene and Propylene Polymerizations: Preparation and Activity.* Industrial & Engineering Chemistry Research, 1997. **36**(4): p. 1224-1237.
21. Estenoz, D.A. and M.G. Chiovetta, *Olefin polymerization using supported metallocene catalysts: Process representation scheme and mathematical model.* Journal of Applied Polymer Science, 2001. **81**(2): p. 285-311.
22. Kristen, M., *Supported metallocene catalysts with MAO and boron activators.* Topics in Catalysis, 1999. **7**(1): p. 89-95.
23. Fink, G., et al., *Propene Polymerization with Silica-Supported Metallocene/MAO Catalysts.* Chemical Reviews, 2000. **100**(4): p. 1377-1390.
24. Kaminsky, W. and H. Winkelbach, *Influence of supported metallocene catalysts on polymer tacticity.* Topics in Catalysis, 1999. **7**(1): p. 61-67.
25. McKenna, T.F. and J.B.P. Soares, *Single particle modelling for olefin polymerization on supported catalysts: A review and proposals for future developments.* Chemical Engineering Science, 2001. **56**(13): p. 3931-3949.
26. Hutchinson, R.A., C.M. Chen, and W.H. Ray, *Polymerization of olefins through heterogeneous catalysis X: Modeling of particle growth and morphology.* Journal of Applied Polymer Science, 1992. **44**(8): p. 1389-1414.
27. McKenna, T. and V. Mattioli, *Progress in describing particle growth for polyolefins: a look at particle morphology.* Macromolecular Symposia, 2001. **173**(1): p. 149-162.
28. Alexiadis, A., et al., *Mathematical Modeling of Homopolymerization on Supported Metallocene Catalysts.* Macromolecular Materials and Engineering, 2004. **289**(5): p. 457-466.
29. Dube, M.A., et al., *Mathematical Modeling of Multicomponent Chain-Growth Polymerizations in Batch, Semibatch, and Continuous Reactors: A Review.* Industrial & Engineering Chemistry Research, 1997. **36**(4): p. 966-1015.
30. Hoel, E.L., C. Cozewith, and G.D. Byrne, *Effect of diffusion on heterogeneous ethylene propylene copolymerization.* AIChE Journal, 1994. **40**(10): p. 1669-1684.
31. Kanellopoulos, V., et al., *Comprehensive Analysis of Single-Particle Growth in Heterogeneous Olefin Polymerization: The Random-Pore Polymeric Flow Model.* Industrial & Engineering Chemistry Research, 2004. **43**(17): p. 5166-5180.
32. Kittilsen, P. and H.F. Svendsen, *Three-level mass-transfer model for the heterogeneous polymerization of olefins.* Journal of Applied Polymer Science, 2004. **91**(4): p. 2158-2167.
33. Soares, J.B.P., T. McKenna, and C.P. Cheng, *Coordination polymerization*, in *Polymer Reaction Engineering*, J.M. Asua, Editor. 2007, Blackwell Publishing Ltd.
34. Chakravarti, S. and W.H. Ray, *Kinetic study of olefin polymerization with a supported metallocene catalyst. III. Ethylene homopolymerization in slurry.* Journal of Applied Polymer Science, 2001. **81**(12): p. 2901-2917.
35. Hutchinson, R.A. and W.H. Ray, *Polymerization of olefins through heterogeneous catalysis. VIII. Monomer sorption effects.* Journal of Applied Polymer Science, 1990. **41**(1-2): p. 51-81.

36. Bonini, F., V. Fraaije, and G. Fink, *Propylene polymerization through supported metallocene/ MAO catalysts: Kinetic analysis and modelling.* Journal of Polymer Science Part A: Polymer Chemistry, 1995. **33**(14): p. 2393-2402.
37. Veera, U.P., G. Weickert, and U.S. Agarwal, *Modeling monomer transport by convection during olefin polymerization.* AIChE Journal, 2002. **48**(5): p. 1062-1070.
38. Severn, J.R., *Methylaluminoxane (MAO), Silica and a Complex:The "Holy Trinity" of Supported Single- site Catalyst*, in *Tailor-Made Polymers Via Immobilization of Alpha-Olefin Polymerization Catalysts*, J.R. Severn and J.C. Chadwick, Editors. 2008, Wiley-VCH: Weinheim, Germany. p. 95-138.
39. Weickert, G., et al., *The particle as microreactor: catalytic propylene polymerizations with supported metallocenes and Ziegler-Natta catalysts.* Chemical Engineering Science, 1999. **54**(15-16): p. 3291-3296.
40. Fink, G., et al., *The particle-forming process of SiO_2-supported metallocene catalysts.* Macromolecular Symposia, 2001. **173**(1): p. 77-88.
41. Bergaya, F., B.K.G. Theng, and G. Lagaly, *Handbook of clay science*. Developments in clay science ;1. 2006, Amsterdam ; Boston ; London: Elsevier. xxi, 1224 p.
42. Meunier, A., *Clays*. 2005, Berlin ; New York :: 9783540271413. xiii, 472 p.
43. Moore, D.M. and R.C. Reynolds, *X-ray diffraction and the identification and analysis of clay minerals*. 2nd ed ed. 1997, Oxford ; New York :: Oxford University Press. xviii, 378 p.
44. Murray, H.H., *Occurrences, Processing and Applications of Kaolins, Bentonites, Palygorskitesepiolite, and Common Clays*. Applied Clay Mineralogy. Vol. Volume 2. 2007, Amsterdam;: Elsevier.
45. Brindley, G.W. and G. Brown., *Crystal structures of clay minerals and their X-ray identification*. Monograph / Mineralogical Society. Vol. 5. 1980, London: Mineralogical Society.
46. Lagaly, G., *Clay Colloids*, in *Developments in Clay Science*, F. Bergaya, B.K.G. Theng, and G.L. (Editor), Editors. 2006, Elsevier: Amsterdam. p. 141-245.
47. Jolly, W.L., *Principles of inorganic chemistry*. 1984, New York: McGraw-Hill.
48. Heller-Kallai, L., *Themally Modified Clay Minerals*, in *Developments in Clay Science*, F. Bergaya, B.K.G. Theng, and G.L. (Editor), Editors. 2006, Elsevier: Amsterdam. p. 289-308.
49. Ainsworth, C.C., J.M. Zachara, and R.L. Schmidt, *Quinoline sorption on Na-montmorillonite; contributions of the protonated and neutral species.* Clays and Clay Minerals, 1987. **35**(2): p. 121-128.
50. Slade, P.G., et al., *Crystal structure of a vermiculite-anilinium intercalate.* Clays and Clay Minerals, 1987. **35**(3): p. 177-188.
51. Mizutani, T., T. Takano, and H. Ogoshi, *Selectivity of Adsorption of Organic Ammonium Ions onto Smectite Clays.* Langmuir, 1995. **11**(3): p. 880-884.
52. Alexandre, M. and P. Dubois, *Polymer-layered silicate nanocomposites: preparation, properties and uses of a new class of materials.* Materials Science and Engineering: R: Reports, 2000. **28**(1-2): p. 1-63.
53. Sinha Ray, S. and M. Okamoto, *Polymer/layered silicate nanocomposites: a review from preparation to processing.* Progress in Polymer Science, 2003. **28**(11): p. 1539-1641.
54. Yano, K., A. Usuki, and A. Okada, *Synthesis and properties of polyimide-clay hybrid films.* Journal of Polymer Science Part A: Polymer Chemistry, 1997. **35**(11): p. 2289-2294.

55. Kodgire, P., et al., *PP/clay nanocomposites: Effect of clay treatment on morphology and dynamic mechanical properties.* Journal of Applied Polymer Science, 2001. **81**(7): p. 1786-1792.
56. Giannelis, E.P., R. Krishnamoorti, and E. Manias, *Polymer-Silicate Nanocomposites: Model Systems for Confined Polymers and Polymer Brushes*, in *Polymers in Confined Environments*. 1999, Springer: Berlin / Heidelberg. p. 107-147.
57. Lagaly, G., M. Ogawa, and I. Dékány, *Clay Mineral Organic Interactions*, in *Developments in Clay Science*, F. Bergaya, B.K.G. Theng, and G.L. (Editor), Editors. 2006, Elsevier: Amsterdam.
58. Ruitz-Hitzky, E. and A.V. Meerbeek, *Clay Mineral And Organic–Polymer Nanocomposite*, in *Developments in Clay Science*, F. Bergaya, B.K.G. Theng, and G.L. (Editor), Editors. 2006, Elsevier: Amsterdam.
59. Scott, S.L., et al., *Highly dispersed clay-polyolefin nanocomposites free of compatibilizers, via the in situ polymerization of [small alpha]-olefins by clay-supported catalysts.* Chemical Communications, 2008(35): p. 4186-4188.
60. Rong, J., et al., *Novel organic/inorganic nanocomposite of polyethylene. I. Preparation via in situ polymerization approach.* Journal of Applied Polymer Science, 2001. **82**(8): p. 1829-1837.
61. Jeong, D.W., et al., *The effect of water and acidity of the clay for ethylene polymerization over Cp2ZrCl2 supported on TMA-modified clay materials.* Journal of Molecular Catalysis A: Chemical, 2003. **206**(1-2): p. 205-211.
62. Liu, C., et al., *Preparation of functionalized montmorillonites and their application in supported zirconocene catalysts for ethylene polymerization.* Journal of Polymer Science Part A: Polymer Chemistry, 2002. **40**(11): p. 1892-1898.
63. Lee, D.-h., et al., *Polyethylene/MMT nanocomposites prepared by in situ polymerization using supported catalyst systems.* Science and Technology of Advanced Materials, 2005(5): p. 457.
64. Mitra, A. and D.A. Atwood, *Aluminum Organometallics*, in *Comprehensive organometallic chemistry III*, D. Michael, P. Mingos, and R.H. Crabtree, Editors. 2007, Elsevier: Amsterdam ; Boston.
65. Hedley, C.B., G. Yuan, and B.K.G. Theng, *Thermal analysis of montmorillonites modified with quaternary phosphonium and ammonium surfactants.* Applied Clay Science, 2007. **35**(3-4): p. 180-188.
66. Dubois, P., M. Alexandre, and R. Jérôme, *Polymerization-filled composites and nanocomposites by coordination catalysis.* Macromolecular Symposia, 2003. **194**(1): p. 13-26.
67. Novokshonova, L., et al., *Heterogenized methylaluminoxane and isobutylaluminoxane as activators for metallocene catalysts.* Kinetics and Catalysis, 2006. **47**(2): p. 251-256.
68. Zhang, J., R.K. Gupta, and C.A. Wilkie, *Controlled silylation of montmorillonite and its polyethylene nanocomposites.* Polymer, 2006. **47**(13): p. 4537-4543.
69. Zhang, J., E. Manias, and C.A. Wilkie, *Polymerically Modified Layered Silicates: An Effective Route to Nanocomposites.* Journal of Nanoscience and Nanotechnology, 2008. **8**: p. 1597 - 1615.
70. Ray, S., et al., *In situ polymerization of ethylene with bis(imino)pyridine iron(II) catalysts supported on clay: The synthesis and characterization of polyethylene-clay nanocomposites.* Journal of Polymer Science Part A: Polymer Chemistry, 2005. **43**(2): p. 304-318.
71. He, A., et al., *Preparation of exfoliated isotactic polypropylene/alkyl-triphenylphosphonium-modified montmorillonite nanocomposites via in situ intercalative polymerization.* Polymer, 2006. **47**(6): p. 1767-1771.

72. Huang, Y., K. Yang, and J.-Y. Dong, *An in situ matrix functionalization approach to structure stability enhancement in polyethylene/montmorillonite nanocomposites prepared by intercalative polymerization.* Polymer, 2007. **48**(14): p. 4005-4014.
73. Ciardelli, F., et al., *Nanocomposites based on polyolefins and functional thermoplastic materials.* Polymer International, 2008. **57**(6): p. 805-836.
74. Heinemann, J., et al., *Polyolefin nanocomposites formed by melt compounding and transition metal catalyzed ethene homo- and copolymerization in the presence of layered silicates.* Macromolecular Rapid Communications, 1999. **20**(8): p. 423-430.
75. Shin, S.-Y.A., et al., *Polyethylene-clay hybrid nanocomposites: in situ polymerization using bifunctional organic modifiers.* Polymer, 2003. **44**(18): p. 5317 - 5321.
76. Yang, F., et al., *Preparation and properties of polyethylene/montmorillonite nanocomposites by in situ polymerization.* Journal of Applied Polymer Science, 2003. **89**(13): p. 3680-3684.
77. Jin, Y.-H., et al., *Polyethylene/Clay Nanocomposite by In-Situ Exfoliation of Montmorillonite During Ziegler-Natta Polymerization of Ethylene.* Macromolecular Rapid Communications, 2002. **23**(2): p. 135-140.
78. Xu, J.-T., Q. Wang, and Z.-Q. Fan, *Non-isothermal crystallization kinetics of exfoliated and intercalated polyethylene/montmorillonite nanocomposites prepared by in situ polymerization.* European Polymer Journal, 2005. **41**(12): p. 3011-3017.
79. Wei, L., T. Tang, and B. Huang, *Synthesis and characterization of polyethylene/clay-silica nanocomposites: A montmorillonite/silica-hybrid-supported catalyst and in situ polymerization.* Journal of Polymer Science Part A: Polymer Chemistry, 2004. **42**(4): p. 941-949.
80. Kuo, S.-W., et al., *Syntheses and characterizations of in situ blended metallocence polyethylene/clay nanocomposites.* Polymer, 2003. **44**(25): p. 7709-7719.
81. Novokshonova, L., et al., *Partially Hydrolyzed Alkylaluminums as the Active Heterogenized Components of Metallocene Catalysts.* Kinetics and Catalysis, 2005. **46**(6): p. 853-860.
82. Bergman, J.S., et al., *Synthesis and characterization of polyolefin–silicate nanocomposites: a catalyst intercalation and in situ polymerization approach.* Chem. Commun., 1999: p. 2179 - 2180.
83. Ushakova, T., et al., *Olefin polymerization on immobilized zirconocene catalysts containing alkylaluminoxanes synthesized on the support surface.* Kinetics and Catalysis, 2007. **48**(5): p. 669-675.
84. Novokshonova, L., et al., *Heterogenization of metalorganic catalysts of olefin polymerization and evaluation of active site non-uniformity.* Macromolecular Symposia, 2004. **213**(1): p. 147-156.
85. Liu, C., T. Tang, and B. Huang, *Zirconocene catalyst well spaced inside modified montmorillonite for ethylene polymerization: role of pretreatment and modification of montmorillonite in tailoring polymer properties.* Journal of Catalysis, 2004. **221**(1): p. 162-169.
86. Suga, Y.Y., JP), Uehara, Yumito (Yokkaichi, JP), Maruyama, Yasuo (Yokohama, JP), Isobe, Eiji (Yokohama, JP), Ishihama, Yoshiyuki (Yokkaichi, JP), Sagae, Takehiro (Yokkaichi, JP), *Method for polymerizing olefins using a novel catalyst*. 1999, Mitsubishi Chemical Corporation (Tokyo, JP): United States.
87. Carnahan, E.M. and G.B. Jacobsen, *Supported Metallocene Catalysts.* CATTECH, 2000. **4**(1): p. 74-88.

88. Scott, S.G., CA, US), Peoples, Brian (Goleta, CA, US), Rojas, Rene (Bosque, CL), Tanna, Akio (Nakahara-ku, JP), Shimizu, Fumihiko (Yarimizu, JP), *Method for forming exfoliated clay-polyolefin nanocomposites*. 2008: United States.
89. Chester, A.W.C.H., NJ), Murray, James G. (East Brunswick, NJ), *Catalysts for olefin polymerization comprising the reaction product of organotitanium and organochromium with zeolites*. 1984, Mobil Oil Corporation (New York, NY): United States.
90. Weiss, K., et al., *Polymerisation of ethylene or propylene with heterogeneous metallocene catalysts on clay minerals.* Journal of Molecular Catalysis A: Chemical, 2002. **182-183**: p. 143-149.
91. Suga, Y.M., JP), Maruyama, Yasuo (Tokyo, JP), Isobe, Eiji (Kawasaki, JP), Suzuki, Toru (Yokohama, JP), Shimizu, Fumihiko (Yokohama, JP), *Catalyst for polymerizing an olefin and method for producing an olefin polymer*. 1994, Mitsubishi Kasei Corporation (Tokyo, JP): United States.
92. Xie, W., et al., *Thermal Degradation Chemistry of Alkyl Quaternary Ammonium Montmorillonite.* Chemistry of Materials, 2001. **13**(9): p. 2979-2990.
93. Frankowski, D.J., et al., *Stability of Organically Modified Montmorillonites and Their Polystyrene Nanocomposites After Prolonged Thermal Treatment.* Chemistry of Materials, 2007. **19**(11): p. 2757-2767.
94. Mittal, V., *Gas permeation and mechanical properties of polypropylene nanocomposites with thermally-stable imidazolium modified clay.* European Polymer Journal, 2007. **43**(9): p. 3727-3736.
95. Araujo, E., et al., *Thermal and mechanical properties of PE/organoclay nanocomposites.* Journal of Thermal Analysis and Calorimetry, 2007. **87**(3): p. 811-814.
96. Tang, T.C., CN), Wei, Liangming (Changchun, CN), Huang, Baolong (Changchun, CN), *Process for preparation of polyolefin/inorganic component nanocomposite by in-situ polymerization*. 2003, Changchun, Institute Of Applied Chemistry Chinese Academy Of Science (Jilian, CN): United States.
97. Alexandre, M., et al., *Polyethylene-layered silicate nanocomposites prepared by the polymerization-filling technique: synthesis and mechanical properties.* Polymer, 2002. **43**(8): p. 2123-2132.
98. Lagaly, G. and R. Fahn, in *Ullmanns Encyklopädie der technischen Chemie*. 1983: Weinheim. p. 311.
99. Takashashi, T., et al., Polym. Preprints, 2002. **43**: p. 1259.
100. Mariott, W.R., N.C. Escudé, and E.Y.-X. Chen, *Stereoregular P(MMA)-clay nanocomposites by metallocene catalysts: In situ synthesis and stereocomplex formation.* Journal of Polymer Science Part A: Polymer Chemistry, 2007. **45**(13): p. 2581-2592.
101. Mariott, W.R. and E.Y.-X. Chen, *Stereochemically Controlled PMMA-Exfoliated Silicate Nanocomposites Using Intergallery-Anchored Metallocenium Cations.* Journal of the American Chemical Society, 2003. **125**(51): p. 15726-15727.
102. Pavlidou, S. and C.D. Papaspyrides, *A review on polymer-layered silicate nanocomposites.* Progress in Polymer Science, 2008. **33**(12): p. 1119-1198.
103. Ke, Y.C. and P. Stroeve, *Polymer-Layered Silicate and Silica Nanocomposites*. 2005, Elsevier Science: Amsterdam. p. 119-209.
104. Bhattacharya, S.N., M.R. Kamal, and R.K. Gupta., *Polymeric nanocomposites: theory and practice*. 2008, Munich: Carl Hanser Publishers.

105. Zanetti, M., S. Lomakin, and G. Camino, *Polymer layered silicate nanocomposites.* Macromolecular Materials and Engineering, 2000. **279**(1): p. 1-9.
106. Nagel, E.J., V.A. Kirillov, and W.H. Ray, *Prediction of Molecular Weight Distributions for High-Density Polyolefins.* Industrial & Engineering Chemistry Product Research and Development, 1980. **19**(3): p. 372-379.
107. Floyd, S., et al., *Polymerization of olefins through heterogeneous catalysis. III. Polymer particle modelling with an analysis of intraparticle heat and mass transfer effects.* Journal of Applied Polymer Science, 1986. **32**(1): p. 2935-2960.
108. Gorval, E.G., P. Svejda, and S.M.P. Mutsers, *Sorption and Desorption of n-Alkanes in Polypropylene Polymerized in the Gas Phase.* Industrial & Engineering Chemistry Research, 2000. **40**(3): p. 814-825.
109. Ferrero, M.A. and M.G. Chiovetta, *Catalyst fragmentation during propylene polymerization: Part I. The effects of grain size and structure.* Polymer Engineering & Science, 1987. **27**(19): p. 1436-1447.
110. Yang, F., et al., *Preparation and properties of polyethylene/montmorillonite nanocomposites by in situ polymerization.* Journal of Applied Polymer Science, 2003. **89**(13): p. 3680-3684.
111. Yang, K., Y. Huang, and J.-Y. Dong, *Efficient preparation of isotactic polypropylene/montmorillonite nanocomposites by in situ polymerization technique via a combined use of functional surfactant and metallocene catalysis.* Polymer, 2007. **48**(21): p. 6254 - 6261.
112. Maneshi, A., J. Soares, and L.Simon, *In-situ polymerization method for preparation of polyolefin/clay nanocomposites: Review*.
113. Ho, D.L., R.M. Briber, and C.J. Glinka, *Characterization of Organically Modified Clays Using Scattering and Microscopy Techniques.* Chemistry of Materials, 2001. **13**(5): p. 1923-1931.
114. Ho, D.L. and C.J. Glinka, *Effects of Solvent Solubility Parameters on Organoclay Dispersions.* Chemistry of Materials, 2003. **15**(6): p. 1309-1312.
115. Yariv, S., *Organo-Clay Complexes & Interactions*, in *Organo-Clay Complexes & Interactions*, S. Yariv and H. Cross, Editors. 2002, Marcel Dekker, Inc.
116. Laubengayer, A.W., J.D. Smith, and G.G. Ehrlich, *Aluminum-Nitrogen Polymers by Condensation Reactions1.* Journal of the American Chemical Society, 1961. **83**(3): p. 542-546.
117. Sangokoya, S.A.B.R., LA), *Tertiary amino-aluminoxane halides*. 1995, Albemarle Corporation (Richmond, VA): United States.
118. Sangokoya, S.A.B.R., LA), *Teritary amino-aluminoxane halides*. 1995, Albemarle Corporation (Richmond, VA): United States.
119. Biswas, K., et al., *Remarkably Stable $(Me_3Al)_2$•DABCO and Stereoselective Nickel-Catalyzed AlR_3 (R: Me, Et) Additions to Aldehydes.* ChemInform, 2005. **36**(31).
120. Klendworth, D.D.W.C., OH, US), Reinking, Mark K. (Mason, OH, US), *Process for making polyolefin compositions containing exfoliated clay*. 2005, Equistar Chemicals, LP (Houston, TX, US): United States.
121. Bala, P., B.K. Samantaraya, and S.K. Srivastava, *Synthesis and characterization of Na-montmorillonite-alkylammonium intercalation compounds.* Materials Research Bulletin, 2000. **35**(10): p. 1717-1724.
122. Atiqullah, M., H. Hammawa, and H. Hamid, *Modeling the solubility of ethylene and propylene in a typical polymerization diluent: some selected situations.* European Polymer Journal, 1998. **34**(10): p. 1511-1520.

123. Chanzy, H., et al., *Nascent structures during the polymerization of ethylene.* Colloid & Polymer Science, 1973. **251**(8): p. 563-576.
124. Scheirs, J., S.W. Bigger, and O. Delatycki, *Structural morphology and compaction of nascent high-density polyethylene produced by supported catalysts.* Journal of Materials Science, 1991. **26**(12): p. 3171-3179.
125. Keller, A. and F.M. Willmouth, *On the morphology and orgin of the fibres observed in Nascent Ziegler polyethylene.* Die Makromolekulare Chemie, 1969. **121**(1): p. 42-50.
126. Muñoz-Escalona, A. and A. Parada, *Factors affecting the nascent structure and morphology of polyethylene obtained by heterogeneous Ziegler--Natta catalysts: 2. Crystallinity and melting behaviour.* Polymer, 1979. **20**(7): p. 859-866.
127. Ray, S.S. and M. Bousmina, *Poly(butylene sucinate-co-adipate)/montmorillonite nanocomposites: effect of organic modifier miscibility on structure, properties, and viscoelasticity.* Polymer, 2005. **46**(26): p. 12430-12439.
128. Chaiko, D.J.N., IL), *Composite materials with improved phyllosilicate dispersion*. 2004, The University of Chicago (Chicago, IL): United States.
129. Knoke, S., et al., *Early Stages of Propylene Bulk Phase Polymerization with Supported Metallocene Catalysts.* Macromolecular Chemistry and Physics, 2003. **204**(4): p. 607-617.